LIQUID CRYSTAL MEDIATED BIOASSAY

FOR PROTEIN DETECTION

VERA JOANNE RETUYA ALIÑO

NATIONAL UNIVERSITY OF SINGAPORE

2012

LIQUID CRYSTAL MEDIATED BIOASSAY

FOR PROTEIN DETECTION

VERA JOANNE RETUYA ALIÑO

(ChE, University of San Carlos)

A THESIS SUBMITTED

FOR THE DEGREE OF DOCTOR OF PHILOSOPHY

DEPARTMENT OF
CHEMICAL & BIOMOLECULAR ENGINEERING

NATIONAL UNIVERSITY OF SINGAPORE

2012

DECLARATION

I hereby declare that this thesis is my original work and it has been written by me in its entirety. I have duly acknowledged all the sources of information which have been used in the thesis.

This thesis has also not been submitted for any degree in any university previously.

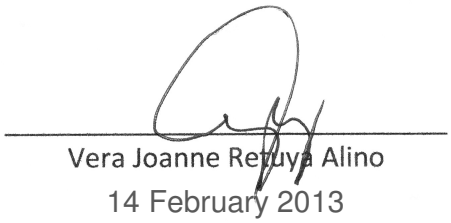

Vera Joanne Retuya Alino

14 February 2013

ACKNOWLEDGEMENTS

I would like to extend my gratitude and my heartfelt thanks to the following people who, in one way or another, helped in the completion of this research study.

First and foremost, I would like to express my deepest and most sincere gratitude to my supervisor and thesis adviser, A/P Yang Kun-Lin, for his suggestions and meticulous scrutiny of the thesis manuscript. His words of encouragement and constant surveillance on the progress of the study motivated and helped me to go beyond my comfort zone. I would also like to thank my thesis panel, A/P Yung Lanry, Prof. Feng Si-Shen and A/P Tong Yen-Wah, for their professional commitment, patience, and scholarly comments, which greatly improved the flow and quality of the research output.

Worthy of mention is Prof. Saif A. Khan, for lending his expertise on microfluidics and sharing his knowledge on fluid dynamics which helped greatly in my research. I am grateful to my final year project (FYP) students, for their invaluable help during the experimental ground work. I would also like to thank all my lab mates and office mates, for providing a friendly atmosphere and therapeutic environment which was conducive to working. I would like to individually mention

Pravien, Laura and Siok Lian. They are seniors in wisdom yet ones who exuded youth and grace in sharing their knowledge unconditionally. Moreover, to Mr. Boey, Ms. Chai Keng, Susan, Evan, Doris and Vanessa who all in their own way helped me with the small yet important matters. Thanks to my true-blooded classmates and generous researchers, Noome, Kate, Egg, and Panu, for their steadfast reminders to be humble when the going gets tough. To my dear friends and relatives, whom I sometimes neglected, I hope that you all would accept this thesis as 167-pages worth of an apology.

Everlasting indebtedness goes to my parents, Ed and Nen, and to my only sibling, brother Earl, for their trust, pride, and confidence in me as I pursued my doctoral degree. I would like to give a shout out to my husband, Mattwho has been so patient and stood by me through the good and trying times - I'm coming home.

Last and never the least, endless thanks and praise goes to GOD ALMIGHTY, for in His time, this dream has become a reality.

VERA JOANNE RETUYA ALIÑO

TABLE OF CONTENTS

SUMMARY

Proteinuria refers to a condition when the urine protein concentration is higher than the normal. People with this condition have a greater risk of developing chronic kidney disease (CKD). Detecting protein biomarkers such as HSA (human serum albumin), IgG (immunoglobulin G), and Trf (transferrin) in urine samples is a standard procedure for the early detection, diagnosis of kidney problems and the prognosis of patients with CKD. However, current detection methods still face the issue of balancing cost and sensitivity, not to mention these methods are laboratory based and require trained personnel to execute the complex, laborious, and often time consuming procedures. The aim of this work is to address these issues by exploring the use of liquid crystals (LC) for the development of label-free detection of proteins with better stability, higher sensitivity and faster response. It is anticipated that the development of LC-based microfluidic protein assays can be used as a low cost and portable device.

The objective of developing LC-based protein assays is accomplished in two different systems: on solid surfaces and in aqueous solutions. To detect proteins on a solid surface, we first studied how to induce homeotropic orientations of LCs by using surface modifications. LC-based protein assay was developed by depositing a layer of antibody on the surface to specifically attract HSA, a target protein, to the surface. Then, we incorporated a thin LC layer as a readout system such that the presence of

protein in urine samples can be detected as optical signals. In combination with dilution protocols, this assay can be used to estimate the concentration range of the protein simply by counting the number of bright spots. The results show that concentrations of HSA can be measured accurately in the range of 20 – 3000 μg/mL both in buffer solutions and urine samples collected from patients diagnosed with CKD.

Next, to detect proteins in aqueous solutions, we develop an assay in which probe proteins are immobilized on the surface of LC droplets rather than on solid surfaces. The advantage of this assay is that the binding of antibodies to the probe proteins can be transduced by the LC droplets directly without the need for additional steps. The orientational transitions occur at concentrations of proteins that are three orders of magnitude lower than previously reported in solid substrate systems. Several methods have been reported to produce emulsified LC droplets. However, obtaining LC droplets with a narrow distribution range in a reproducible fashion remains a challenge. This problem is addressed in the third part of the thesis. We report a simple means of producing uniform LC droplets by flushing inkjet-printed LC droplets with aqueous solutions in an open channel. This is the first study showing that LC can be used as "ink" for inkjet printing to produce identical LC droplets of various sizes. We also discuss under what conditions the printed LC droplets can be flushed and released from the surface. Using this technology, we are able to tailor the optical behaviors and surface properties of the emulsified LC droplets for biosensing applications.

Lastly, we develop a microfluidic protein assay where LC dots are embedded in the microfluidic channels as microscopic protein sensors. The stability of the surface-supported LC dots under fluid flow is also studied. Through this design, we are able to estimate the concentration of the protein in the solution simply by counting the number of bright sections of LC dots along the channel. Moreover, this protein assay provides a real-time sensing solution to monitor the proteins in microfluidic devices without protein labeling or complex instrumentation to read the signals.

In summary, we have developed LC-based protein assays that can detect and quantify proteins both on the surface and in solution. Unlike the traditional urine dipstick, both LC-based systems detect proteins which are specifically targeted. In addition, because these developed systems are sensitive and do not require additional complex instrumentations, they are good candidates to become a portable and low-cost protein assay which can provide a faster and simpler alternative for the fast profiling of CKD patients.

LIST OF TABLES

LIST OF FIGURES

LIST OF ABBREVIATIONS

A

AEAPS	(3-(2-aminoethylamino)propyl) trimethoxysilane
AHSA	Anti-Human Serum Albumin
AIgG	Anti-Human Immunoglobulin G

B

BSA	Bovine Serum Albumin

C

CKD	Chronic Kidney Disease
CTAB	Cetyl Trimethylammonium Bromide
Cy3–AHSA	Cy3–Labeled Anti-Human Serum Albumin
Cy3–AIgG	Cy3–Labeled Anti-Human Immunoglobulin G
Cy3–HSA	Cy3–Labeled Human Serum Albumin
Cy3–IgG	Cy3–Labeled Human Immunoglobulin G
Cy3–PEI	Cy3–Labeled Polyethyleneimine

D

DI	Deionized Water
DMOAP	N,N-dimethyl-N-octadecyl-3-aminopropyltrimethoxysilyl chloride
DOD	Drop-on-demand
DTT	Dithiothreitol
DSCG	Disodium cromoglycate

E

ELISA	Enzyme-Linked Immunosorbent Assay

F

FIA	Fluorescence Immunoassay
FITC	Fluorescein Isothiocyanate
FITC–AHSA	Fluorescein Isothiocyanate–Labeled Anti-Human Serum Albumin
FITC–HSA	Fluorescein Isothiocyanate–Labeled Human Serum Albumin
FITC–HTrf	Fluorescein Isothiocyanate–Labeled Human Transferrin
F/P	Final Dye/ Protein Ratio

G

GA	Glutaraldehyde

H

HF	Hydrofluoric Acid
HPLC	High Performance Liquid Chromatography
HSA	Human Serum Albumin
HSA–LC droplet	LC droplets coated with Human Serum Albumin
HTrf	Human Transferrin

I

IgG	Human Immunoglobulin G
IgG–LC droplet	LC droplets coated with Human Immunoglobulin G
IN	Immunonephelometry
ITA	Immunoturbidimetric Assay

L

LC	Liquid Crystal
LOD	Limit of Detection
LPEI	Linear Poly(ethylene imine)

M

MS	Mass Spectrophotometer

N

Na_2CO_3	Sodium Carbonate
$NaBH_3CN$	Sodium Cyanoborohydride

P

PAH	Poly(allylamine hydrochloride)
PBS	Phosphate-Buffered Saline
PBS–T20	Phosphate-Buffered Saline with Tween 20
PDI	Polydispersity index
PDMS	Poly(dimethylsiloxane)
PEI	Polyethyleneimine
PEI–T20	Polyethyleneimine with Tween 20
POC	Point-of-care
PSS	Poly(sodium-4-styrene sulfonate)
PVA	Polyvinyl alcohol

R

RIA	Radioimmunoassay

S

SDS	Sodium Dodecyl Sulfate
SE3030	Polystyrene and Ethylene Oxide block copolymer
SPR	Surface Plasmon Resonance

T

TEA	(Triethoxysilyl) butanal
Tween 20	Polyethylene Glycol Sorbitan Monolaurate

OTHERS

5CB	4-pentyl-4'-cyano-biphenyl (Liquid Crystals)
A	Surface Area
c	Contact diameter
C	Concentration
D	Diameter
F	Surface free energy
h	Height of the LC droplet
K	Elastic modulus strain
n	Director of the LC
NA	Avogadro's Number
R_D	Mean urine dipstick reading
R_E	Electrophoresis dipstick reading
R_{LC}	Mean LC-based assay reading
S_i	Spreading parameter
$SA_{LC/water}$	Interfacial area of the 5CB (LC)
V	Volume
v	Linear velocity
W	Surface anchoring energy per unit area
γ	Surface Tension
Γ	Surface Density
Φ_v	Volumetric Flow rate
Φ_c	Critical volumetric flow rate

CHAPTER 1

INTRODUCTION

1.1 Background of the Study

In recent years, chronic kidney disease (CKD) has become a worldwide public health problem (Afzali et al. **2007;** Goligorsky et al. **2007;** Snyder and Pendergraph **2005**). The use of early predictive biomarkers for the diagnosis of CKD can significantly improve the prognosis of this disease. Proteins in urine such as human serum albumin (HSA), human immunoglobulin G (IgG), and human transferrin (HTrf) are one of the most reliable biomarkers of CKD (Barratt and Topham **2007;** Bazzi et al. **2001;** Gonzalez-Buitrago et al. **2007;** Liu et al. **2006;** Pedraza-Chaverri et al. **2006;** Viberti et al. **1982b;** Woo and Lau **1998**). In addition, because they are excreted from the body, these urinary biomarkers provide great advances in understanding the kidney function and offer enormous potential in clinical applications as they require minimal invasive procedures in doing so. Currently, the analysis of proteins in urine is commonly done by using dipstick tests (Gyure **1977**). This type of test, however, can only detect HSA and tends to give false readings because of the lack of specificity (Constantiner **2005;** Grootendorst et al. **2009;** Jimbo **2007;** Mathiesen et al. **1984;** Mladenovic **2004;** Schrier **2007;** Viberti et al. **1982a;** Viberti et al. **1982b**). There are also several other tests readily available for the detection of urinary proteins such as radioimmunoassay (RIA) (Alexander **1980;** Bernard and Lauwerys **1983;** Comper et al. **2004a**), enzyme-linked immunosorbent assay (ELISA) (Bernard and Lauwerys **1983;** Torffvit and Wieslander **1986;** Watts et

al. **1986**), and nephelometry (Carroll and Temte **2000;** Marre et al. **1987;** Thakkar et al. **1997**). These tests have higher sensitivity and accuracy, yet they suffer from several drawbacks (Bernard and Lauwerys **1983**). Firstly, they require labeling that may either be expensive (e.g. enzymes for ELISA) and/or hazardous (e.g. radioisotopes for RIA). Labeling can also affect the bioactivity of the proteins. Secondly, these methods have complex procedures and require larger sample volumes and longer processing times (~12 h). Lastly, they require sensitive and bulky instrumentation which may be difficult to be used in point-of-care (POC) applications. Because of these limitations, there is a need to develop a new assay that is more sensitive, label-free and easier to operate.

For the past decade, several studies have successfully demonstrated the principles of using liquid crystals (LCs) for the detection of surface-adsorbed proteins through optical outputs (Bi et al. **2007;** Clare and Abbott **2005;** Gupta et al. **1998;** Jang et al. **2005;** Kim and Abbott **2001;** Kim and Abbott **2002;** Kim et al. **2000;** Luk et al. **2005;** Luk et al. **2003;** Shah and Abbott **2001;** Skaife et al. **2001;** Tingey et al. **2004;** Xue et al. **2008;** Xue et al. **2009**). These principles can be summarized as follows. First, when a thin layer of LC is supported on a solid surface, the orientations of LC are determined by the surface property. Therefore, when proteins are adsorbed on the surface, the surface property changes and that affects the orientations of the LC at the interface. The disturbance of the orientational ordering of the LCs at the interface propagates to other LC molecules in bulk (over a distance up to tens of micrometers), resulting in global transition in the orientation of the

molecules. Such distorted orientational profile will trigger a transition in the optical signal of LC that is observable under polarized light microscopy or simply, by the naked eye as shown in Figure 1.1. Secondly, this sharp transition only occurs when the surface density of proteins reaches a critical value. The protein concentration in the solution that leads to this critical surface density is called **critical concentration**.

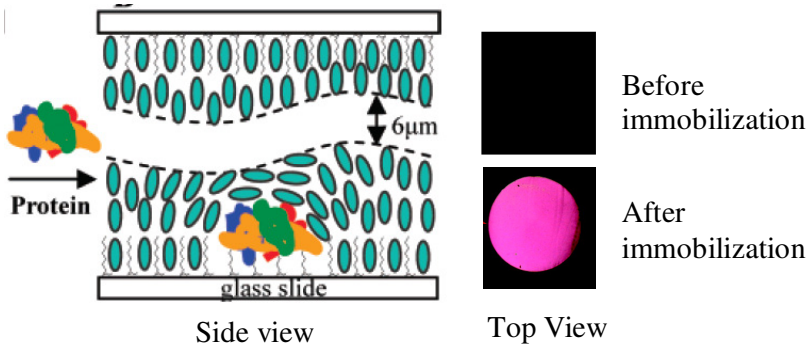

Figure 1.1 Orientational profiles of 5CB in an LC optical cell with a separation distance of ~6μm. The presence of protein immobilized on one of the surfaces changes the homeotropic orientation of the LC to a tilted or planar orientation at the interface causing a distinct optical signal. This signal is in sharp contrast to the dark background in the surrounding area with no protein (Xue and Yang 2008).

Protein detection using LC-based assay is highly sensitive because it has been reported that the assay can differentiate a difference of 1 μg/mL in protein concentration (Xue and Yang **2008**). A dark-to-bright LC response is also a useful feature for tests that require a simple yes or no answer. Thus, the use of LC material in assays can eliminate the need of labeling materials (e.g. fluorescent or radioactive), and has sensitivity that matches traditional analytical methods. However, the LC-based assay still has several setbacks that need to be addressed. For instance, it still

requires incubation, rinsing, and fabrication of LC cells before analysis. Also, at this stage, it is extremely difficult to determine the total amount of protein in solution. The inability to quantify the proteins as well as the design constraints poses a practical problem when LC is used to diagnose patients with CKD.

In this thesis, we first exploit LC for developing protein assays in two different configurations: on solid surfaces and in aqueous solutions. In the first configuration, we address the quantification of protein concentration by developing a dilution protocol such that the amount of proteins can be determined simply by counting the number of bright LC dots in the cell. In the second configuration, we develop an assay in which probe proteins are immobilized on the surface of LC droplets rather than on solid surfaces. The advantage of this assay is that the binding of antibodies to the probe proteins can be transduced by the LC droplets directly without the need for additional steps. The orientational transitions occur at concentrations of proteins that are three orders of magnitude lower than those previously designed on solid surfaces. Both systems have their own positive features and the advantage of being label-free making them ideal candidates to be further developed as a portable and low-cost protein assay.

However, to immobilize proteins on the surface of LC droplets, uniform and stable LC droplets dispersed in aqueous solutions are needed. In the past, the production of LC droplets mainly relies on vortex or sonication of LC. Both methods

often result in emulsified LC droplets with a broad size distribution (Lavrentovich **1998;** Zou et al. **2011;** Zou and Fang **2010**). Because of this limitation, new techniques that enable the preparation of LC droplets with an uniform size and surface properties are needed. Currently, only few methods are available for producing monodisperse LC droplets. These methods include templating and microfluidic methods. In the former, silica particles were coated with multiple layers of polyelectrolyte to create a polymer capsule. The silica core is then etched with hydrofluoric acid, and the hollow space is filled with LC. Meanwhile, the latter uses either flow focusing (Hamlington et al. **2007;** Shklyaev and Shen **2009**) or co-flowing liquid streams (Umbanhowar et al. **2000**) to squeeze and break off a stream of LC into spherical droplets. However, both methods are still time-consuming and not convenient. Therefore, we aim to develop a simple and reliable method for producing uniform LC droplets, which can be used to develop our protein assays.

Lastly, miniaturized microfluidic protein assay has several advantages over traditional one, because the former requires less sample volumes and has faster assay time (Sia and Whitesides **2003**). Nevertheless, it still requires bulky and complex instrumentation for signal readouts, and that limits its practical applications. In this thesis, we aim to develop a miniaturized protein assay where LC can be incorporated inside the microfluidic channels for signal readout. Therefore, the use of bulky instrumentation can be avoided, and the detection can simply rely on naked eye. Several issues related to the stability of LC droplets inside microfluidic channels are also investigated in details in this thesis.

1.2 Scope and Objectives

In this thesis, we aim to develop LC-based protein assays to detect and quantify the amount of proteins in unknown samples. Ideally, the assay should be able to produce results with good reproducibility, high sensitivity, fast response and low sample consumption. In addition, it will not require the use of additional instrumentations, making it suitable for point of care usage. The research results described herein may be considered as an important first step for the development of a low-cost, POC diagnostic device for CKD.

The structure of this thesis is outlined in Figure 1.2. In **Chapter 3**, the changes in the optical appearances of LCs to HSA adsorbed on anti-human serum albumin (AHSA)-decorated solid surfaces are exploited for developing label-free protein immunoassays. The concept of this method is based on the high sensitivity of the orientational ordering of LCs to minute changes on a solid surface. A thin layer of LC is incorporated as a readout system such that the HSA density immobilized on the surface (from the HSA in the urine samples) can be detected as optical signals. In combination with dilution protocols, this assay can be used to estimate the concentration range of HSA simply by counting the number of bright spots. It is anticipated that this assay can provide a faster and simpler alternative for the diagnosis and prognosis of patients with kidney diseases without using expensive and bulky equipment.

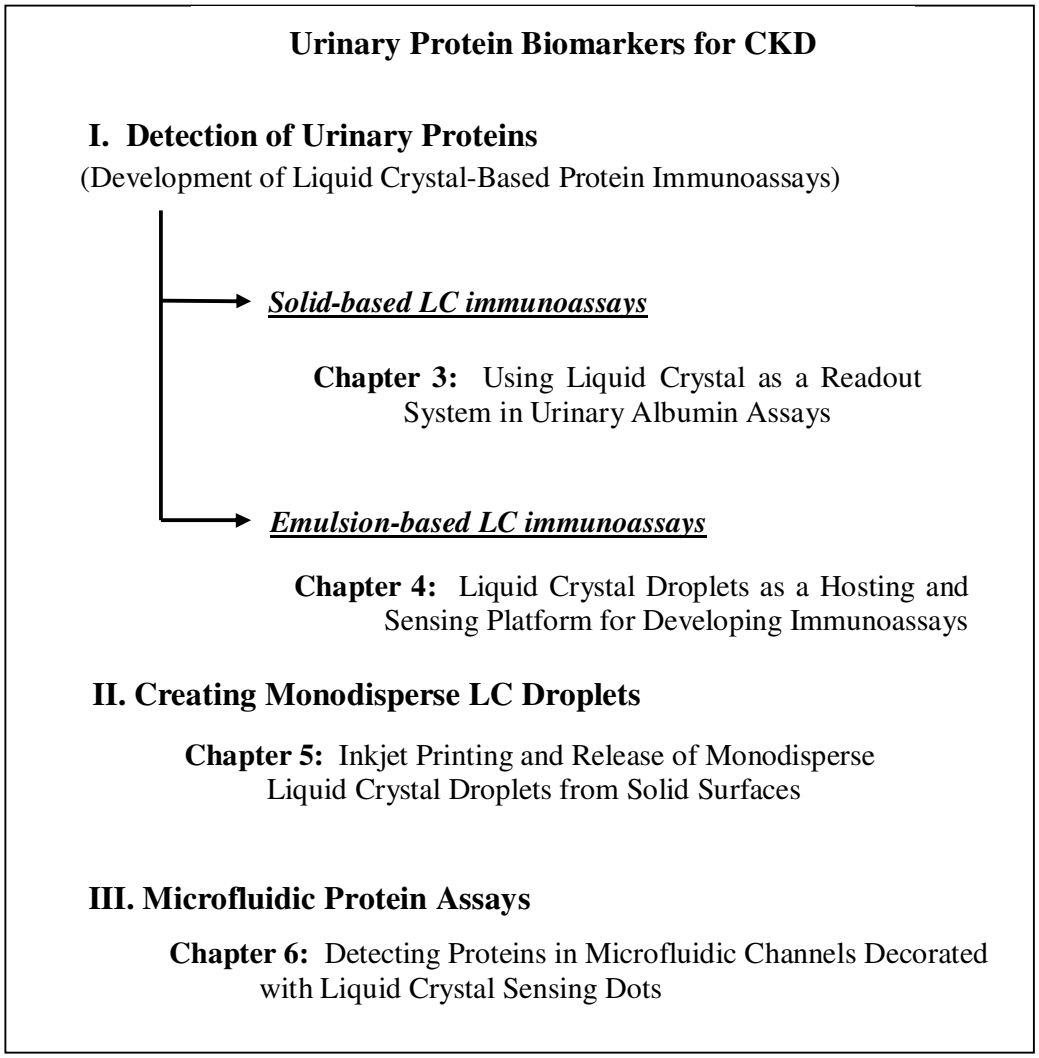

Figure 1.2 Thesis Outline

Dispersion of LC as emulsion droplets in polymers and aqueous solutions has attracted much attention in the recent years, because large surface areas and orientational ordering of these LC droplets give unique optical and mechanical properties (Lockwood et al. **2006;** Volovik and Lavrentovich **1983**). In **Chapter 4**,

we report an immunoassay in which probe proteins are immobilized on the surface of LC droplets rather than on solid surfaces. The advantage of this immunoassay is that the binding of antibodies to the probe proteins can be transduced by the LC droplets directly without any additional steps. For example, when we incubate the LC droplets decorated with HSA (HSA-LC droplets) in a solution containing AHSA, these droplets change their orientations from radial to bipolar configuration. In contrast, when we incubate the HSA-LC droplets in a solution containing anti-human immunoglobulin G (AIgG), no changes are observed. The change of orientational configuration indicates the formation of antigen-antibody immunocomplex on the surface of the LC droplets. From this work, we show that the sensitivity of this platform is higher than that of protein assays developed on solid surfaces. Since the immunoassay using LC droplets is label-free and gives a unique optical response, it has the potential to be used directly in the solution as a portable and low-cost immunoassay.

The emulsified LC droplets used above was prepared through vortexing, which innately produces droplets with broad size distribution. Recent studies show that the size of the LC droplets can affect their optical behaviour (Gupta et al. **2009b**). Hence, only a limited number of droplets with similar sizes were used during the analysis of the protein immunoassay in Chapter 4. Therefore, in **Chapter 5**, we aim to address this issue by producing LC droplets with uniform size using a two-step method. The first step investigates the possibility of using 5CB, a nematic LC, as "ink" in inkjet printers to dispense LC droplets in desired locations. The second aim

is to lift off these LC droplets from solid surfaces to form free LC droplets in aqueous solution. We also investigate the unanimous response of these monodisperse LC droplets created by a simple chemical reaction. Using this two-step method, we are able to control the size of the LC droplets and use them as chemical sensors.

Finally, miniaturization of protein assays is accomplished by using microfluidic devices with LC sensing dots embedded within the channels. In **Chapter 6,** we first exploit inkjet printing to generate LC dots, and study the behaviors of these LC dots under flow conditions. By using the optical appearance of the LC dots, we are able to observe the adsorption of bovine serum proteins (BSA) in microfluidic channels in real time. Moreover, the concentration of BSA can be estimated by counting the number of bright sections of LC dots. This design offers a real-time sensing solution to monitor the proteins in microfluidic devices without labeling or the use of complex instrumentation. This microfluidic protein assay also requires less sample volume and the response time is fast.

CHAPTER 2

LITERATURE REVIEW

In this chapter, we review literatures related to kidney diseases and their biomarkers (i.e. urinary proteins). This chapter also discusses the conventional means of detecting these urinary proteins and the limitations of the methods. Moreover, this chapter tackles on the recent developments of liquid crystals (LCs) and their potential applications for the detection and quantification of protein mixtures. Lastly, we discuss the evolution of inkjet printing technology from their conventional usage to their exploitation for other diverging applications.

2.1 Overview of Kidney Diseases

2.1.1 Normal Kidneys and Their Function

Kidneys play a vital role in the body. Their main function is to remove waste products and excess water from the blood. The kidneys filter the blood through their tiny units called nephrons which are made up of a glomerulus and a tubule as shown in Figure 2.1. As the first step in filtration, blood is delivered to the glomeruli. Here, waste products and excess water are filtered from the blood while red blood cells, proteins, and large molecules are retained. The filtrate is collected in a sac called the Bowman's capsule and drains into the tubule. The tubules, lined with highly functional cells, further process the filtrate. They re-absorb useful substances escaped from the glomeruli and deliver them back to the bloodstream while discharging the rest into the bladder as urine.

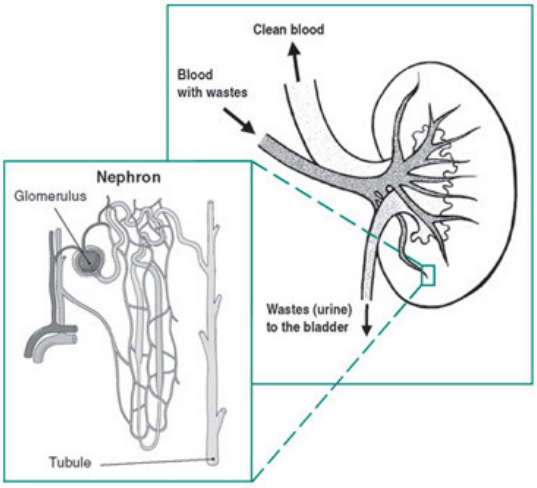

Figure 2.1 Nephron, a unit structure of kidney. A nephron consists of a glomerulus and a tubule where the sieving of wastes and re-absorption of useful substances take place, respectively.

2.1.2 Chronic Kidney Disease and Acute Kidney Failure

Kidney diseases can be classified as either chronic kidney disease (CKD) or acute kidney failure (AKF). CKD refers to the gradual and progressive loss of kidney function (Afzali et al. **2007**). Though it may be a result of primary autoimmune diseases of the kidneys themselves, CKD is mainly caused by other diseases such as diabetes (Gilbert et al. **1994;** Hillege et al. **2002;** Marks et al. **2003;** Sukhija et al. **2006**) or hypertension (Anavekar et al. **2004;** Cheng et al. **2007;** Contois et al. **2006;** Ellekide et al. **1997**). Among the 768 cases per million residents in 2009, diabetes and hypertension accounted for 61.7% and 10%, respectively, for kidney failure according to the Singapore Renal Registry (Choong **2009**). High levels of blood-sugar caused by diabetes can overload the kidney filters, whereas high blood pressure caused by hypertension can damage the kidney's capillaries. As a result, the kidney

loses its normal function, and waste products such as creatinine and residual proteins can leak into the urine (Cheng et al. **2007**). Depending upon the severity, CKD has 5 different stages of which stage 5 is the worst. At this stage, (the so-called end-stage kidney disease), all kidney functions are lost. Thus, in order to keep patients alive, either dialysis or kidney transplantation must be performed.

On the other hand, AKF is a sudden and dramatic loss of kidney function. It usually occurs as the result of sudden interruption in the blood supply to the kidney, damage to the kidney itself, or obstruction in the urinary tract. Some causes of AKF include accidents, injuries or complications from surgery where the kidneys are deprived of normal blood flow for an extended period of time. Unlike CKD, the kidneys can often recover from AKF, allowing the patient to resume a normal life. Nevertheless, due to the rapid deterioration of kidneys during a short period of time (over days or weeks), it is highly critical to distinguish AKF from CKD in order to properly manage the associated illness.

2.2 Biomarkers for Kidney Disease

2.2.1 Glomerular Filtration Rate (GFR) and Creatinine

Glomerular filtration rate (GFR) is often used to screen for early kidney damage or for signs of deteriorating kidney functions of those who have been diagnosed with kidney diseases (Jimbo **2007;** Stevens and Levey **2009**). GFR is

defined as the flow rate (mL/min) of the filtrate passing through the kidney per surface area of the body (1.73 m^2, the average surface area of the human body). As shown in Table 2.1, as CKD progresses, GFR becomes significantly lower.

Table 2.1 Stages of CKD and Corresponding GFR (Jimbo 2007)

CKD Stage	Description	GFR (mL/min/1.73m^2)
1	Slight kidney damage with normal or increased filtration	> 90
2	Mild decrease in kidney function	60-89
3	Moderate decrease in kidney function	30-59
4	Severe decrease in kidney function	15-29
5	Kidney failure requiring dialysis or transplantation	< 15

There are a number of filtered substances whose measurement may be used to estimate GFR including blood urea nitrogen (BUN), serum creatinine and creatinine from urine. The most widely used method is measuring the amount of serum creatinine. Creatinine is a waste product in the blood that comes from two sources: decomposition of meat products in the diet and secretion due to muscle use. Creatinine production changes due to several factors: age, gender, race or ethnicity, and muscle mass (Schrier **2007**). In addition, the production of creatinine in the blood can take longer than one or two days to reach a clinically significant level, and

irreversible damage might already have set in during the time between injury and diagnosis. Since the amount of creatinine excreted varies, the calculated GFR values can be inaccurate. Because of this limitation, using GFR alone for the diagnosis of kidney disease is inadequate. Thus, other biomarkers are needed to detect early deterioration of kidney functions. Among these biomarkers, the most reliable ones are the urinary proteins. These biomarkers also do not require any invasive methods, and thus are more feasible to use.

2.2.2 Urinary Proteins, Biomarkers for CKD

One of the symptoms for kidney dysfunction is proteinuria (Barratt and Topham **2007;** Gonzalez-Buitrago et al. **2007**). Proteinuria is characterized by the presence of proteins in urine. There are two types of proteinuria. Glomerular proteinuria occurs as a consequence of defects in the glomerular permselective properties, which leads to the leakage of plasma proteins into the urinary tract. On the other hand, tubular proteinuria results from the failure of the tubule to reabsorb relatively small amounts of protein back into the bloodstream. Studies have shown that some proteins can be used as biomarkers to predict the location of kidney damage (Barratt and Topham **2007;** Bazzi et al. **2001;** Woo and Lau **1998**). For example, human serum albumin (HSA), immunoglobulin G (IgG) and transferrin (Trf) are useful biomarkers for glomerular damages while other urinary proteins such as α_1-microglobulin, retinol-binding protein, β_2-microglobulin are useful biomarkers for tubular dysfunction. Table 2.2 lists some properties of these urinary proteins and their

reported abnormal values. Amongst these protein biomarkers, HSA is the most abundant protein because it comprises about 60% of human blood. Moreover, because the HSA molecule is relatively small, it is often among the first proteins to enter the urine after glomerular damage. Microalbuminuria, a type of proteinuria with HSA concentrations between 30-300 µg/mL from 24-h samples in the urine, is the first sign of kidney problems (Stevens et al. **2006;** Vallon et al. **2006**). Therefore, microalbuminuria should be detected early for proper treatment of the disease.

Table 2.2 Urinary Proteins as CKD Biomarkers

Kidney Damage	Urinary Proteins	Molecular Weight (kDa)	Abnormal Concentration (µg/mL)
Glomerular Damage	HSA	67	20
	Trf	80	2
	IgG	150	4
Tubular Dysfunction	α_1-microglobulin	26-33	4
	Retinol-binding protein	< 33	0.30
	β_2-microglobulin	12	0.10

2.3 Detection of Urinary Proteins

2.3.1 Urine dipstick test

Admitted patients with diabetes or high blood pressure are often mandated to receive a urine dipstick test to help doctors identify potential kidney problems. The detection principle of the urine dipstick is based on the colorimetric response of a chemical indicator, bromophenol blue, to HSA (Barratt and Topham **2007**). Nevertheless, it gives inaccurate readings with LOD ≥ 300 µg/mL (Barratt and Topham **2007;** Gonzalez-Buitrago et al. **2007**), thereby giving both false positive and false negative results (Constantiner **2005;** Grootendorst et al. **2009;** Jimbo **2007;** Mathiesen et al. **1984;** Mladenovic **2004;** Schrier **2007;** Viberti et al. **1982a**). False negative results for proteinuria occur when urine is extremely diluted or when other monoclonal globulin proteins such as Bence Jones proteins are present in large amounts. False positive results occur when urine is highly concentrated, when urine pH is > 8, and/or when the dipstick has been immersed for too long (> 30 s).

2.3.2 Conventional means for urinary protein detection

An immunoassay is a test that makes use of the formation of antibody-antigen complexes to detect either target antigens or antibodies in samples (Deshpande **1996;** Gizeli and Lowe **2002;** Rogers **1997**). Antibodies (also known as immunoglobulins) are gamma globulin proteins which are found in blood or other body fluids of vertebrates. They have two main regions: the carbohydrate region (F_c) and the

receptor site region (F_{ab}). There are only two specific receptor sites on the antibody; both of them are located in the F_{ab} region (Deshpande **1996**). The optimum situation for an antibody to be available for interaction with the antigen is for the F_c portions to be bound to a surface as shown in Figure 2.2.

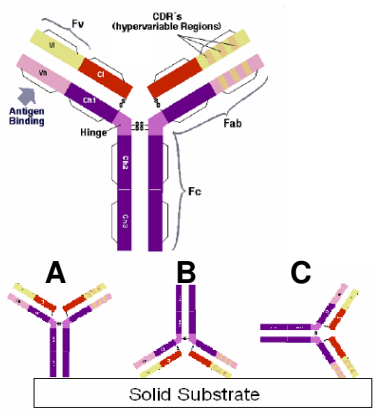

Figure 2.2 Basic Structure of Immunoglobulins. Random orientations of immunoglobulin are obtained during passive adsorption. (A) Optimal interaction with antigen; (B) Minimal interaction with antigen (both receptor sites are immobilized on the surface); and, (C) Partially active antibodies.

The most widely used conventional clinical diagnostic tests for detecting urinary proteins are radioimmunoassay (RIA), fluoroimmunoassay (FIA), enzyme-linked immunosorbent assay (ELISA), immunoturbidimetric assays (ITA), and nephelometry (Alexander **1980;** Bernard and Lauwerys **1983;** Carroll and Temte **2000;** Choi et al. **2004;** Comper et al. **2004a;** Lian et al. **2007;** Marre et al. **1987;** Thakkar et al. **1997;** Torffvit and Wieslander **1986;** Watts et al. **1986;** Woo and Lau **1998**). In general, these assays are all immunoassays. RIA has high sensitivity, low detection limits (16 ng/mL for HSA), and low operating costs. Nevertheless, due to the requirements for radioactive materials during the labelling processes, RIA requires

special containment and has stability problems (Bernard and Lauwerys **1983**). FIA (Choi et al. **2004**) can also detect HSA concentrations between 20-600 µg/mL with high sensitivity. However, this method requires the labelling of proteins with fluorescent dyes, which lead to the following limitations: (a) photobleaching or quenching effects may occur resulting in false results; (b) the number of binding sites of the proteins is reduced since some sites are tagged with fluorescent dyes; and, (c) broad emission spectra of fluorescent dyes lead to a higher LOD. Another method applied to detect HSA is ELISA (Bernard and Lauwerys **1983**) which can measure concentrations between 1-25 µg/mL. Although this method is routinely used in medical diagnosis, it is relatively time-consuming (~ 12 h), and it also requires labelling of proteins with enzymes (Bernard and Lauwerys **1983;** Torffvit and Wieslander **1986;** Watts et al. **1986**).

ITA involves the binding of antigen protein to the antibody that has been adsorbed to latex particles, resulting to agglutination. The agglutination is detected as a change in absorbance, which in turn determines the amount of the proteins found in the solution. ITA can be used to detect many different proteins. It gives a linear response for HSA between 5-400 µg/mL and 3-1000 µg/mL for IgG. ITA requires, however, large amounts of antibodies to detect these proteins (Thakkar et al. **1997**).

Nephelometry, a newer technique with full automation, has become a main method for quantifications of urinary protein. It offers great precision but requires the

use of sophisticated facilities and rigidly matched reagents, thus limiting its application for point-of-care applications (Carroll and Temte **2000;** Marre et al. **1987;** Thakkar et al. **1997;** Woo and Lau **1998**).

2.4 Advances in Protein Assays

2.4.1 Microfluidic Protein Assays

Conventional protein assays have long processing time, complex assaying procedures and require a large samples volume. These issues motivate researchers to replace these conventional assays with microfluidic technology. Microfluidic protein assays allow the integration of other several procedures (e.g. sample filtration, extraction, and protein separation) into a single miniaturized chip which makes the device more compact in size and minimizes the sample processing and handling (Burns **2002;** Meldrum and Holl **2002;** Sia and Whitesides **2003**). In addition, at small scales (microns to millimetres), the assay time and the sample volumes are reduced which can lower the procedural costs (Barry and Ivanov **2004**). However, the post column analysis of peptides and/or proteins in microfluidic devices still requires the bulky analytical instruments such as mass spectrophotometer (MS) (Chan et al. **1999;** Gao et al. **2001;** Jiang et al. **2001**), ultraviolet-visible (UV/Vis) spectrometer (Ou et al. **2009**) or ultraviolet laser induced fluorescence (UV-LIF) spectrometer (Hellmich et al. **2005**). For example, Hellmich et al. incorporated a clear window display on the channels in order to detect the 84 nM avidin protein using UV-LIF

spectrometer (Hellmich et al. **2005**). Chan et al. used a fused-silica capillary to connect the outlet of the PDMS channel to the electrospray ionization-mass spectrometer (ESI-MS) in order to detect rat serum albumin (Chan et al. **1999**). Meanwhile, Ziegler and co-workers detect fluorescently labeled C-reactive protein (CRP) with a sensitivity of 0.9 ng/mL on immobilized antibodies patterned on the surface using fluorescence spectroscopy (Ziegler et al. **2008**). These analytical instruments cause a constraint should these microfluidic protein assays be used for POC applications.

2.4.2 Label-free Techologies for Protein Detection

Although the conventional immunoassays have high sensitivity, they usually require labeling such as enzyme, fluorescence or radioactive isotopes. Thus, there is a need for other techniques which do not require labeling. For example, quartz crystal microbalance (QCM) is a popular label-free method for protein detection (Futami et al. **2005;** Keuren et al. **2003;** Luo et al. **2006;** Malmsten et al. **1996;** Metzger et al. **1999;** Sakai et al. **1995;** Sakai et al. **1997;** Sakti et al. **2001;** Vashist et al. **2006**), QCM consists of a quartz crystal attached to two electrodes. When a voltage is applied to the electrodes, the crystal oscillates at its resonant frequency. When solution containing protein HSA is flowed on the quartz crystal, the HSA binds to the surface and a change in the mass of the crystal changes the resonant frequency of the QCM device. QCM, however, may give false readings due to nonspecific adsorption of other proteins onto the surface of the crystal (Keuren et al. **2003**). In addition, this

equipment is sensitive to environmental conditions and cannot be used for POC applications. High performance liquid chromatography (HPLC) (Comper et al. **2004b;** Iwata **2001;** Konta et al. **2007;** Liu et al. **2009**), and chip electrophoresis (Chan and Herold **2006**) can also be used to detect urinary HSA in a label-free manner. HPLC has recently been used to identify urinary HSA because it can detect both reactive and nonimmunoreactive albumins. Questions regarding the results of the HPLC method, however, were raised because several other urinary globulins (i.e. α_1-acid glycoprotein, α_1-antitrypsin, transferrin) coeluted with HSA during the process (Sviridov et al. **2006**). Furthermore, Chan and Herold developed an assay that uses chip electrophoresis for the diagnosis of microalbuminuria (Chan and Herold **2006**). They showed that this assay also measures total microalbuminuria without any discernable interference from other common urine proteins.

2.5 Liquid Crystals (LCs)

Recently, the use of LCs in protein assays has attracted the attention of many researchers mainly due to its label-free detection capability. In this section, we discuss the properties of LCs, their detection principle and their current applications in biomolecules and protein detection.

LCs are materials possess physical properties that are intermediate between conventional liquids and solids (Collings and Hird **1997**). They can flow like liquids,

yet the arrangement of molecules within them can exhibit structural orders like solids. There are three types of LCs that have been discovered so far: thermotropic, lyotropic and polymeric. Among these three, thermotropic LCs have been studied extensively and have many applications in display technologies.

2.5.1 Thermotropic LCs

Thermotropic LCs, as the name implies, are LCs that highly depend on temperature. These molecules only exhibit LC properties within a certain temperature range. When the temperature is below a nematic transition temperature, the molecules are in a crystalline state, and when the temperature exceeds the isotropic transition temperature, the molecules are in an isotropic (liquid) state and lose their ordered structure. Thermotropic LCs can exist in three phases: nematic, cholesteric, and smectic. The difference of these phases is their preferred molecular orientations as depicted in Figure 2.3. Nematic LC exhibits long-range molecular orientational ordering but shows no positional ordering. The average orientation of the nematic LC molecules is characterized by one axis of symmetry called the director.

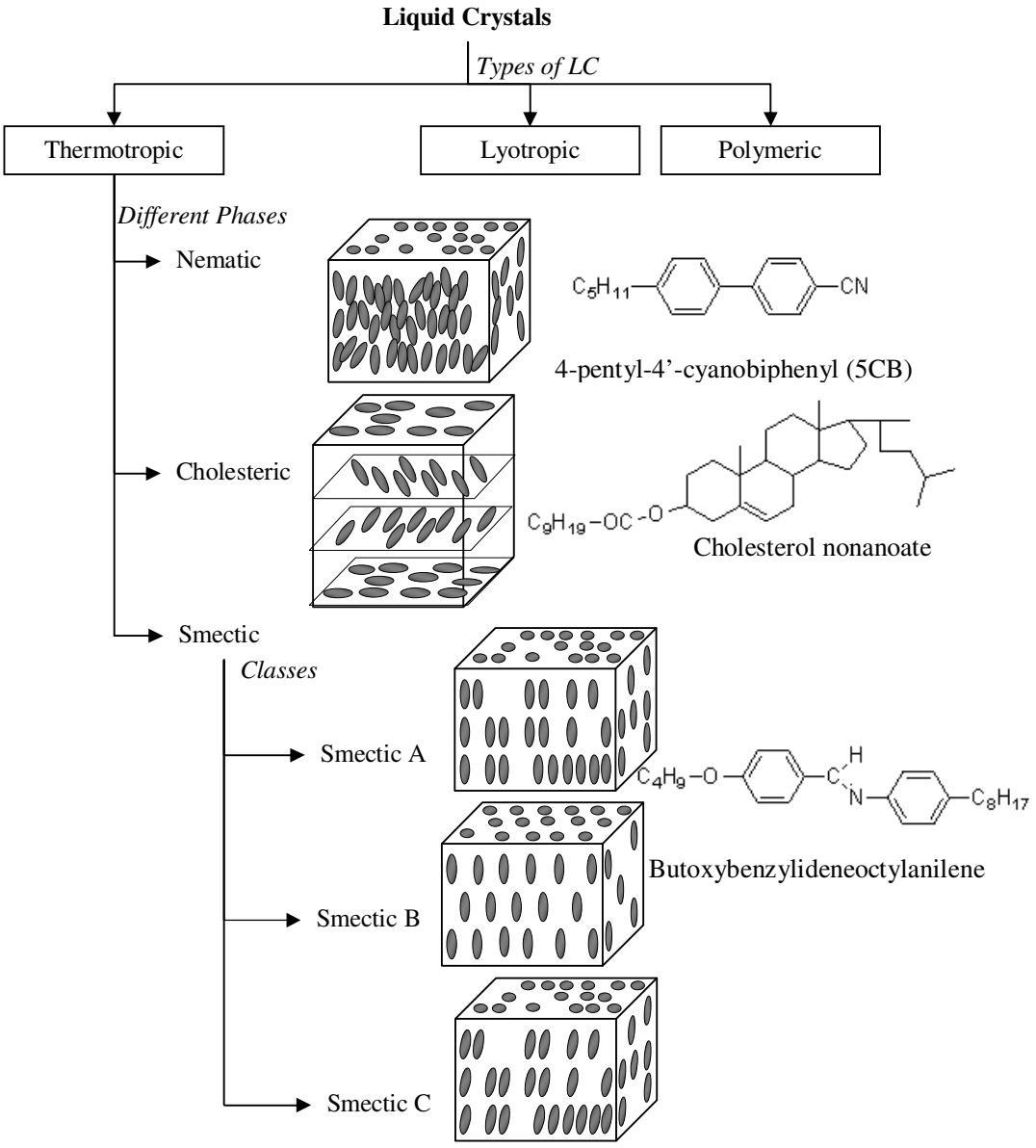

Figure 2.3 Orientations of molecules in different LC phases (Khoo and Wu 1993).

The director can be reoriented by presence of analytes or by an external field such as an electric or magnetic field. Smectic phase is more ordered than nematic in a way that the molecules tend to align themselves in layers or planes. The type of smectic phase is mostly identifiable by the tilt angle with respect to the planes (smectic A or C) or by its particular positional ordering (smectic B arranged in hexagonal networks). The last thermotropic LC phase is the cholesteric phase. These are nematic mesogenic molecules that favor an orientation between molecules at a slight angle to one another creating a layered structure with the director in each layer twisted with respect to those above and below it.

The significance of the LC molecular structures and orientations to its optical properties is made clear when viewed using polarizers. Normally, a linearly polarized light is produced when an unpolarized light is passed through a polarizer whose axis is in line with the desired linear polarization as shown in Figure 2.4A. This means that only the component which is parallel to the polarizer's axis will emerge while the perpendicular component is absorbed. Therefore, if the polarized light is sent through another polarizer (analyzer) that is oriented at 0º of the light's axis, the emerging light is the same. For crossed polarizers, the analyzer is oriented at 90º to the first polarizer. This means that no component of the original light is parallel to the direction of the analyzer, and no light emerges (Figure 2.4B).

The presence of LC between the crossed polarizers, however, allows light to pass through as shown in Figure 2.4C. When a beam of light enters the LC, the light can be considered as a combination of an ordinary ray and an extraordinary ray travelling at different velocities. As the beam of light exits from the LC, the two rays recombine and create a phase difference that causes the polarization state to be changed. This intrinsic property is known as **birefringence or double refraction**. The intensity of the transmitted light is determined by the angle between the director of the LC and the optical axis of one of the polarizers. When the orientation of the director of the LC is at 45º to one of the polarizers leads to a maximum transmission; aligning the optical axis of the LC with either of the input or output polarizers' optical axes gives the minimum transmission. Therefore, when the directors are parallel to the first polarizer (director is pointing perpendicular to the surface), the LC is in a **homeotropic orientation** (Kocevar and Musevic **2003**). If, however, the director is perpendicular to the first polarizer (director lies parallel in the plane of the surface) then the LC is in a **planar orientation** (Price and Schwartz **2006**).

Because of their innate structures, LCs display characteristic optical and electronic properties such as birefringence, dielectric and diamagnetic. LC molecules have long range molecular interactions which mean they can communicate their orientation to one another. Change in the orientational behaviour of LCs due to

surface properties provides a promising label-free detection mechanism to report biomolecules that adsorb on the surface.

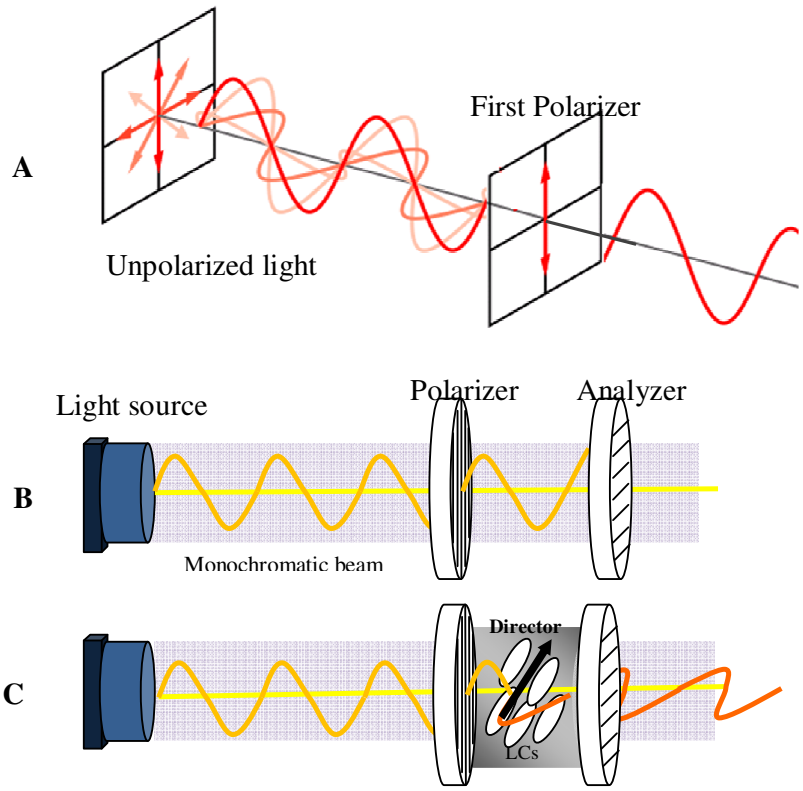

Figure 2.4 Polarization state of light. (A) Light passing through a single polarizer. Light passing through crossed polarizers (B) without LCs; (B) with LCs orienting along the director. Light's polarization state changes due to the birefringence property of LCs causing some light to pass through the analyzer (Wilson and Hawkes **1998**).

2.5.2 Orientations of LCs on Solid Surfaces

When a film of LC is supported on a solid surface, the orientational profile of LC within the film is determined by the surface properties of the solid surface. For example, when proteins adsorb on the surface, the surface properties change and trigger an orientational transition of the LC near the interface. This orientational change is then communicated through long-range electrostatic interactions up to 100 μm away (Kim and Abbott **2001**), resulting in an amplification of the minute change into an orientational transition of the bulk LC. Because of the birefringent property of LCs, the global orientational transition is accompanied by a measurable optical signal. Thus, in order for minute changes to be monitored, the LC should be oriented in a more uniform manner on the surface. This can be realized by surface modifications prior to the adsorption of proteins.

Several strategies of surface modifications have been proposed in the past to make LCs adopt a planar orientation. These strategies include, but not limited to, oblique deposition of films (Jang et al. **2005;** Shah and Abbott **2001;** Skaife et al. **2001**), manual rubbing, and periodic grating structures (Bi et al. **2007;** Kim and Abbott **2001;** Kim et al. **2000**). Kim et al., for example, detected anti-BSA using manually rubbed films of bovine serum albumin (BSA) (Kim and Abbott **2001;** Kim and Abbott **2002;** Kim et al. **2000;** Nelson et al. **2002**). This rubbing process led to an anisotropic structure on the surface which oriented LCs uniformly. When the slide

was exposed to non-specific proteins, these proteins did not bind to the surface even at 100 nM. Thus, the planar orientation of LC was not perturbed (Kim et al. **2000**). Nevertheless, when anti-BSA bound to the surface-immobilized BSA, the anisotropic structure of the surface was erased and the planar orientation of the LC was disrupted. However, one challenge in this approach is the difficulty to control the rubbing force. In order to improve the LC-based protein detection system, Luk et al. used SAMs (mixed monolayers presenting nitrilotriacetic acid and tri(ethylene glycol) to functionalize surfaces of gold films which were deposited in an oblique angle of incidence (Luk et al. **2003**). Still, minute deviations in the orientation of LCs relative to the amount of proteins adsorbed are extremely difficult to measure. Also, the system is highly dependent on how the gold is deposited, and is limited by the availability of the gold evaporator.

Recently, Xue and Yang developed a LC-based protein assay that does not require rubbing techniques or oblique deposition of gold films (Xue and Yang **2008**). They demonstrated that through the chemical functionalization of the slides with hydrocarbon-terminated silanes such as N,N-dimethyl-N-octadecyl-3-aminopropyltrimethoxysilyl chloride (DMOAP) they can modify the surface property and align LC supported on the surface in a perpendicular (homeotropic) orientation. Using this LC-based protein assay, they were able to detect AIgG proteins as low as 0.31 μg/mL. However, this type of system requires several steps before final results

can be obtained. Hence, real-time detection of proteins are still very difficult at this stage.

2.5.3 Orientations of LCs in Emulsions

An emulsion is a mixture of two immiscible liquids, one of which is dispersed (from a hundreds of nanometers to a micrometer in size) in a continuous phase of the other (Bibette **1991;** Mason et al. **2006;** McClements and Weiss **2005**). In general, emulsions are only metastable, and the droplets tend to coalesce over time. A large part of the research on emulsions is thus devoted to maintain stability of the dispersion, to monitor interactions between droplets, and tailor surface properties of droplets to prevent coalescence. There are many studies dealing with emulsions of LCs. For instance, Poulin and co-workers reported an inverted LC emulsion system in which LC forms a continuous phase with water dispersed as droplets (Poulin et al. **1997**). Most studies, however, are focused on direct LC emulsion system where LCs are dispersed in a continuous phase (normally water).

When the LCs are in droplets form (dispersed phase), they mainly assume three orientational ordering: bipolar, preradial and radial configuration (Lavrentovich **1998**). Bipolar ordering is characterized by a parallel orientation of the LC molecules at the interface. Such configuration can be seen with two points of defects at opposite edge of the droplets under crossed polarizers. Preradial and radial droplets, on the other hand, are characterized by a perpendicular orientation of the LC molecules at

the interface and the configuration can be seen by a single point of defect either at the edge (preradial) or the center (radial/hedgehog) of the droplets under crossed polarizers. The orientation of the LCs is determined by the free energy of each droplet, *F*, which is influenced by the balance between the orientation-dependent surface free energy and the elastic strain free energy within the droplets (Lavrentovich **1998;** Lin et al. **2011**):

$$F = \int W dA + \frac{K}{2} \int (\nabla n)^2 dV \qquad [2.1]$$

where W is the surface anchoring energy per unit area (A), K is the elastic modulus strain of the LC, n is the director of the LC, and V is the volume of the droplet.

Emulsions of LCs can be easily made by using vortex or sonication of LCs. These procedures often result in LC droplets having a wide size distribution as shown in Table 2.3. Although the size can be narrowed by crystallization fractionation techniques (Bibette **1991**), this method requires most of the unwanted LC droplets to be discarded, and that is costly and time-consuming. On the other hand, some studies have shown the preparation of monodispersed LC droplets by using silica templating or microfluidics (see Table 2.4). Silica templating involves a layer-by-layer deposition of polyelectrolytes on the surfaces of the silica templates. Silica cores were removed by immersing in hydrofluoric acid (HF), and then filled with LC. Creating monodispersed LC droplets via silica templating has the advantage of

producing small-size LC droplets up to 0.7 μm. However, safety issues associated with HF hampers the application of this method (Sullivan and Krieger 2001). In addition, it is often difficult to completely remove the cores (Donath et al. **1998**). Meanwhile, Hamlington and co-workers, reported the use of microfluidic channels having a flow-focusing structure to create spherical LC droplets (Hamlington et al. **2007**). Microfluidic technology can produce LC droplets in large quantity, but it is difficult to prepare LC droplets of different sizes which are dependent of the dimensions of the microfluidic channel.

Table 2.3 Production of LC droplets (Polydisperse)

	Method	LC	Continuous Phase	LC configuration (droplet size, μm)	Reference	Journal
Polydisperse LC droplets	Vortex	E7	Polyurethane (TU50A)	Radial (3 – 6 μm)	(Erdmann et al. 1990)	Phys. Rev. Lett.
	Vortex	E7	Epoxy (E-51)	Bipolar (2 – 20 μm)	(Ding and Yang 1992)	Jpn. J. Appl. Phys
	Vortex	5CB	H_2O with SDS	Radial (23 – 50 μm)	(Poulin et al. 1997)	Science
	Vortex	5CB	H_2O	Radial (20 μm)	(Lavrentovich 1998)	Liq. Cryst.
	Vortex	5CB	LPEI	Radial (1 – 8 μm)	(Kinsinger et al. 2010)	Langmuir
	Sonication	E7	PDMS based	Radial (~10 μm)	(Loudet et al. 2000)	Langmuir
	Sonication	5CB	H2O w/ surfactants (SDS, T20, T40)	Radial (4 – 55 um)	(Heppenstall-Butler et al. 2005)	Liq. Cryst.
	Sonication	5CB	DLEPC	Radial (1 – 10 μm)	(Tjipto et al. 2006)	Nano Lett.
	Sonication	E7	H_2O with SDS	Radial (1 – 5 μm)	(Tixier et al. 2006)	Langmuir
	Sonication	E7	SDS/SE3030	Bipolar (0.2 – 0.5μm)	(Tongcher et al. 2006)	Langmuir
	Sonication	DSCG	PVA	Radial (4 – 10 μm)	(Simon et al. 2007)	Langmuir
	Sonication	DSCG	PAAm	Bipolar (15 – 25 μm)	(Simon et al. 2007)	Langmuir
	Sonication	5CB	PSSH-terminating	Radial (< 0.6 μm) Bipolar (>1.2 μm)	(Zou and Fang 2010)	Langmuir
	Sonication	5CB	PSSNa-terminating	Bipolar (0.5 – 2 μm)	(Zou and Fang 2010)	Langmuir
	Sonication	5CB	PDADMAC-terminating	Radial (0.3 – 2 μm)	(Zou et al. 2011)	J. Phys. Chem. B
	Sonication	5CB	PSS-terminating	Bipolar (0.3 – 2 μm)	(Zou et al. 2011)	J. Phys. Chem. B

Table 2.4 Production of LC droplets (Monodisperse)

	Method	LC	Continuous Phase	LC configuration (droplet size, µm)	Reference	Journal
Monodsiperse LC droplets	Silica Template	5CB	PSS – PAH	Bipolar (5 µm)	(Sivakumar et al. 2008)	Chem. Mater.
	Silica Template	5CB	PSS – PAH w/ SDS	Radial (8 µm)	(Gupta et al. 2009a)	Langmuir
	Silica Template	5CB	PSS – PAH w/o SDS	Bipolar (8 µm)	(Gupta et al. 2009a)	Langmuir
	Silica Template	5CB	PSS– PAH	Radial (0.7 – 1 µm) Bipolar (3 – 10 µm)	(Gupta et al. 2009b)	Angew. Chem. Int. Ed.
	Microfluidic	5CB	Ether	Radial (5 µm)	(Umbanhowar et al. 2000)	Langmuir
	Microfluidic	5CB	Silicone oil, 20 cSt	Radial (54 µm)	(Hamlington et al. 2007)	Liq. Cryst.

* lyotropic liquid crystal

Over the past decade, interest in using emulsified LC droplets as sensing platforms gradually gains momentum. LC droplets are better than LC films due to their higher surface areas and uniform distribution in aqueous solutions (Lockwood et al. **2006**). Initial studies were done on the effects of lipids and surfactants, such as sodium dodecylsulfate (SDS), on the orientations and optical textures of LC droplets (Lin et al. **2011**). Based on this result, Sivakumar *et al*. demonstrated the ability of LC droplets in aqueous solution to differentiate positive (+) and negative (–) gram bacteria based on the presence of lipids on the former (Sivakumar et al. **2009**).

2.6 Inkjet Technology

Inkjet printing technology has been used for printing paper documents, reproducing digital images or characters in modern society (Mohebi and Evans **2002**). The main feature of inkjet printing technology is that it can dispense microliter- to picoliter-sized ink droplets at a specific location with high precision (Delaney et al. **2009**). In addition, automatically controlled printing procedures reduce the experimental variations to a great extent. Piezoelectric and thermal inkjet printing are by far the most commonly used systems. In thermal inkjet printing, liquid is heated locally to form vapor that expands and ejects the liquid near the nozzle as a droplet. In contrast, piezoelectric printing uses a piezoelectric material which deforms under an applied voltage, causing liquid to be ejected from the nozzle as a droplet as shown in

Figure 2.5. Such mechanism gives piezoelectric inkjet printing an advantage over thermal inkjet printing, because the former prevents ink from degradation (Allain et al. **2004;** Scoutaris et al. **2011**).

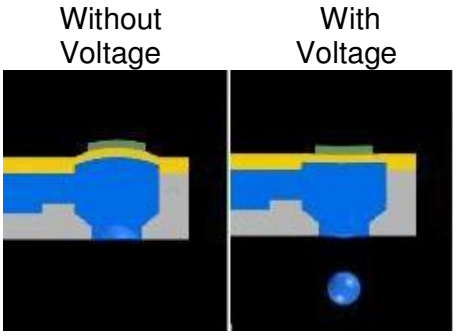

Figure 2.5 Schematic diagram of piezoelectric inkjet printer.

Recently, interest in using inkjet printing technology to print different materials emerges, thanks to the recent development in electronic printers. For example, Volkman and co-workers used inkjet printing to create conductive thin films by depositing silver and copper nanoparticles on surfaces (Volkman et al. **2004**). Other unconventional ink such as alkanethiolate (Bietsch et al. **2004**), pre-hydrolized silane (Danzebrink et al. **2002**), fine zirconia (Zhao et al. **2002**), and organic polymers (Stutzmann et al. **2003**) were also reported to be compatible with inkjet printing. Furthermore, some research groups use inkjet printing to deliver biological molecules including oligopeptides, proteins, and antibodies, etc (Allain et al. **2004;** Kim et al. **2010;** Scoutaris et al. **2011;** Sumerel et al. **2006;** Zheng et al. **2011**). Allain *et al.* ,for

example, created an assay for *Bacillus anthracis*, by printing *B. anthracis* target DNA on a membrane followed by DNA hybridization with complementary probes (Allain et al. **2004**). Unlike other approaches for microarray fabrication (e.g. contact printing), inkjet printing does not require the contact of the printing head with the surface. Hence, it reduces contamination and damage to the surface, making inkjet printing more attractive (Harris et al. **2000**). Despite the successful applications of inkjet printing for printing different materials in the past, the use of LCs as "ink" in inkjet printers has not been reported before. It is possible that LCs have high viscosity, make them difficult to be dispensed smoothly.

CHAPTER 3

USING LIQUID CRYSTAL AS A READOUT SYSTEM

IN URINARY ALBUMIN ASSAYS

3.1 Introduction

As mentioned in Chapter 2.2.2, human serum albumin (HSA) is commonly used as a biomarker in urine samples for detecting CKD. Nevertheless, current point-of-care diagnosis of CKD relies on urine dipstick test which has some notable disadvantages. For example, it lacks high sensitivity and often gives false positive or negative results (Mladenovic 2004). Although there are other analytical methods better than the urine dipstick test, there are still some disadvantages associated with these tests. FIA, for instance, requires labelling proteins with fluorescent molecules, and that may lead to changes in binding abilities of proteins if fluorescent labels occupy binding sites. ELISA methods involve complex procedures that require longer processing times (~5 h) (Baker et al. 2002). RIA has a detection limit of 16 ng/mL, but it requires labelling proteins with radioactive isotopes (Moore **2002**). ITA is simple and rapid, but it requires large amounts of antisera (Rifai et al. **2000**). IN and chip electrophoresis have higher precision and sensitivity but require bulky and expensive machines (Baker et al. 2002). Because of these limitations, there is a need to develop an HSA assay that is more sensitive, label-free and easier to operate.

In this study, we investigate the feasibility of using a bioassay, which features a thin layer of liquid crystals (LCs) as a readout system, to detect the presence of HSA in urine samples. When LCs are supported on a solid surface, they are known to change their orientation rapidly in response to small perturbations on the surface

(Clare and Abbott **2005;** Dickert et al. **1993;** Gupta and Abbott **1997;** Gupta et al. **1998;** Luk et al. **2003;** Shah and Abbott **2001;** Skaife et al. **2001**). This phenomenon has been exploited in the past to develop LC-based assays by Abbott's group (Gupta and Abbott **1997;** Gupta et al. **1998;** Luk et al. **2003**). However, such assays often require the immobilization of antigens on obliquely deposited gold films to obtain uniform orientation of the LCs. When the slide is incubated in sample solutions containing antibodies, antibodies can bind to the surface antigens and erase the surface topography. This subtle change in the surface properties disrupts the orientation of the LCs, and that leads to changes in the optical appearance of the LCs. Recently, to eliminate the need of gold films, we used glass slides coated with *N*,*N*-dimethyl-*N*-octadecyl- 3-aminopropyltrimethoxysilyl chloride (DMOAP) to align the LCs perpendicularly to the surface (Lai et al. **2009;** Xue et al. **2009;** Xue and Yang **2008**). In this assay, the optical appearance of the LCs depends on the total surface protein density. When the surface density exceeds a critical value, the orientations of the LCs are disrupted. As a results, appearance of LCs in that region turns from dark to bright. However, because of its "all-or-nothing" characteristics, this type of assay is only qualitative and cannot be used to quantify the concentration of real samples like urine which has a wide concentration range.

To address this issue, we aim to develop an LC-based assay that can detect and quantify HSA in the solution. We also aim to distinguish CKD patients by using this assay with urine samples collected from two groups of diabetic patients: those

diagnosed with CKD and those without (control group), and compare the test results with urine dipsticks and chip electrophoresis.

3.2 Experimental Section

3.2.1 Materials

Glass slides were purchased from Marienfield (Germany). *N*,*N*-dimethyl-*N*-octadecyl-3-aminopropyltrimethoxysilylchloride (DMOAP), dithiothreitol (DTT), human serum albumin (HSA), fluorescein isothiocyanate-labelled human serum albumin (FITC–HSA), human transferrin (HTrf), fluorescein isothiocyanate-labelled human transferrin (FITC–HTrf), anti-HSA (AHSA) and fluorescein isothiocyanate-labelled anti-HSA (FITC–AHSA) were purchased from Sigma-Aldrich (Singapore). Liquid crystal, 4-pentyl-4'-cyano-biphenyl (5CB) was purchased from Merck (Japan). Phosphate-buffered saline (PBS) 10× and polyethylene glycol sorbitan monolaurate (Tween 20, biotechnology grade) were both obtained from first BASE (Singapore). All aqueous solutions were prepared using deionized water with a resistance of 18.2MΩ cm^{-1} (Millipore).

3.2.2 Collection and Storage of Urine Samples

Urine samples from diabetic patients diagnosed negative of CKD (control group) and diabetic patients with CKD (CKD patients) were collected by the National

University Hospital, Singapore. Several aliquots (10μL each) were then prepared from these urine samples and stored at -70 °C upon collection. Prior to use, the aliquots were thawed at room temperature and diluted with PBS buffer (0.1 M, pH 7.4). All samples were used within two weeks from collection (Klasen et al. **1999**).

3.2.3 Preparation of Protein Solutions

AHSA (FITC–AHSA) stock solution with a concentration of 1000 μg/mL was prepared by dissolving 1000 μg of AHSA (FITC–AHSA) in 1mL of PBS buffer (0.1 M, pH 7.4). The stock solution was stored at 4 ºC. Prior to use, the stock solution was diluted with PBS buffer to obtain the final concentration. Stock solutions for HSA, HTrf, FITC–HSA, and FITC–HTrf were also prepared in a similar way except that surfactant Tween 20 (0.001%) was added to PBS buffer to prevent nonspecific adsorption of proteins on surfaces (Batteiger et al. **1982;** Dong et al. **2008**).

3.2.4 Surface Modification and Characterization

Procedures for surface modification of glass slides can be found in our past publications (Xue et al. **2009;** Xue and Yang **2008**). Briefly, glass slides were first soaked in a 5% (v/w) Decon-90 (a commercially available detergent) for 2 h, and then sonicated for 15 min. The glass slides were then rinsed thoroughly with DI water, blow-dried with N_2 gas and stored at room temperature. Clean glass slides were immersed in 0.1% (v/v) of DMOAP solution for 5 min. After rinsing and blow drying, the slides were heated at 100 ºC in vacuum for 15 min. To immobilize AHSA

on a DMOAP-coated slide, a clean Lifter slip was placed on top of the slide and 40 μL of AHSA solution was dispensed on the surface. After 2 h, the slide was rinsed with PBS buffer for 3 min, DI water and then blow dried with nitrogen gas.

Static water contact angles of AHSA-decorated slides were measured by using a water contact angle goniometer (AST, U.S.A.). In a typical run, a drop of water (1 μL) was automatically dispensed on the sample surface, and the image of the droplet on the surface was captured by using the software provided by the manufacturer.

Ellipsometric thicknesses were measured by using a Stokes ellipsometer equipped with a 6328 Å HeNe laser (Gaertner, U.S.A). The sample wafer was cut into pieces (~2cm × 2cm) and placed at the sample holder. The incident light was kept fixed at 70º, and a wavelength of 632 nm was used to determine the film thickness. For each sample, 3 different locations were measured. The thickness was obtained by using the software provided by the manufacturer.

To estimate the actual AHSA surface density after rinsing, we spotted FITC–AHSA solutions on a DMOAP-coated slide. After 2 h of incubation in a humidified chamber, the slide was rinsed with PBS buffer for 3 min, DI water and then blow dried with nitrogen gas. Finally, fluorescence intensity of each spot was measured and the corresponding AHSA surface density was estimated by using the calibration curve (see the Appendix A). The fluorescence intensity was measured by using a

microarray scanner (GenePix 4100A, Molecular Devices, U.S.A.) under an excitation wavelength of 532 nm (gain = 600, pixel size = 10μm).

3.2.5 HSA Immobilization and Detection

To prepare a sample slide, droplets (~0.1 μL) of HSA solutions were spotted onto the AHSA-decorated slide in an array format using an automated dispenser (Biodot AD1500, U.S.A.). After 30 min of incubation in a humidified chamber, the slide was rinsed with PBS buffer for 3 min. Finally, the sample slide was rinsed with deionized water and blow dried with nitrogen gas. Protein selectivity of the assay was also done by using solutions containing 25 μg/mL HTrf. Fabrication of an LC optical cell can be found elsewhere (Lai et al. **2009;** Xue et al. **2009;** Xue and Yang **2008**). Briefly, an LC cell (10 mm × 26 mm) was constructed by pairing the sample glass slide with a DMOAP-coated glass slide face-to-face with two spacers (~6 μm) secured tightly with binder clips at both ends of the cell. The LC cell was then filled with 5CB, and the optical appearances were observed under crossed polarizers in the transmission mode.

3.2.6 Dilution Protocols

Two dilution protocols were developed to reduce the HSA concentration before analysis. Firstly, we prepared one set of standard HSA solutions to cater for HSA concentrations in the proteinuria range (3000, 1000, 300, 150 and 100 μg/mL). Subsequently, each HSA solution was sequentially diluted 200, 60, 20, 10 and 5x

(dilution protocol I) and each diluent was dispensed to the AHSA-decorated slide, forming a 5 × 5 microarray. This array was incubated for 30 min, allowing the binding of HSA to AHSA. After being rinsed and blow dried, the surface was used to prepare an LC cell. Secondly, another set of standard HSA solutions was also prepared to cater for lower HSA concentrations in the microalbuminuria range (200, 150, 100, 50 and 20 μg/mL). Each solution from the second set was sequentially diluted 12, 9, 6, 3, and 1× (dilution protocol II). Similarly, each diluent was dispensed to the AHSA-decorated slide and the microarray was then made into an LC cell which is later analyzed under crossed-polarizers.

3.2.7 Chip Eletrophoresis and Urine Dipstick

Chip electrophoresis was performed by using a bioanalyzer (Agilent, U.S.A.) together with Protein 230 LabChip kit. Sample preparation was done following the manufacturer's protocols.(AgilentTechnologies **2006**) About 4 μL of the urine sample was placed in a 100μL centrifuge tube with 2 μL of the denaturing solution containing 1M DTT as the reducing agent. The mixture was heated, diluted with deionized water and then loaded onto the sample wells in the chip along with the protein ladder. Data analysis was done using the Agilent 2100 Expert software. The urine samples were also analyzed using Albustix Reagent Strips (Bayer, U.S.A.). The urine dipstick was dipped directly into the urine sample and the excess urine was removed by running the edge of the strip against the rim of the urine container. The

sample was then analyzed after 60 s by comparing the reagent side of test area with the corresponding color chart provided by the manufacturer.

3.3 Results and Discussion

3.3.1 Immobilization of AHSA on Solid Surfaces and Surface Characterization

In order to capture HSA, we deposit a layer of AHSA, which binds specifically to HSA, on the DMOAP-coated slide. To monitor the amount of AHSA deposited, we compared the water contact angles and ellipsometric thicknesses before and after the immobilization of AHSA on the surface. Figure 3.1 shows that when 10 μg/mL AHSA is used, the water contact angle decreases from 86 ± 0.5° to 85.6 ± 0.4°. This slight decrease in water contact angle implies that some of the DMOAP-coated surface is occupied by the AHSA molecules, thus rendering the surface more hydrophilic. The presence of AHSA is also evident by the increase of the ellipsometric thickness from 0 ± 0.40 nm to 0.71 ± 0.41 nm. This value, however, is lower than the typical value for a monolayer of AHSA adsorbed on the surface (5.0 ± 1.0 nm) (Heideman et al. **1993;** Lechuga et al. **1995;** Schipper et al. **1995**), suggesting that the surface coverage is around 14%. The amount of the AHSA in the solution also affects the amount of AHSA adsorbed on the surface. This is shown by the progressive decline of water contact angle (from 85.6 º ± 0.4º to 80.7 º ± 0.8º) and the increase in the ellipsometric thickness (from 0.71 ± 0.41 nm to 4.14 ± 0.09 nm) when the AHSA is increased from 10 μg/mL to 100 μg/mL.

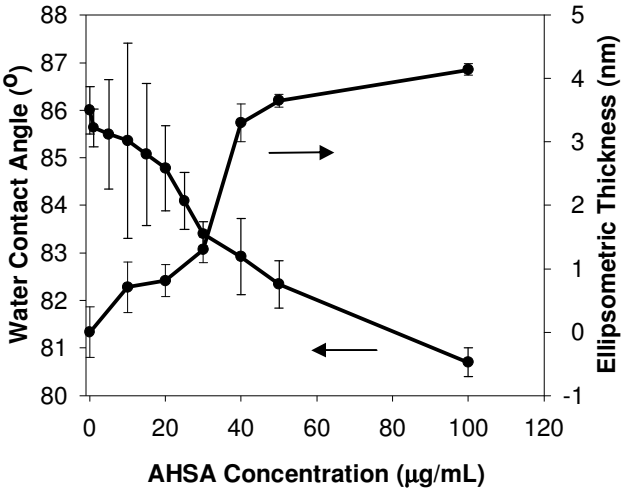

Figure 3.1 Effect of surface-immobilized AHSA on (A) surface water contact angle (B) and ellipsometric thickness on DMOAP-coated glass slides. Increasing the AHSA concentration lowers the water contact angle but increases the ellipsometric thickness.

To investigate the orientational behaviour of 5CB supported on various AHSA-decorated slides, we used these slides to fabricate LC cells. Figure 3.2 shows the optical appearance of these LC cells under crossed polarizers. We note that when 10 µg/mL to 30 µg/mL AHSA are used, the LC cells appear dark. These solutions give equivalent AHSA surface densities in the range of 0.5 ± 0.1 pmol/cm^2 to 1.6 ± 0.1 pmol/cm^2 (see Appendix A.1). In these cases, although AHSA molecules adsorb on the surfaces, these densities are not able to disrupt the homeotropic orientation of the LCs supported on the surface. On the other hand, when 40 µg/mL AHSA is used, the AHSA surface density reaches 2.1 ± 0.2 pmol/cm^2 and the surface-immobilized AHSA molecules disrupt the LCs supported on the surface resulting in a bright image. Further increase in the AHSA surface density causes the surface to completely light up. Although higher AHSA surface density is preferred in order to capture more

HSA, if the density of the AHSA is too high, then its presence will disrupt the uniform orientation of the LCs and render the assay ineffective for HSA detection. Therefore, the optimum AHSA surface density for the LC-based HSA assay of 2.1 ± 0.2 pmol/cm^2 which has an equivalent surface coverage of 70%.

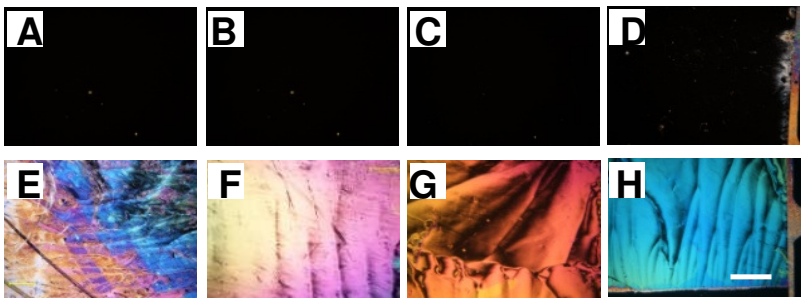

Figure 3.2 Optical appearance of the LC cells (under crossed polarizers) made from DMOAP-coated slides immobilized with different concentrations of AHSA. (A-H) AHSA concentrations used are 10, 20, 30, 40, 50, 100, 250 and 500μg/mL, respectively. Scale bar is 3mm.

3.3.2 LC-Based HSA Assays

To build HSA assays, we spotted solutions containing different HSA concentrations (5–50 μg/mL) on AHSA-decorated slides. These slides were rinsed, blow dried and analyzed by using the LC method. Figure 3.3A shows the optical appearance of the LC cell viewed under crossed polarizers. We note that the optical appearance of the LCs shows bright colors in regions where the HSA concentrations are greater than or equal to 15 μg/mL, however, the optical appearance of the LCs remains dark when the HSA concentrations are lower than 15 μg/mL. This result suggests that when the

HSA concentration is above 15 μg/mL, the surface density of HSA is high enough to disrupt the orientation of the LCs supported on the surface (Figure 3.3C).

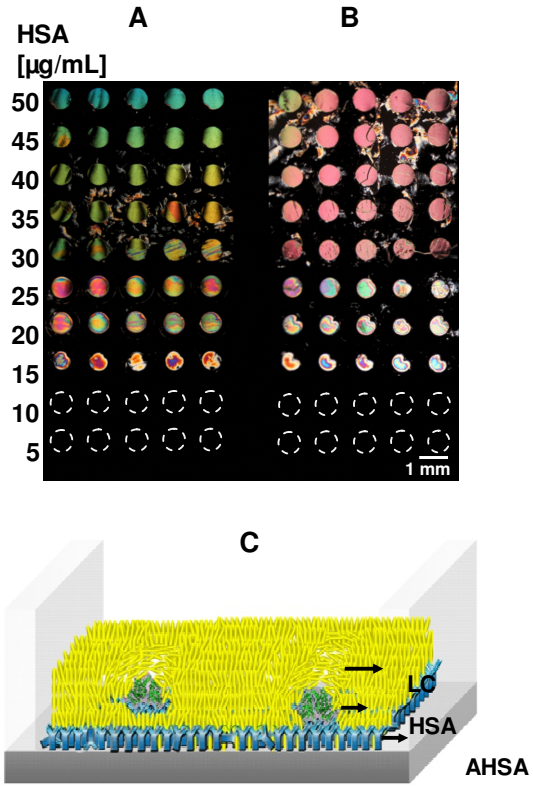

Figure 3.3 Optical appearance of the LC cells (under crossed polarizers) made from AHSA-decorated slides supporting arrays of (A) PBS buffer containing HSA. (B) urine containing HSA. (C) Schematic illustration of the change in the orientation of the LCs supported in the presence of HSA binding.

A change in the orientation of LCs allows light to pass through the crossed polarizers, thereby producing bright-colored regions. Secondly, this dark-to-bright transition of the optical appearance of the LCs, establishes a clear cut-off at 15 μg/mL HSA (**critical concentration**). This result implies that the orientation of LCs supported on the surface is very sensitive to small changes in the amount of HSA bound to the surface.

Because the goal of this study is to use this LC-based HSA assay for urine samples, we further study whether the presence of salts and other components of urine can interfere with the signal. To do this, we dissolved HSA in urine samples collected from a control group and repeated our experiments. As shown in Figures 3.3A and 3.3B, there is a shift in the birefringence colors across the concentration range from bluegreen to pink and pink to white, respectively. It is possible that the presence of other substances in the solution may influence on the orientation of the LCs. However, other factors such as irregularities on the surface, film thickness, and tensile strength of binder clips (Clare et al. **2006;** Tercero Espinoza et al. **2004;** Xue et al. **2009**) can also cause small changes in the orientations of the LCs (as shown by the nonuniform colors in Figure 3.3A). Because of these factors, it is difficult to quantify the amount of HSA on the surface based on birefringence colors alone. Nevertheless, it is noted that the immunobinding of HSA to immobilized AHSA did not change. This result is in agreement with past studies showing that there are no significant effects from matrix interferences (i.e. pH and ionic strength) on HSA immunobinding in urine. They also showed that such matrix interferences can be offset upon sample dilution.

Next, we spotted solutions containing FITC–HTrf and FITC–HSA to investigate their immunobinding selectivity to the AHSA immobilized on the surface. Fluorescence signal in Figure 3.4A shows that only HSA binds to the immobilized AHSA, and the nonspecific adsorption of HTrf is negligible. We also used unlabelled

HTrf and HSA in the LC-based assay. Polarized-light images in Figure 3.4B are consistent with the fluorescent results; only HSA can bind to the AHSA on the surface to disrupt the orientation of the LCs. There is lesser chance for the adsorption of these nonspecific proteins to occur considering HSA is highly abundant and that the amounts of other proteins in urine are minimal.

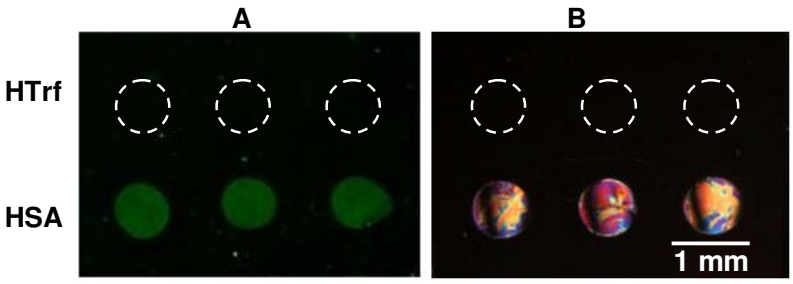

Figure 3.4 Selectivity of the LC-based HSA assay. (A) Fluorescence and (B) Polarized images of HTrf and HSA solutions spotted on AHSA-decorated slides. Protein solutions used are 25 μg/mL.

3.3.3 Detection of HSA in Urine Samples by Using Chip Electrophoresis

To quantify the total amount of HSA present, we run the urine samples using the chip electrophoresis (Agilent Protein 230 LabChip Kit). We first determine the HSA limit of detection (LOD) of the chip electrophoresis to be 20 μg/mL after testing several standard HSA solutions. This value is slightly higher than the results obtained by Chan and Herold (LOD = 5 μg/mL) who used bovine serum albumin (BSA) to represent urinary HSA (Chan and Herold **2006**). Nevertheless, this value only shows that the LOD obtained by the LC-based HSA assay is comparable (15 μg/mL) to that

of the chip electrophoresis. Next, we analyzed the HSA contents of the urine samples collected from 15 patients; 5 of which were taken from the control group (Sample 1–5) while the remaining 10 were taken from the CKD patients (Sample 6–15). Based on the electropherograms, the urine samples from the CKD patients all have HSA levels while those from the control group do not. Using the Agilent 2100 Expert software, we obtained the total amounts of HSA in the urine samples as summarized in Table 3.1.

Table 3.1 HSA Concentrations (μg/mL) Measured by Using Urine Dipstick

Patient No.	Electrophoresis	Dipstick Test	% error[a]
1-5	-	(trace)	NA[b]
6	79	150 – 299	184.2
7	81	150 – 299	177.2
8	103	150 – 299	118.0
9	160	150 – 299	40.3
10	177	300 – 999	266.9
11	184	300 – 999	253.0
12	193	300 – 999	236.5
13	300	300 – 999	116.5
14	1050	1000 – 2999	90.4
15	1200	≥ 3000	NA

[a] $\%\ error = \left| \frac{[R_D - R_E]}{R_E} \times 100\% \right|$

where R_D is mean urine dipstick test reading

R_E is electrophoresis test reading

[b] *not applicable*

To show the HSA detection capability of the urine dipstick method, we tested the same urine samples by using urine dipsticks and compared the results with those from the chip electrophoresis (Table 3.1). Similar to chip electrophoresis, no HSA can be detected in the urine samples from the control group. In contrast, the presence of HSA is detected in the urine samples from the CKD patients. The findings also show that in 6 out of 10 samples from the CKD patients, the dipstick method tends to overestimate the concentrations of HSA. Moreover, the percentage error of the overestimation is significantly large (up to 266.9%).

3.3.4 Detection of HSA in Urine Samples with LC-Based HSA Assays

Finally, we analyzed the same urine samples using the LC-based HSA assay. Figure 3.5 shows the optical appearance of the LC cells made from these urine samples that were directly spotted onto the AHSA-decorated slides. Apparently, urine samples from CKD patients can be distinguished from those without CKD by using the bright colors of LCs. However, it is difficult to determine the amount of HSA in these urine samples based solely on the color intensity produced by the LCs. We also noted that when the HSA concentration in the urine sample is between 1050 μg/mL and 1200 μg/mL, the surrounding areas where the urine samples are spotted also show bright colors. This smearing phenomenon has also been observed previously by Xue *et al.* when high concentrations of protein solution were applied to the surface (Xue and Yang **2008**). Smearing happens probably because HSA form multilayers on the surface and migrate to the surrounding regions during the rinsing and drying steps.

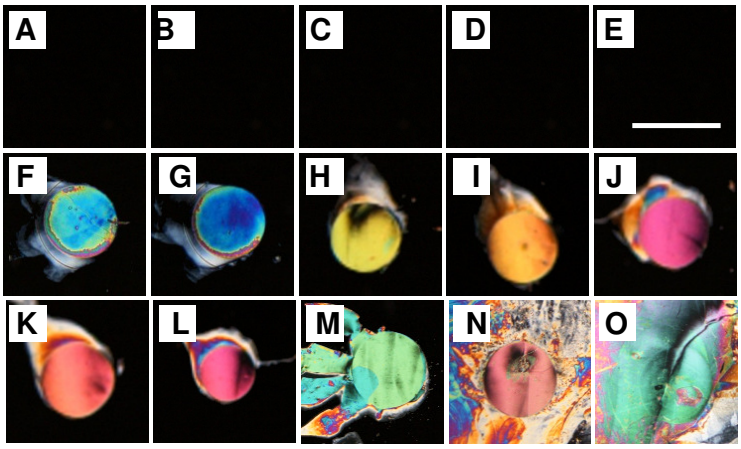

Figure 3.5 Optical appearance of the LC cells (under crossed polarizers) after spotting urine samples 1–5 from the control group (A-E) and urine samples 6–15 from CKD patients (F–O). Scale bar is 1 mm.

To overcome this problem, we developed a dilution protocol in our assay to reduce the amount of HSA in the sample. The dilution protocol was based on the fact that only HSA concentrations above or equal to the critical concentration (≥ 15 μg/mL) produce bright LC spots. To create a reference chart, we first prepared 5 standard solutions having HSA concentrations in the range of 100 – 3000 μg/mL as our first reference (reference I). Each solution was diluted according to the sequential dilution protocol I (consisting of dilution ratios 200×, 60×, 20×, 10× and 5×), and then each diluent was dispensed onto an AHSA-decorated slide. Figure 3.6A shows the optical appearance of the LC cell made from the slide. It is noted that all of the 5 diluents from the 3000 μg/mL HSA solution produce 5 bright spots (first row).

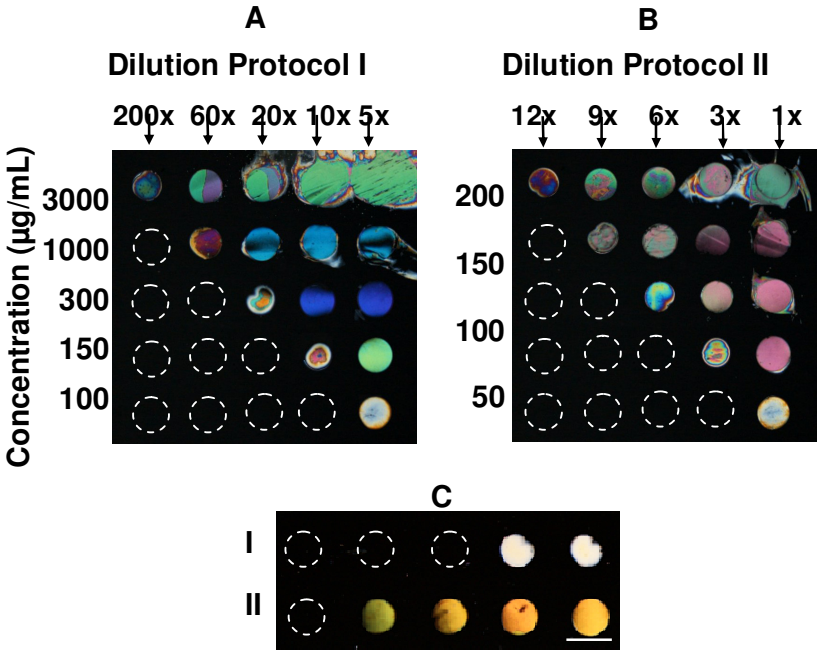

Figure 3.6 Application of dilution protocols in the LC-based assay for estimating the concentration range of HSA. (A) Optical appearance of the LC cell after applying dilution protocol I to 5 different HSA solutions having concentrations in the range of 100–3000µg/mL (B) Optical appearance of the LC cell after applying dilution protocol II to 5 different HSA solutions having concentration in the range of 20–200 µg/mL. (C) Optical appearance of the LC cell obtained from an actual urine sample (Sample #12) using both dilution protocols I and II, respectively. Scale bar is 1mm.

This is anticipated because the HSA concentrations of the diluents (which correspond to HSA solutions of 15, 50, 150, 300, and 600 µg/mL, respectively) are equal to or above the critical concentration. In contrast, when diluents from the 1000 µg/mL standard HSA solution are used (second row), only 4 out of the 5 spots are able to produce bright spots. This is because after diluting 200×, the HSA concentration of the solution is reduced to 5 µg/mL, which is lower than the critical

concentration of HSA; therefore the optical appearance of the LCs in this region remains dark. Although the HSA concentrations in the four other diluents decrease to 17, 50, 100, and 200 μg/mL they are still higher than the critical concentration after the dilution. These solutions can disrupt the LCs supported on the surface thereby producing bright spots. In summary, the number of bright spots corresponds to the number of HSA solutions whose concentrations are higher than or equal to the critical concentration after dilution. In addition, Figure 3.6A shows that the number of bright optical spot is reduced by 1 as the HSA concentration level continues to decrease from 300, 150 and 100 μg/mL. On the basis of this principle, an LC response of 1 bright spot corresponds to an HSA concentration range of 100 – 149 μg/mL, while 2, 3, 4, and 5 bright spots corresponds to HSA concentration ranges of 150 – 299, 300 – 999, 1000 – 2999 and ≥ 3000 μg/mL, respectively.

Dilution protocol I is designed for urine samples which have high HSA concentrations (up to 3000 μg/mL). Because of this, the range per HSA level is larger. In order to have better approximation of the HSA concentration in urine samples, especially at microalbuminuria range, we designed a second dilution protocol (dilution protocol II), which has a different set of dilution ratios (12, 9, 6, 3 and 1×). To develop this dilution protocol, we prepared another set of 5 standard solutions having HSA concentrations ranging from 20 to 200 μg/mL as our second reference (reference II). The diluents were dispensed similar to reference I and an LC cell was made. Figure 3.6B shows how the number of bright spots corresponds to HSA concentration; 1 bright spot is for HSA concentration in the range of 20 – 49

μg/mL while 2, 3, 4, and 5 bright spots correspond to HSA concentration in the ranges of 50 – 99, 100 – 149, 150 – 199, and ≥ 200 μg/mL, respectively.

The amount of HSA in the urine samples from the CKD patients were then quantified using the LC-based HSA assay by employing dilution protocols I and II. LC cells were made and their optical appearances were examined under crossed polarizers. Figure 3.6C shows the optical appearance of LC cells when dilution protocol I and II are applied to a urine sample from a CKD patient. There are two bright spots when the dilution protocol I is used. On the basis of Figure 3.6A, two bright spots correspond to an HSA concentration of 150 – 299 μg/mL, which is 16.3% off the actual HSA concentration (193 μg/mL, estimated by using chip electrophoresis). Nevertheless, this is still more accurate than the urine dipstick test, which gives an error of 236.5% (Table 3.1). In addition, LC-based assays are faster (t~ 3 h) and less laborious than performing electrophoresis (t~ 6 h). Meanwhile, when the same sample was subjected to dilution protocol II, the LC cell produced four bright spots which give a corresponding HSA concentration range of 150 – 199 μg/mL. This value is only 9.6% off the actual HSA concentration as measured by the chip electrophoresis. Table 3.2 summarizes the results obtained from the LC-based HSA assay and their offset errors.

Table 3.2 HSA Concentrations (μg/mL) Measured by Using the Developed Dilution Protocols I and II

Patient No.	Electrophoresis	Dilution Protocol I	% error[a]	Dilution Protocol II	% error
1-5	-	(trace)	NA[b]	(trace)	NA[b]
6	79	≤ 100	NA	50 – 99	5.2
7	81	≤ 100	NA	50 – 99	8.0
8	103	100 – 149	20.9	100 – 149	20.9
9	160	150 – 299	40.3	150 – 199	9.1
10	177	150 – 299	26.8	150 – 199	1.4
11	184	150 – 299	22.0	150 – 199	5.7
12	193	150 – 299	16.3	150 – 199	9.6
13	300	300 – 999	116.5	≥ 200	NA
14	1050	1000 – 2999	90.4	≥ 200	NA
15	1200	1000 – 2999	66.6	≥ 200	NA

[a] $\%\ error = \left| \frac{[R_{LC} - R_E]}{R_E} \times 100\% \right|$

where R_{LC} is mean LC-based assay reading

R_E is electrophoresis test reading

[b] *not applicable*

3.4 Conclusion

In summary, we have developed an LC-based HSA assay which can be used to detect HSA in urine samples. The LCs supported on the AHSA-decorated slides are

disrupted by the presence of HSA molecules, thereby producing bright optical signals which are easily distinguishable. Moreover, the quantification of the amounts of HSA present in the sample was successfully achieved using the developed dilution protocols. The results from the LC-based HSA assay show better accuracy than urine dipsticks especially when the samples contain low HSA concentration. This LC-based HSA assay may find potential application in the diagnosis and prognosis of diabetic patients having CKD.

CHAPTER 4

LIQUID CRYSTAL DROPLETS AS A HOSTING AND SENSING PLATFORM FOR DEVELOPING IMMUNOASSAYS

4.1 Introduction

Over the past decade, liquid crystals (LCs) have been exploited in the development of label-free platforms for detecting chemical and biological agents (Birchall et al. **2008;** Brake et al. **2003b;** Gupta et al. **1998;** Hoogboom et al. **2006;** Shah and Abbott **2001;** Skaife et al. **2001;** Xue et al. **2009;** Xue and Yang **2008**). The detection principle is based on the highly sensitive orientational response of LCs to minute changes of solid surfaces supporting the LCs. The LCs at the surface can then communicate their orientations through the bulk, causing global changes in orientations and generating optical textures that can be readily observed with the naked eye under cross polarizers. Recently, this mechanism has been exploited to detect the presence of proteins on solid surfaces (Birchall et al. **2008;** Gupta et al. **1998;** Skaife et al. **2001;** Xue et al. **2009;** Xue and Yang **2008**) or at aqueous/LC interfaces(Bi et al. **2009a;** Bi and Yang **2010;** Hartono et al. **2008;** Hartono et al. **2009a;** Hartono et al. **2009b;** Hartono et al. **2010**). In Chapter 3, for example, we demonstrated an LC-based protein immunoassay which allows the detection and quantification of different antibodies after they bind to surface-immobilized antigens (Aliño and Yang **2011**) . This LC-based protein immunoassay offers advantages over conventional immunoassays because it does not require labeling of proteins or complex instrumentation. However, it still requires several steps before the test results can be obtained. These steps include surface treatments, antigen and antibody immobilization, rinsing and drying, and fabrication of LC cells. Therefore, there is a

need to design a simpler and more straightforward immunoassay with minimal number of steps.

In the past, researchers have shown interest in dispersing LCs into small droplets (Di Profio et al. **2001;** Di Profio et al. **2002;** Golemme et al. **1998;** Gupta et al. **2009b;** Heppenstall-Butler et al. **2005;** Kleman and Lavrentovich **2006;** Lanzo et al. **1999;** Lockwood et al. **2008;** Nicoletta et al. **1999;** Nicoletta et al. **2001;** Simon et al. **2007;** Sivakumar et al. **2008;** Sivakumar et al. **2009;** Tixier et al. **2006;** Tjipto et al. **2006;** Tongcher et al. **2006**) because of their applications in various electro-optical devices such as optical switches and light valves (Di Profio et al. **2001;** Di Profio et al. **2002;** Golemme et al. **1998;** Lanzo et al. **1999;** Nicoletta et al. **1999;** Nicoletta et al. **2001**). Recently, it has been proposed that LC droplets in aqueous solutions can be exploited for sensing applications (Simon et al. **2007;** Tjipto et al. **2006;** Tongcher et al. **2006**). Using LC droplets as a sensing platform is advantageous because these droplets are homogenous, mobile and have large surface areas. Several methods for the fabrication and characterization of LC droplets have been reported (Gupta et al. **2009b;** Heppenstall-Butler et al. **2005;** Lockwood et al. **2008;** Simon et al. **2007;** Sivakumar et al. **2008;** Sivakumar et al. **2009;** Tjipto et al. **2006;** Tongcher et al. **2006**). Tongcher, *et. al.* for instance, produced stable LC droplets in aqueous solutions by using hydrophobe such as hexadecane to suppress molecular diffusion degradation (Ostwald ripening) and coalescence by collision (Tongcher et al. **2006**). In addition, they also reported that ionic and steric surfactants such as sodium dodecyl sulfate (SDS) and polystyrene and ethylene oxide block copolymer (SE3030) can

improve the stability of the LC droplets. Similarly, Simon and co-workers reported the dispersion and stabilization of LC droplets in aqueous solutions containing water-soluble polymers (Simon et al. **2007**). More recently, Sivakumar, *et. al.* created monodispersed LC droplets by using silica particles coated with polyelectrolytes as templates. Later, the silica core was etched with hydrofluoric acid (HF) and the hollow polyelectrolyte templates were filled with LCs (Sivakumar et al. **2008**). This method, however, is time-consuming and labor intensive. In addition, because HF is hazardous and can penetrate tissue (Muriale et al. **1996;** Sullivan and Krieger **2001;** Wang and Stein **2008**), this method requires special handling. Hence, this system has limitations in practical sensing applications.

In this work, we aimed to detect proteins in solution by using LC droplets as a platform for hosting protein immunoassays. So far, there is still no report of using LC droplets for hosting immunoassays. We also studied the immobilization of proteins on the surface of LC droplets and investigated how the presence of protein and immunocomplexes affects the orientation of the LCs inside the droplets. Herein, we focused on detecting two model antibodies, anti-human immunoglobulin G (AIgG) and anti-human serum albumin (AHSA) in the solution.

4.2 Experimental Section

4.2.1 Materials

Glass slides were purchased from Marienfield (Germany). Human immunoglobulin G (IgG), anti-human immunoglobulin G (AIgG), human serum albumin (HSA), anti-human serum albumin (AHSA), polyethylene imine (PEI, 50 wt %), pluronic 188 (poloxamer), poly(vinylalcohol) (PVA), glutaraldehyde (GA, 50 wt %), sodium carbonate (Na_2CO_3), ethanolamine, sodium cyanoborohydride ($NaBH_3CN$), and hexadecane were purchased from Sigma-Aldrich (Singapore). Thermotropic liquid crystal, 4-pentyl-4'-cyano-biphenyl (5CB) was purchased from Merck (Japan). Cy3-labelling kit (Cy3 Mono-Reactive Dye Pack) was purchased from Amersham Biosciences (U.S.A.). Phosphate buffer saline (PBS) 10X, and polyethylene glycol sorbitan monolaurate (Tween 20, biotechnology grade) were both obtained from 1st BASE (Singapore). All aqueous solutions were prepared using deionized (DI) water with a resistance of 18.2 $M\Omega\ cm^{-1}$ (Millipore).

4.2.2 Preparation of Protein Solutions

AIgG stock solution with a concentration of 1 mg/mL was prepared by dissolving 1 mg of AIgG in 1 mL of PBS buffer (0.1 M, pH 7.4). The stock solution was stored at 4 ºC. Stock solutions of IgG, HSA and AHSA were also prepared in a similar way. To obtain the final concentration, the stock solution was diluted with PBS buffer. Meanwhile, AIgG and AHSA solutions used for immunobinding

reactions were prepared by diluting the stock solution with PBS-T20 buffer (0.1 M PBS buffer containing 0.21 wt % of Tween 20) (Batteiger et al. **1982;** Dong et al. **2008**).

4.2.3 Fluorescence Labeling of Proteins

Proteins AIgG, IgG, AHSA and HSA were first dissolved in 0.1 M of carbonate buffer (pH 9.3) to a final concentration of 1 mg/mL. Then, these proteins were fluorescently labeled by using a Cy3-labelling kit following the manufacturer's protocol. The resulting Cy3-labeled proteins were named: Cy3-AIgG, Cy3-IgG, Cy3-AHSA and Cy3-HSA, respectively. Purification of these Cy3-labeled proteins was done by dialysis against PBS buffer using a dialysis membrane (Fisher) with a 3.5 kDa cutoff pore size for 18 h. From the absorbance readings at 280 and 552 nm, the final dye/protein ratio (F/P) is approximately 6-8. Cy3-labeled PEI (Cy3-PEI) was also prepared in a similar way, except that 5 mg/mL of PEI in carbonate buffer was used. The dye/monomer ratio was 1:95.

4.2.4 Preparation of LC Droplets in Water

First, 5CB was mixed with hexadecane (3% w/w, as a hydrophobe) for 10 min. Next, the 5CB with hexadecane was added to DI water containing 1 wt % PEI at a ratio of 1:20 (5CB: water). The mixture was then sheared using a vortex mixer (FinePCR, Korea) at 3000 rpm for 5 min. The mixture was left overnight to settle the LC droplets. Finally, the aqueous solution was decanted to obtain LC droplets at a

ratio of 1:4 (5CB: water). To monitor the PEI surface density, we also prepared LC droplets using 0, 0.01, 0.05, 0.1, 0.5, 1.0, 1.5, 2.0, 2.5 and 3.0 wt% Cy3-labeled PEI. The PEI surface densities of the prepared LC droplets were then estimated by using a calibration curve (see Appendix B).

4.2.5 Effects of Glutaraldehyde (GA) on the LC Droplets

Approximately 100 μL of the LC droplets was diluted with 500 μL of PBS buffer. Then, approximately 20 μL of GA solution was added to the LC droplets and the emulsion was incubated at different time intervals (0 min, 5 min, 15 min, 30 min, 1h, 4h, and 12h). The GA solution was prepared from PBS buffer containing different concentrations of GA (0.1, 0.5, and 1.0 wt %) and 0.1 mM of $NaBH_3CN$. (***Note:*** *Higher $NaBH_3CN$ concentration may cause instability and aggregation*). After the reaction, excess GA solution was removed and the LC droplets were rinsed with PBS buffer twice. The droplets were then immersed in 500 μL PBS-T20 buffer for 30 min before image analysis.

4.2.6 Immobilization of Proteins on the LC Droplets

After the reaction with GA, excess GA solution was removed and the LC droplets were rinsed twice with fresh PBS buffer. The buffer was decanted until a final volume of 250 μL is reached. In order to immobilize the proteins, the emulsion was added with 100 μL of PBS buffer which contains either 50 μg/mL of IgG or HSA and incubated for 30 min. The protein-decorated LC droplets (denoted as IgG-LC and

HSA-LC droplets, respectively) were then rinsed with PBS-T20 buffer to remove the excess proteins. Finally, 10 μL of PBS buffer containing 0.1 mM ethanolamine and 0.1 mM $NaBH_3CN$ was added to passivate any excess aldehyde groups (Chua et al. **2009;** Zheng et al. **2005**). After 15 min of incubation, the protein-decorated LC droplets were rinsed and suspended with 250 μL of PBS-T20 buffer.

4.2.7 Immunobinding Experiments

The protein-decorated LC droplets were immersed in 100 μL of PBS-T20 buffer containing different concentrations of AIgG or AHSA at room temperature for 15 min. After the immunobinding, the LC droplets were rinsed with PBS-T20 twice. The droplets were immersed in the PBS-T20 buffer for 30 min before image analysis.

4.2.8 Image Analysis of LC droplets

LC droplets were first loaded into an optical cell composed of two glass slides and two pieces of spacer with a thickness of ~300 μm. This particular thickness is selected to ensure that the LC droplets can move freely and two droplets do not overlap in the same optical path during analysis. The sample was shaken well before loading into the cell. Bright-field, crossed polars, and fluorescence images of the LC droplets were acquired using an optical microscope (Nikon ECLIPSE LV100POL, Japan) equipped with a digital camera. The sizes (diameters) of the droplets were measured using imaging software from Nikon (NIS-Elements D). Because LC droplets have a wide range of size distributions, we only analyzed and compared LC

droplets between 60 and 85 μm in the immunoassay. Fluorescence images were captured under a fluorescence filter set (Nikon HYQ). Experiments were performed in triplicates, and images were taken at three different locations of the optical cell.

4.3 Results and Discussion

4.3.1 LC Droplets Coated with PEI

In the present study, the surface of LC droplets was coated with a thin layer of PEI to allow the immobilization of proteins on the LC droplets. Therefore, we first studied how to control the surface density of PEI on the LC droplets by varying the PEI concentration. Figure 4.1 shows that the surface density of PEI on the LC droplets increases proportionally to the PEI concentration. When the PEI concentration is 3.0 %, the surface density of PEI can be as high as $125 \pm 2 \times 10^{-7}$ nm^{-2}. It should be noted that having a higher PEI surface density is favored because it gives more reactive amine groups to immobilize the proteins. However, we noted that the concentration of PEI also affects the size of the LC droplets.

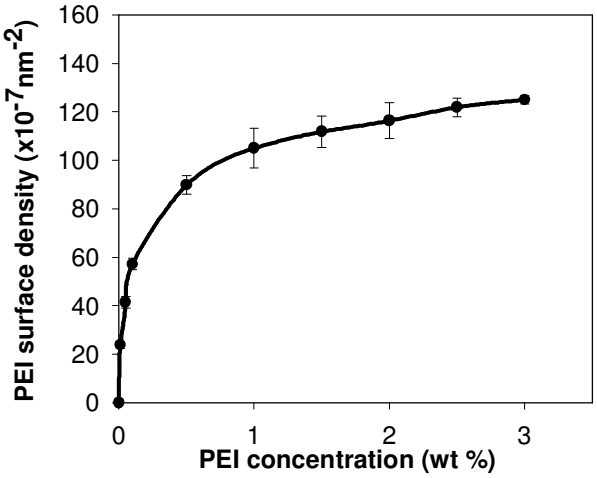

Figure 4.1 Effect of PEI concentration on the surface density of PEI on the LC droplets.

Table 4.1 shows that when the PEI concentration is 0.01 %, the LC droplet size is 107 ± 38 μm, and the size gradually decreases with increasing PEI concentration. For example, when the PEI concentration is 1.0 %, the droplet size decreases to 61 ± 20 μm. This phenomenon is probably caused by the increase in the viscosity of the PEI solution (Pal **1996**). When the viscosity is higher, the shear stress is also stronger. Hence, smaller droplets are produced.

Table 4.1 Effect of PEI Concentration on LC Droplet Size (μm) and Stability

Days	**PEI Concentration**				
	0.01 wt %	**0.10 wt %**	**1.00 wt %**	**1.50 wt %**	**2.00 wt %**
0	107 ± 38	69 ± 34	61 ± 20	56 ± 13	55 ± 18
2	115 ± 51	71 ± 33	65 ± 18	58 ± 19	61 ± 30
6	131 ± 71	93 ± 41	67 ± 19	60 ± 25	63 ± 21
14	225 ± 223	106 ± 28	74 ± 28	75 ± 18	76 ± 17
20	308 ± 156	157 ± 50	76 ± 17	78 ± 17	73 ± 15

In addition, increasing the PEI concentration also causes a higher density of PEI on the surface of the LC droplets. Because of electrostatic repulsion and steric hindrance, Ostwald ripening and coalescence of LC droplets (which also contributes to the larger LC droplet size) become more difficult. Although there is a decreasing trend in the droplet size, the decrease in the droplet size is negligible when we further increase the PEI concentration above 1.0 %. Aside from having higher amine groups on the surface, it is also important to obtain LC droplets with good long-term stability. Therefore, LC droplet size was monitored as a function of storage time. As shown in Table 4.1, the sizes of the LC droplets prepared from 0.01 % and 0.1 % of PEI solution gradually increase to 308 ± 156 μm and 157 ± 50 μm, respectively, over a period of 20 days, indicating that the LC droplets prepared by using these two PEI concentrations are not stable. The size of LC droplets prepared from 1.0 % PEI solution, however, only increases to 76 ± 17 μm after 20 days. Because 1.0 % PEI

solution provides higher amine surface density and better stability for LC droplets, we used 1.0 % PEI solution to prepare LC droplets in our subsequent experiments.

4.3.2 Optical Textures and Orientations of LC droplets

Next, we studied the optical textures of the LC droplets coated with PEI. Under a microscope, we found two points of defects (boojums) at the edge of the droplets as indicated by the white arrows (Figure 4.2A). We also investigated the birefringence of the LC by viewing them under cross polarizers. The polarized-light image displays bright spherical dots with dark dimples where the boojums are located. Both figures suggest that the LC inside the droplets exhibits a bipolar configuration (Ding and Yang **1992;** Erdmann et al. **1990**). These results are consistent with other reports showing that the orientation of LC inside a droplet larger than 3μm has a bipolar configuration when the LC orients parallel to the surface (Gupta et al. **2009b;** Kleman and Lavrentovich **2006;** Sivakumar et al. **2008;** Tjipto et al. **2006**).

On the other hand, when we dispersed the LC droplets into PBS-T20 buffer, only a single boojum located at the center of the droplets was observed (Figure 4.2B). Under cross polarizers, each LC droplet has a dark cross in it. Therefore, we conclude that the orientation of the LC in these droplets has a radial configuration. This configuration occurs when the LC at the interface orients perpendicularly to the surface of the droplets.

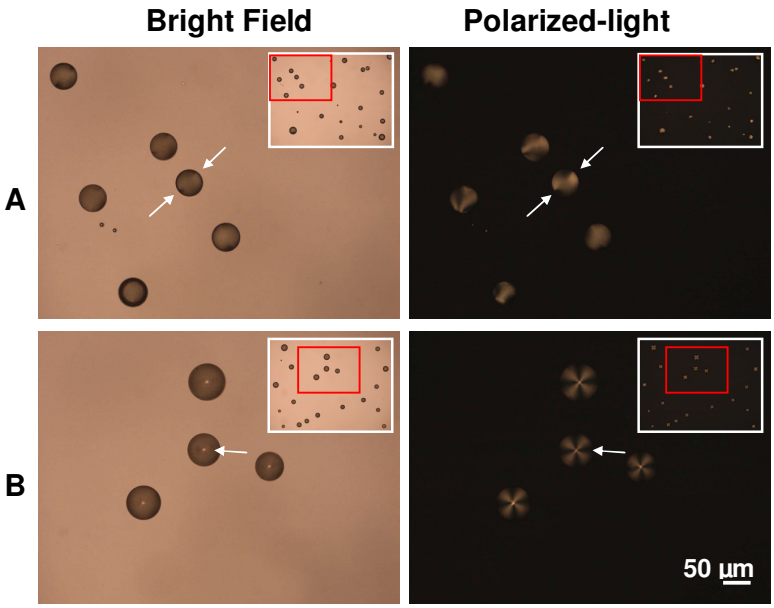

Figure 4.2 Images of the LC droplets (A) before and (B) after the immersion of LC droplets in PBS-T20 buffer. This figure shows that the orientation of LCs inside the LC droplets changes from bipolar to radial configuration in the presence of Tween 20.

On the basis of the above results, we propose that Tween 20, because of its amphiphilic properties, can permeate through the PEI layer and concentrate on the surface of the LC droplets. Thus, the presence of Tween 20 dictates the orientation of the LC in the droplet. A similar phenomenon has been observed when thin films of LC are exposed to aqueous solutions containing surfactants such as sodium dodecyl sulfate (SDS) (Lockwood et al. **2006;** Lockwood et al. **2008;** Price and Schwartz **2008**). A schematic illustration of the orientation of the LC in the droplet before and after the addition of Tween 20 is shown in Figure 4.3.

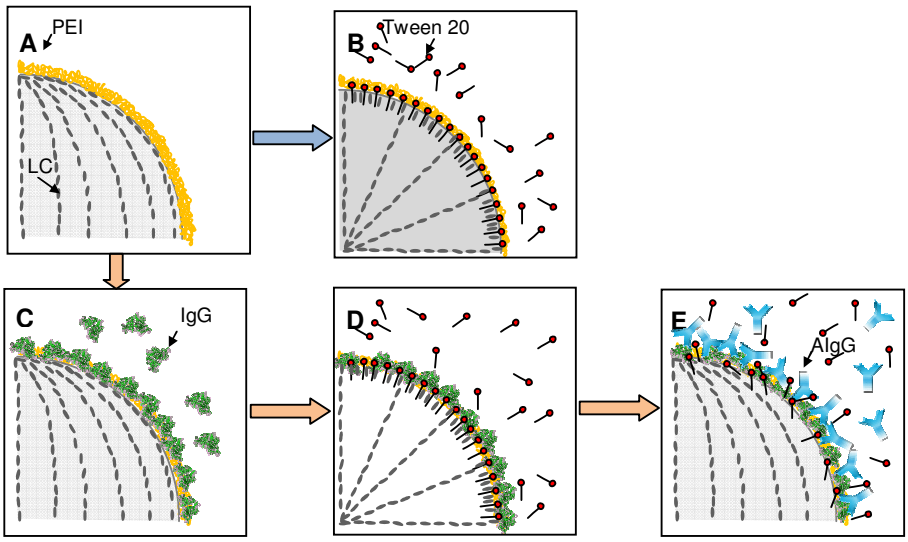

Figure 4.3 Schematic illustration of the LC droplet during chemical functionalization and protein immobilization. (A) A LC droplet in PBS buffer exhibits a bipolar configuration. (B) Addition of PBS-T20 buffer induces an orientational transition from a bipolar to a radial configuration. (C) Immobilization of IgG on the surface of the LC droplet. (D) After rinsing the IgG-LC droplet with PBS-T20, the LC droplet exhibits a radial configuration. (E) Immunocomplex formation on the surface changes the LC orientation to a bipolar configuration.

4.3.3 Effect of Chemical Modifications on the Orientations of LC

To immobilize IgG on the surface of the LC droplet, the PEI–coated LC droplets were functionalized with GA to provide aldehyde groups for protein immobilization. Figure 4.4 shows the effects of the GA concentration on the orientation of the LC inside the droplets. After 15 min, the LC droplets still exhibit a radial configuration when GA is 0.1% or 0.5%. When the GA concentration is increased to 1%, however, the orientation of the LC changes to a bipolar configuration. This result confirms that the orientation of LC at the interface can be

affected by the chemical functionality and the surface density of functional molecules. When the incubation time is increased to 1h, the amount of GA immobilized on the LC droplet surface increases as shown by the change in the configuration of the LC from radial to bipolar. Because a radial configuration is preferred, the GA concentration and incubation time were fixed at 0.5% and 15 min, respectively, in the following experiments.

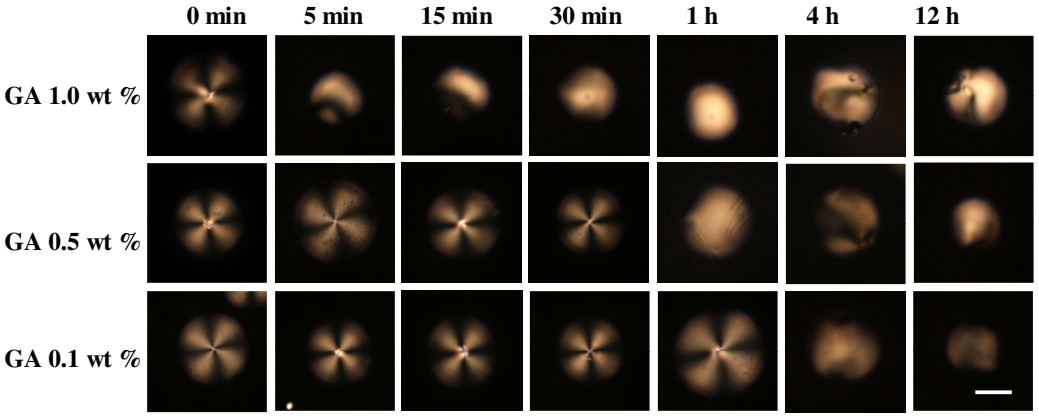

Figure 4.4 Effect of GA concentrations and incubation times on the optical appearance of LC droplet (under crossed polars). Scale bar is 25 μm.

4.3.4 Effect of Protein Surface Densities on the Orientations of LC

We studied the effects of protein surface densities on the orientations of LC by incubating the LC droplets in different protein concentrations (Figure 4.5). From the figure, we observed that, when the IgG concentration is greater than 50 μg/mL, the LC orientation inside the droplets already changes to bipolar prior to the immunobinding reaction. This indicates that the IgG molecules alone can disrupt the

LC at the interface, provided that its surface density is high enough. Therefore, an upper limit exists for the immunoassay. The same principle also holds true for HSA–LC droplets, but the upper limit is slightly higher at 100 μg/mL. This difference can be explained by the smaller size of HSA (MW_{HSA} of 67 kDa) than IgG (MW_{IgG} of 150 kDa). At 50 μg/mL, the equivalent surface densities for IgG and HSA are $14 \pm 1 \times 10^{-3}$ and $32 \pm 1 \times 10^{-3}$ nm^{-2}, respectively.

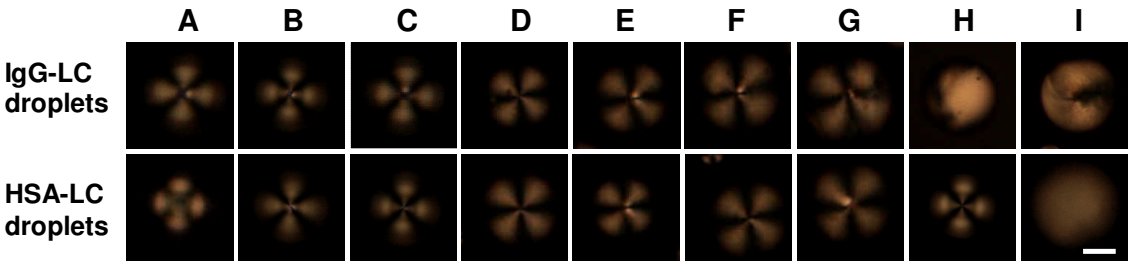

Figure 4.5 Effect of protein surface densities on the optical appearance of LC droplet (under crossed polars). (A) 0, (B) 0.01, (C) 0.02, (D) 0.1, (E) 1, (F) 10, (G) 50, (H) 100, (I) 200 μg/mL. Scale bar is 25 μm.

4.3.5 Detecting Antibodies Using Immunobinding Reaction

To investigate whether AIgG can bind to IgG immobilized on the surface of LC droplets, we first incubated IgG-LC droplets in PBS-T20 buffer containing either fluorescently labeled Cy3-AIgG or Cy3-AHSA as shown in Figure 4.6.

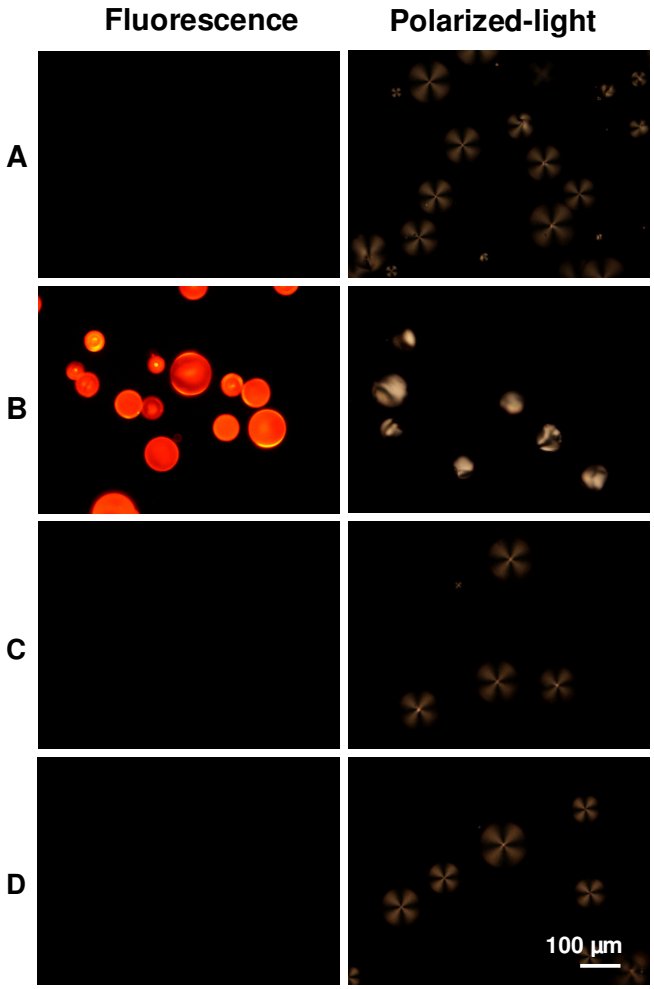

Figure 4.6 Fluorescence (left) and polarized-light (right) images of LC droplets. (A) IgG-LC droplets before the addition of antibody solutions, (B) IgG-LC droplets after the addition of AIgG, (C) IgG-LC droplets after the addition of AHSA, and (D) LC droplets (without IgG coating) after the addition of AIgG. Successful binding of AIgG to the IgG-LC droplets can be seen from the red fluorescence and bipolar configuration. 50 µg/mL of AHSA and AIgG solutions are used.

Fluorescently-labeled antibodies were used in this study because fluorescence provides direct evidence regarding the antigen-antibody immunobinding reaction.

However, we point out that in our LC-based immunoassay, the fluorescently-labeled antibodies are not necessary. After 15 min of incubation, the IgG-LC droplets were rinsed and re-suspended in 250 μL of PBS-T20 buffer. The red fluorescence in Figure 4.6B indicates that AIgG binds to the IgG immobilized on the surface of the LC droplets. On the other hand, no fluorescence can be observed after the reaction with Cy3-AHSA (Figure 4.6C) or in LC droplets without IgG coating (Figure 4.6D). This result suggests that the binding of Cy3-AIgG to IgG is specific.

Next, we compared the optical textures of the IgG-LC droplets before and after the immunoreaction using unlabeled antibodies, AIgG and AHSA. The polarized-light images indicate that the LC orientation inside the IgG-LC droplets changes to a bipolar configuration after the reaction with AIgG. After comparing the polarized-light and fluorescence images, we attribute the change of LC orientation (from radial to bipolar) to the formation of the immunocomplex when AIgG binds to the surface of the IgG-LC droplets. We further propose that the large size of the immunocomplex is able to displace some Tween 20 molecules from the LC surface or blocks the permeation of Tween 20 into the LC, thus causing the changes in the LC orientation. In contrast, the LC orientation inside the IgG-LC droplet retains its radial configuration after the addition of AHSA. This result further confirms that the change is due to the formation of the immunocomplex on the surface of the LC droplets.

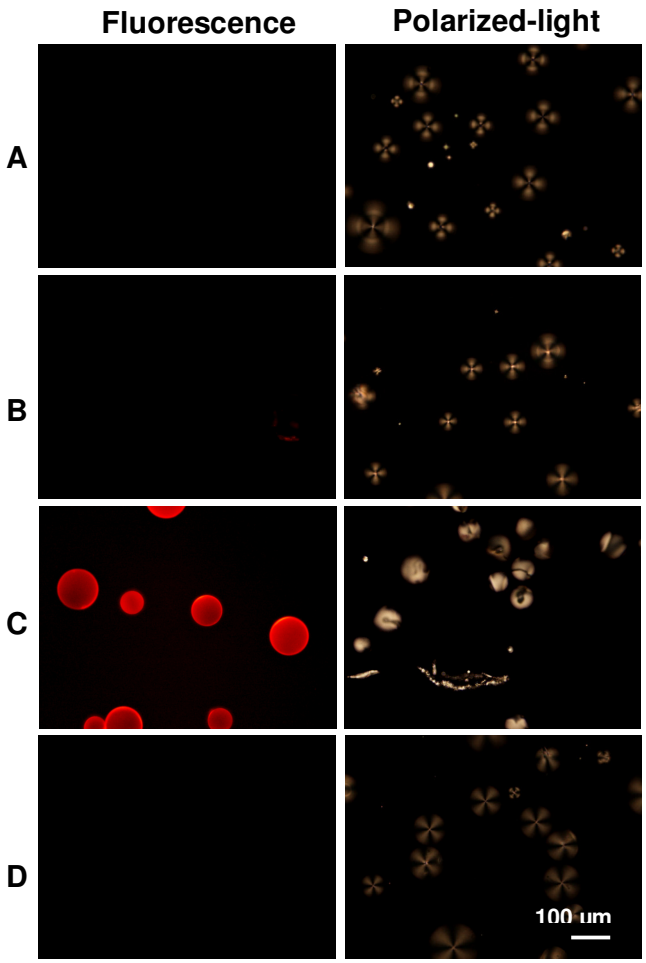

Figure 4.7 Fluorescence (left) and polarized-light (right) images of LC droplets. (A) HSA-LC droplets before the addition of antibody solutions, (B) HSA-LC droplets after the addition of AIgG, (C) HSA-LC droplets after the addition of AHSA, and (D) LC droplets (without HSA coating) after the addition of AHSA. Successful binding of AHSA to the HSA-LC droplets can be seen from the red fluorescence and bipolar configuration. 50 µg/mL of AHSA and AIgG solutions are used.

To investigate whether this LC-based immunoassay can be applied to detect AHSA, we repeated the experiment by using HSA-LC droplets. Fluorescence and polarized-light images before (Figure 4.7A) and after (Figure 4.7B) the immersion of

HSA-LC droplets in PBS-T20 buffer containing AIgG suggests that AIgG does not bind to HSA immobilized on the surface of the LC droplets. This is evident by the lack of fluorescence and the radial configuration of the LCs. Similarly, no fluorescence can be observed after the immersion of LC droplets without HSA in PBS-T20 buffer containing AHSA (Figure 4.7D). This finding suggests that there is no binding on the passivated surface. In contrast, when HSA-LC droplets are immersed in an AHSA solution (Figure 4.7C), appearance of red fluorescence indicates that AHSA binds to the HSA on the surface. This is accompanied by the change in the LC orientation from a radial to a bipolar configuration.

4.3.6 Limit of Detection (LOD) of the LC-Based Immunoassay

To test the LOD of the LC-based immunoassay, we incubated IgG–LC droplets into PBS–T20 buffer containing different concentrations of AIgG. On the basis of the change in the LC orientation (from a radial to a bipolar configuration), we can detect AIgG when its concentration is as low as 0.01 μg/mL (Figure 4.8). Similarly, when we used HSA–LC droplets, we can detect AHSA when its concentration is as low as 0.02 μg/mL. Below this concentration, the HSA–LC droplets still retains its radial configuration even after the immunobinding reaction. This is probably because the amount of the HSA–AHSA complex on the surface is too low to disrupt the orientation of the LCs at the surface, thus setting a lower limit of the immunoassay.

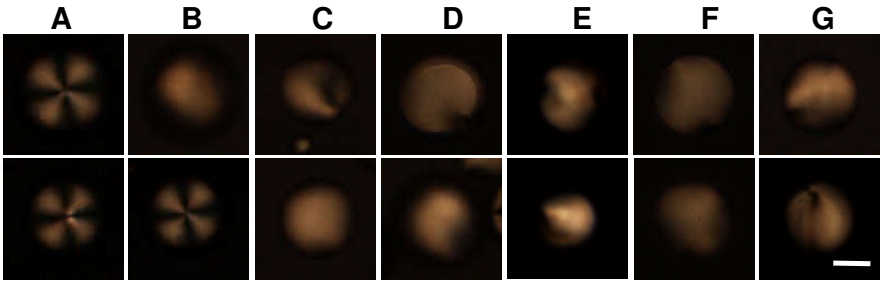

Figure 4.8 Polarized-light images of LC droplets after the immersion of these droplets into antibody solution. (Top) IgG-LC droplets in buffer containing AIgG. (Bottom) HSA-LC droplets in buffer containing AHSA. Antibody concentrations used in these experiments are (A) 0, (B) 0.01, (C) 0.02, (D) 0.10, (E) 1, (F) 10, and (G) 100 μg/mL. Scale bar is 25 μm.

4.4 Conclusion

We have demonstrated that LC droplets can be used as a hosting and sensing platform for developing protein immunoassays. We also demonstrated that the LC droplets remained stable at 1 wt% of PEI. The presence of the specific protein can be directly monitored by the optical texture produced by the LC droplet. This sensing mechanism is based on the formation of immunocomplexes between antibodies and antigens immobilized on the surface of the LC droplets. The immunocomplex is able to disrupt the homeotropic ordering at the interface of the LC droplets, to cause a bipolar configuration and distinct optical readout signals.

CHAPTER 5

INKJET PRINTING AND RELEASE OF MONODISPERSE LIQUID CRYSTAL DROPLETS FROM SOLID SURFACES

5.1 Introduction

Liquid crystals (LCs) as emulsion droplets in polymers and aqueous solutions have attracted much attention in recent years because of their large surface areas as well as their unique optical properties (Lockwood et al. **2006;** Volovik and Lavrentovich **1983**). Unlike isotropic liquids, molecules in LC droplets assume three types of orientational ordering: bipolar, preradial and radial configuration. The orientational ordering of LC droplets is highly sensitive to boundary conditions and/or external fields, making them suitable for biological and chemical sensing applications (Aliño et al. **2011;** Di Profio et al. **2001;** Di Profio et al. **2002;** Golemme et al. **1998;** Gupta et al. **2009a;** Kinsinger et al. **2010;** Lanzo et al. **1999;** Lin et al. **2011;** Nicoletta et al. **1999;** Nicoletta et al. **2001;** Sivakumar et al. **2009;** Tjipto et al. **2006**). For example, in Chapter 4, we have demonstrated the detection of antibody molecules in aqueous solutions by using LC droplets. When antibody forms a immunocomplex with an immobilized antigen on the surface of a LC droplet, the orientational configuration of the droplet changes readily from radial to bipolar (Aliño et al. **2011**).

LC droplets are often produced via homogenization of LC in water, with emulsifying agents such as water-soluble polymers (e.g. polyethyleneimine, PEI) (Aliño et al. **2011;** Simon et al. **2007;** Sivakumar et al. **2008;** Tjipto et al. **2006;** Zou et al. **2011;** Zou and Fang **2010**), surfactants (e.g. sodium dodecyl sulfate, SDS)

(Tongcher et al. **2006**), and nonpolar liquids (e.g. hexadecane) (Aliño et al. **2011;** Tongcher et al. **2006**). For instance, LC droplets of 15 to 36 μm can be created vortexing (Simon et al. **2007**) whereas smaller LC droplets of 180 to 630 nm in diameter can be prepared by using ultrasonification (Tongcher et al. **2006**).

The LC droplets used in Chapter 4 were produced via vortexing. Droplets prepared using this method, however, usually have a broad size distribution. In Chapter 4, we are able to bypass this problem by choosing only a fraction of the size distribution (60 – 85 μm) while discarding the rest. This creates a problem in real applications since the size of the LC droplet can affect the orientational ordering within each LC droplet (Gupta et al. **2009b**). Using only a fraction of the LC droplets is also not cost-effective. Therefore, it is important to control the size of the LC droplets. A number of methods have been proposed in the literature for the preparation of LC droplets with uniform sizes (Donath et al. **1998;** Gupta et al. **2009b;** Hamlington et al. **2007;** Priest et al. **2008;** Shklyaev and Shen **2009;** Sivakumar et al. **2008;** Umbanhowar et al. **2000**). For example, uniform silica particles coated with multiple layers of polyelectrolytes were used as templates to prepare uniform LC droplets (Donath et al. **1998**). The silica cores were first etched with hydrofluoric acid (HF), and then the hollow polymer capsules were filled with LCs. Nanosize (~700 nm) LC droplets can be prepared using this method (Gupta et al. **2009b**), but the procedure is tedious and is not suitable for large-scale production. In contrast, flow focusing microfluidic devices (Hamlington et al. **2007;** Shklyaev and Shen **2009**) or those with co-flowing liquid streams (Umbanhowar et al. **2000**) were

used to squeeze and break off a stream of LCs into spherical droplets. Although the use of microfluidic device is suitable for large scale production (Hamlington et al. **2007**), it is difficult to customize the size of LC droplets because they depend on the dimensions of the channel. Therefore, there is still a need to develop a method for easy preparation of uniform LC droplets whose size can be fine-tuned.

Inkjet printing technology has been around for decades and used widely for reprographic techniques (Mohebi and Evans **2002**). It is fast, precise and fully automatic (Delaney et al. **2009**). The most commonly used inkjet printers are the piezoelectric drop-on-demand (DOD) because they are suitable for producing uniform droplets without affecting the fluid used (Allain et al. **2004;** Scoutaris et al. **2011**). In recent years, many research groups have attempted to use different fluids as "ink" for inkjet printing. Their choice of ink ranges from nanoparticles to biological samples (Allain et al. **2004;** Kim et al. **2010;** Scoutaris et al. **2011;** Sumerel et al. **2006;** Volkman et al. **2004;** Zheng et al. **2011**). However, to the best of our knowledge, LCs have never been used as ink for inkjet printing, probably because most LCs are too viscous to jet smoothly. In this study, we first investigated whether LC 4-pentyl-4'-cyano-biphenyl (5CB) can be used as ink in inkjet printing to create uniform LC droplets. Secondly, we investigated the behaviors of these printed LC droplets under flow conditions. Our aim was to lift off these LC droplets from solid surfaces to form free LC droplets in aqueous solutions. We also studied the feasibility of using these free LC droplets for chemical sensing applications.

5.2. Experimental Section

5.2.1 Materials

Glass slides were purchased from Marienfield (Germany). Polyethyleneimine (PEI, 50 wt %), glutaraldehyde (GA, 50 wt%), (triethoxy-silyl)butanal (TEA), 3-(2-aminoethylamino)propyl)trimethoxysilane (AEAPS), (1H, 1H, 2H, 2H-perfluorooctyl)trichlorosilane (fluorosilane), octadecyltrichlorosilane (OTS) and *N*,*N*-dimethyl-*N*-octadecyl-3-aminopropyltrimethoxysilylchloride (DMOAP) were purchased from Sigma-Aldrich (Singapore). Thermotropic liquid crystal, 4-pentyl-4'-cyano-biphenyl (5CB) and methanol were purchased from Merck (Japan). Phosphate buffer saline (PBS) was acquired from 1st Base (Singapore). All aqueous solutions were prepared using deionized (DI) water with a resistance of 18.2 MΩ cm^{-1} (Millipore).

5.2.2 Surface modifications of glass slides

Hydrocarbon-terminated slides were prepared by immersing clean glass slides into DMOAP solutions (see Section 3.2.4) or heptane solution containing 0.5 mM OTS for 1 h (Aliño and Yang **2011;** Xue et al. **2008**). Fluorine-terminated slides were prepared via vapor deposition by placing 50 μL of fluorosilane next to glass slides under vacuum overnight (Sharpe et al. **2005;** Tada and Nagayama **1995**). Aldehyde-terminated slides were prepared by immersing the slides in methanolic solution

containing 2% (v/v) TEA for 2h (Lai et al. **2009**). Amino-terminated slides were prepared by immersing the glass into aqueous solution containing 2% (v/v) AEAPS in 50C for 1h (Xu et al. **2009**). The slides were then rinsed with DI water and blow-dried with N_2. After functionalization, all slides were placed in a 100 ºC vacuum oven for 15 min to allow cross-linking to occur.

5.2.3 Inkjet printing of LCs

LCs were inkjet-printed on glass slides by using Dimatix Materials Printer DMP-2800 (Fujifilm, USA). First, about 1 mL of LC was placed inside a cartridge (1 pL or 10 pL). The printing height was set at 990 μm. The operating temperature was maintained at 70ºC to lower the viscosity of LC. To ensure that the nozzle was not clogged, the jets were purged for 2 min before printing. The LC was printed at a firing voltage of 25V. The printer was programmed to print LC droplets spaced 150 μm apart (to avoid overlapping of adjacent droplets) on a 25 × 14 mm glass slide in each run. Detailed waveform settings and parameters used can be found in the Appendix C. After printing, the slides were stored overnight to allow the LC droplets to stabilize.

5.2.4 Flushing the LC droplets

A schematic diagram of the experimental setup device is shown in Figure 5.1. The bottom plate of the open rectangular channel was made from a clean glass slide (65 mm × 14 mm). The sides of the channel were made by stacking thin glass slides

(65 mm × 2 mm), on top of one another, giving a total depth of 3 mm. To ensure adequate sealing between the slides, a thin layer of epoxy was applied. The device was secured with binder clips and dried overnight. A clean or functionalized glass slide with printed LC droplets was then placed at one end of the channel.

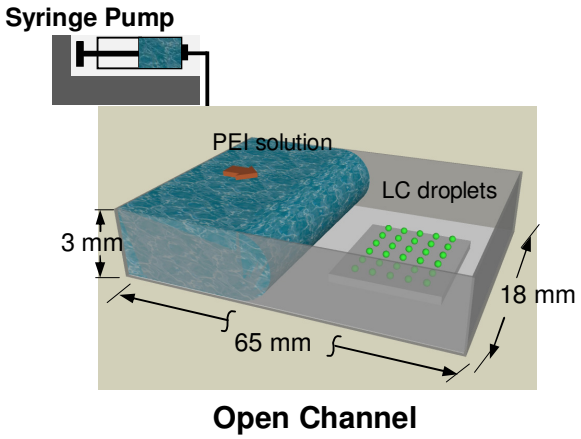

Figure 5.1 Schematic diagram of the experimental setup.

A digital syringe pump NE-4000 (New Era Pump Systems, USA) was used to flush the PEI solution horizontally from the other end of the channel at a constant flow rate. PEI solution was composed of 10 mM of PBS buffer containing 1% PEI to stabilize the LC droplets. The PEI solution was introduced from the other end of the channel with flow rates varying from 2 to 1000 mL/h. Flushing experiments were done in triplicates.

5.2.5 Contact angle and interfacial tension measurements

Procedures for water contact angle measurements of the slides can be found in Section 3.2.4. Meanwhile, interfacial tensions between 5CB, glass, and aqueous PEI solution were measured using pendant drop shape analysis (KSV Cam 200). This method was performed by suspending a drop of 5CB in air (for 5CB-air interfacial tension) or in PEI solution (for 5CB-PEI interfacial tension). The shape of the pendant drop was then analyzed via software to fit Young-Laplace equation of capillarity to estimate interfacial tension (Rotenberg et al. **1983**).

5.2.6 Reaction with glutaraldehyde (GA)

After flushing out LC droplets, about 500 mL of PEI solution was gently pipetted out from the channel and replaced with DI water. Then, GA (5 wt%) solution was added in 10 μL increments into the aqueous solution from one side of the channel. The solution was allowed to diffuse throughout the channel. After 1h, images of the LC droplets were taken under crossed polarizers.

5.2.7 Image analysis of LC droplets

Bright-field and polarized-light images of the LC droplets were acquired by using an optical microscope (Nikon ECLIPSE LV100POL, Japan) equipped with a digital camera. Size diameter of the emulsified LC droplets was measured by using Nikon's imaging software (NIS-Elements D).

5.3 Results and Discussion

5.3.1 Dispensing LC using inkjet

We first carried out some studies to understand parameters that affect the inkjet printing of LC 5CB. In Table 5.1, we list specifications for ink that can be used in inkjet printing. Physical properties of LC 5CB are also listed for comparison.

Table 5.1 Ink requirements for inkjet printing

Properties	Acceptable ranges[1]	LC (5CB)
Viscosity	10 – 12 cP	40 cP
Surface tension	32 – 42 dynes/cm	40 dynes/ cm[2]
Boiling point (°C)	> 100 °C	400 °C[3]
pH	4 – 9	
Specific gravity	> 1	1.016 @ T = 25 °C (nematic)[4]
		0.980 @ T = 70 °C (isotropic)[4]

[1](Fujifilm 2008); [2](Carboni *et al.* **2008**); [3](Gonzalo et al. **1997**); [4](Deschamps et al. **2008**)

From Table 5.1, we can see that the viscosity of 5CB (40cp) is higher than the requirement (10-12 cp), and that prevents 5CB from dispensing smoothly at ambient conditions. To lower the viscosity of 5CB, we increased the temperature to 70 °C. At this temperature 5CB can be dispensed, but the quality of the droplets formed is affected by the voltage settings. Figure 5.2 shows that when the voltage is 40V, some stray spots caused by dissociation of the main stream, can be found on the surface.

The number of stray spots, however, decreases as the voltage is decreased from 40V to 30V. Meanwhile, when the voltage is 15V – 25V, the system enters a "dripping" regime under which a periodic drop emission of the ink can be found near the printing head nozzle (Cordero et al. **2011**). Based on the observation, 25V was chosen to be the optimized voltage. This gives an equivalent Weber number (*We*) of 14.3, Reynolds number (*Re*) of 3.9, and Ohnesorge number (*Oh*) of 0.9. This set of dimensionless numbers falls within the "printable fluid" region (Derby, **2010**). Under this voltage, each printed LC droplet has a diameter of 67.8 ± 1.3μm as shown in Figure 5.2.

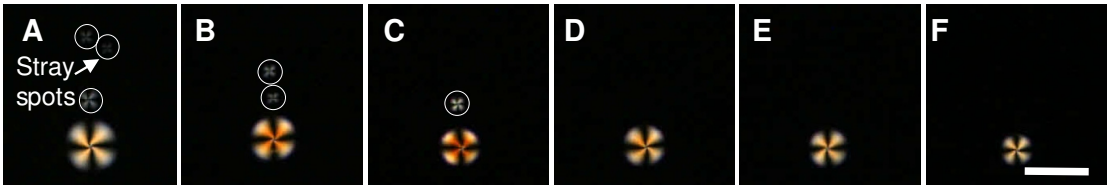

Figure 5.2 Effect of voltage on the printed LC droplets. (A) 40 V, (B) 35 V, (C) 30 V, (D) 25 V, (E) 20 V, and (F) 15 V. The volume of each LC droplet is 10 pL. Increasing the voltage increases the number of stray spots deposited on the surface. Scale bar is 100 μm.

One limitation of the method mentioned above is that the maximum volume of each droplet is either 1pL or 10 pL (depending on the nozzle diameter of the cartridge used). Since the inkjet printer can print on the same spot with high accuracy, we further studied whether the size of each LC droplet could be controlled by printing multiple times on the same spot. Figure 5.3A shows that 1, 2, 4, 6, and 8 pL were produced by spotting 1, 2, 4, 6 and 8 layers using the 1 pL-cartridge while 10, 30, 50, 80 and 100 pL were produced by spotting 1, 3, 5, 8 and 10 layers using the 10pL-

cartridge. Figure 5.3B shows that the diameter of the LC droplet increases with the increasing droplet volume. This result demonstrates that it is possible to control the volume of each printed LC droplet precisely by using inkjet printing.

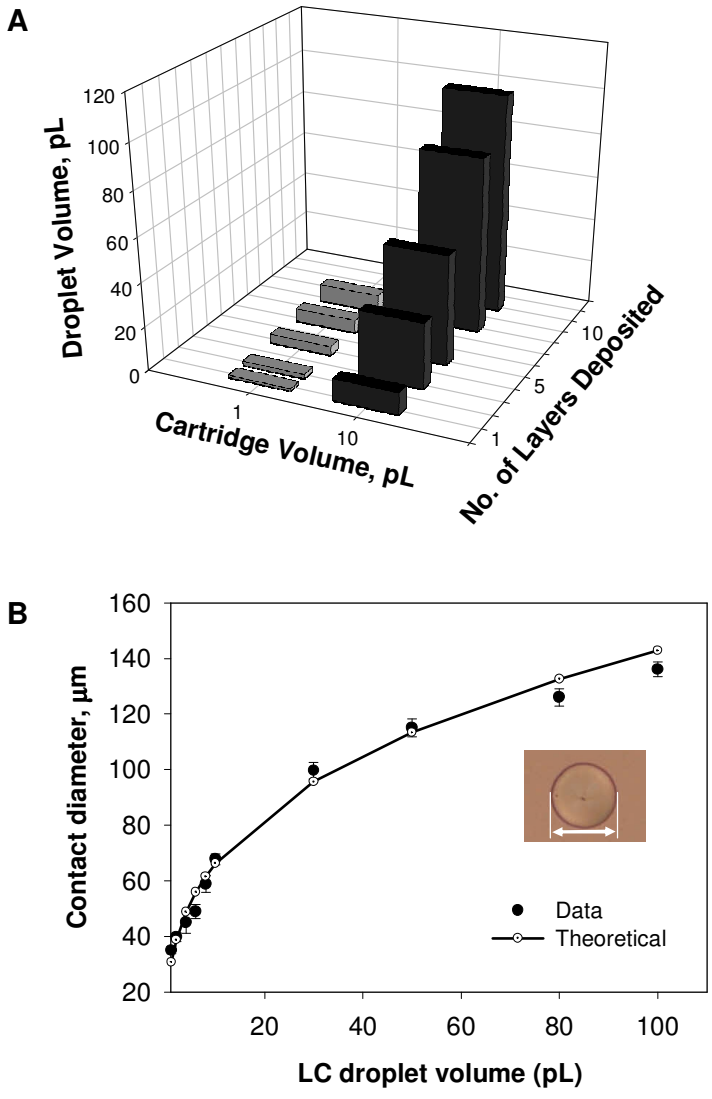

Figure 5.3 (A) Effects of multilayer deposition and cartridge on the LC droplet volume. (B) Contact diameter of the LC droplet as a function of droplet volume.

5.3.2 Releasing LC droplets from solid surfaces to solutions

To release the droplets from the surface, we flushed the LC droplets with PEI solution horizontally at one end of the channel as shown in Figure 5.1. Figures 5.4A and 5.4B show that the LC droplets were easily detached and lifted off from the glass surface into the solution. On the other hand, when the LC droplets were printed on a glass slide coated with DMOAP, they could not be lifted off as shown in Figures 5.4D and 5.4E.

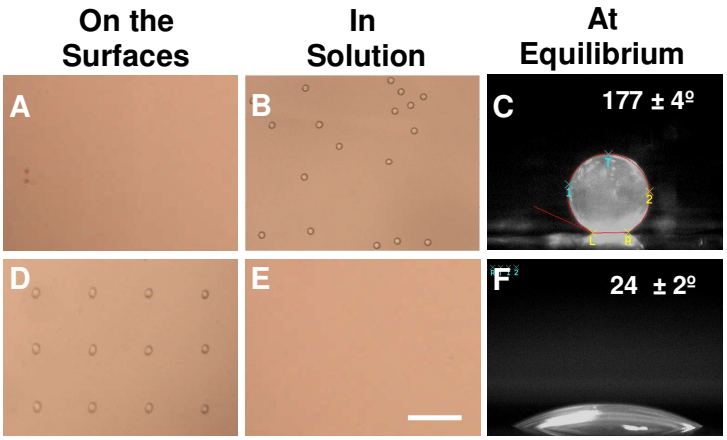

Figure 5.4 Images of the LC droplets on (A-C) clean glass and (D-F) DMOAP-coated glass. LC droplets (A,D) on the surface and (B,E) in the solution after flushing with PEI solution. (C,F) Contact angles of LC immersed in PEI solution under static conditions. Scale bar is 250 µm.

This result is puzzling because LC tends to wet clean glass (rather than DMOAP-coated glass). Therefore, one would expect that the LC droplets could not

be lifted off from a clean glass surface. However, since LC droplets are immersed in an aqueous PEI solution, the interaction between the solution and glass should be taken into account. Behaviors of a three-phase system can be described by using spreading parameters S_i,

$$S_1 = \gamma_{23} - (\gamma_{12} + \gamma_{13}) \quad [5.1]$$

$$S_2 = \gamma_{13} - (\gamma_{21} + \gamma_{23}) \quad [5.2]$$

$$S_3 = \gamma_{12} - (\gamma_{31} + \gamma_{32}) \quad [5.3]$$

where γ is the interfacial tension between two phases. 1, 2 and 3 represent glass, PEI solution and LC respectively (see Appendix C). On the basis of these spreading parameters, there are three different possibilities (Barikbin et al. **2010;** Loxley and Vincent **1998;** Pannacci et al. **2008;** Torza and Mason **1970**): (I) complete wetting when $S_1 < 0$, $S_2 < 0$ and $S_3 > 0$; (II) partial wetting when $S_1 < 0$, $S_2 < 0$, and $S_3 < 0$; and (III) nonwetting when $S_1 < 0$, $S_2 > 0$ and $S_3 < 0$. In the first case, the LC droplet cannot be lifted off from the surface whereas in the third case, the LC droplet can be lifted off from the surface and carried away by the solution. Table 5.2 shows interfacial tensions between two phases and the corresponding spreading parameters. When a clean glass slide is used, the three spreading parameters are all negative (S_1 = - 33.00, S_2 = - 0.02, S_3 = - 32.14). Under a static condition, the LC forms a spherical drop that partially wets the glass surface with a large contact angle (177.0° ± 3.7°) as shown in Figure 5.4C. However, since S_2 is very small, the system is close to the nonwetting category. This is consistent with the large contact angle observed in

Figure 5.4C. Therefore, when the LC is subjected to a flow, it can be easily lifted off from the surface.

Table 5.2 LC Contact Angle, Interfacial Tension, and Spreading Parameters for LC Droplets Supported on Different Surfaces

Surface	Contact Angle (°)	Interfacial Tension (mN/m)	Spreading Parameter, S_i*
Glass	177.0 ± 3.7	γ_{12} = 16.51 γ_{13} = 32.57 γ_{23} = 16.08	S_1 = - 33.00 S_2 = - 0.02 S_3 = - 32.14
DMOAP	24.0 ± 2.2	γ_{12} = 63.62 γ_{13} = 48.93 γ_{23} = 16.08	S_1 = - 96.48 S_2 = - 30.77 S_3 = - 1.39
Aldehyde-terminated	65.3 ± 0.5	γ_{12} = 39.41 γ_{13} = 32.69 γ_{23} = 16.08	S_1 = - 56.02 S_2 = - 22.80 S_3 = - 9.36
Amino-terminated	52.8 ± 3.1	γ_{12} = 40.86 γ_{13} = 31.14 γ_{23} = 16.08	S_1 = - 55.92 S_2 = - 25.80 S_3 = - 6.36
Fluorinated	14.6 ± 0.5	γ_{12} = 84.94 γ_{13} = 69.38 γ_{23} = 16.08	S_1 = -138.24 S_2 = - 31.64 S_3 = - 0.52

* 1- glass 2- water, and 3- LC.

When the DMOAP surface is used, however, the three spreading parameters become S_1 = - 96.48, S_2 = - 30.77, and S_3 = - 1.39. This scenario also belongs to the partial wetting category, but it is closer to the complete wetting category because of the very small negative value of S_3. As shown in Figure 5.4G, the LC droplet has a very small

contact angle (24.0° ± 2.2°) in the PEI solution, suggesting that it is difficult to lift off the LC droplet even under a flow condition.

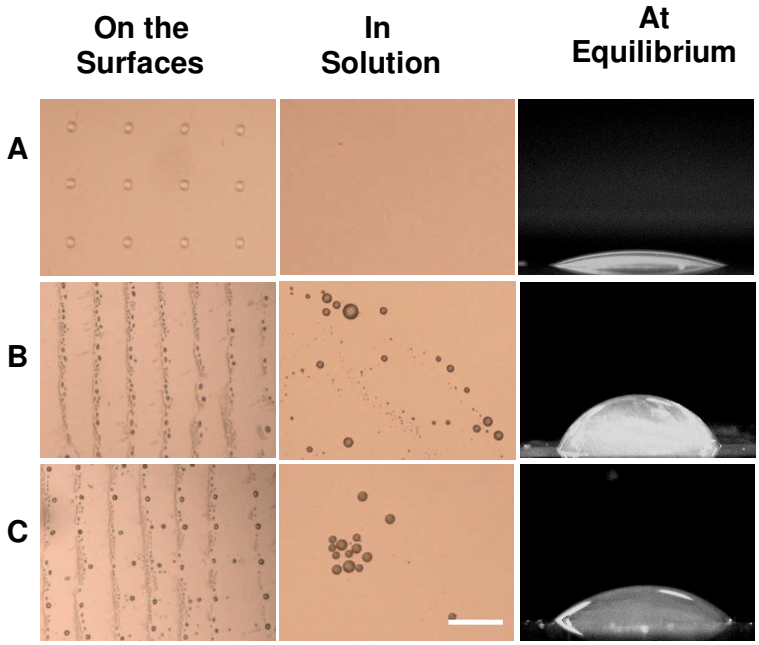

Figure 5.5 Images of the LC droplets on the surface and in the solution after flushing with aqueous PEI solution. Contact angles of LC immersed in aqueous PEI solution and resting on (A) fluorinated, (B) aldehyde-terminated, and (C) amino-terminated surface under static conditions. Scale bar is 250 μm.

We also studied other surfaces with different chemical functionalities (see Figure 5.5). A fluorinated surface has a contact angle of 14.6° ± 0.5°, and three spreading parameters are closer to the complete wetting category, making it similar to the DMOAP surface. Aldehyde-terminated and amino-terminated surfaces are borderline cases between clean glass and DMOAP surface as shown by their contact angles of 65.3° ± 0.5° and 52.8° ± 3.1°, respectively. As a result, some LC droplets can be lifted off from these surfaces, but the process is incomplete. Among all

surfaces tested, the clean glass slide gives the best result because all LC droplets can be lifted off from the surface by using PEI solution. We used clean glass slides for the subsequent experiments.

5.3.3 Effect of flow rates

To determine whether monodisperse LC droplets can be created at different flow rates, we controlled the flow rates of the PEI solution (from 2 to 1000 mL/h) to flush LC droplets (1 pL) supported on glass, and quantified the polydispersity index (PDI) of the emulsified LC droplets. PDI is defined as the standard deviation of the size distribution divided by the mean droplet size (Baroud et al. **2010**). Droplets are considered monodispersed if the PDI is below or equal to 0.05.

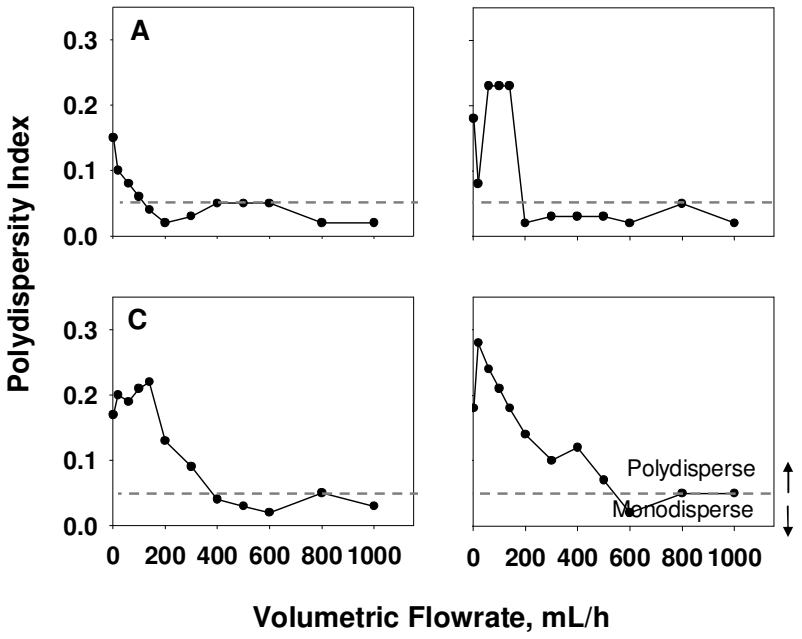

Figure 5.6 Effect of flow rates on the PDI of the emulsified LC droplets. (A) 1 pL, (B) 10 pL, (C) 50 pL, and (D) 100 pL LC droplets.

Figure 5.6 shows PDI of the LC droplets at different flow rates. At a higher flow rates ($\Phi_v \geq 140$ mL/h), the PDI is 0.02 – 0.05, which suggests that the LC droplets are monodispersed. On the other hand, at lower flow rates ($\Phi_v < 140$ mL/h), the droplets have a PDI between 0.06 – 0.15. These results led us to propose a model as shown in Figure 5.7.

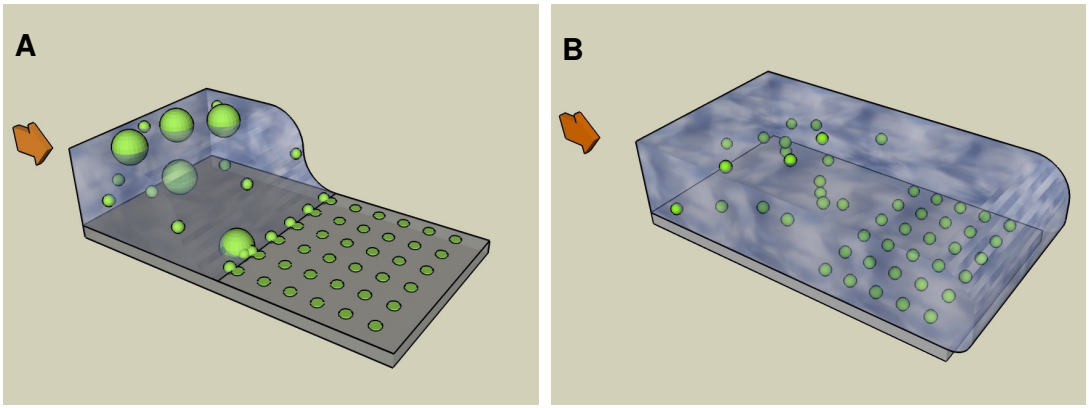

Figure 5.7 Fate of printed LC droplets after flushing with PEI solution under (A) low ($\Phi_v < \Phi_c$) and (B) high ($\Phi_v \geq \Phi_c$) flow rates. The LC droplets are supported on a clean glass slide.

At high flow rates, the LC droplets on the surface are quickly flooded with the PEI solution. In this case, the LC droplets remain in a spherical shape and can be easily lifted off from the surface. At low flow rates, however, the contact line moves too slowly to submerge the LC droplets completely. During this process, part of the LC droplet is submerged in the PEI solution when it meets the contact line, while the remaining part is still in the air. These LC droplets can simply 'ride' the contact line and coalesce and form bigger droplets during this process. While we use the

horizontal setup for illustration, we also show that the printed LC droplets can be released in a vertical setup. Detailed experimental results and two videos are provided in Appendix C.

We also investigated whether we could create monodisperse LC droplets having bigger sizes by multiple printing and flushing. Figure 5.6 shows the PDI for LC droplets having a volume of 10 pL, 50 pL and 100 pL, respectively. At low flow rates, the PDI values for 10 pL, 50 pL, and 100 pL LC droplets range from 0.08 – 0.23, 0.09 – 0.22, and 0.07 – 0.28, respectively. In addition, the critical flow rate (Φ_c), the flow rate needed to reach a PDI of 0.05, increases with the increasing volume of the LC droplet. For example, critical flow rates for 10 pL, 50 pL, and 100 pL LC droplets are 200 mL/h, 400 mL/h, and 600 mL/h, respectively. Using flow rates higher than the critical value, we are able to create free LC droplets with diameters of 30 µm, 50 µm and 62 µm in solutions as shown in Figure 5.8. Interestingly, LC droplets of different sizes have different optical textures. The center of the droplets gives different colors ranging from white, blue, pink and orange for 15 µm, 30 µm, 50 µm, and 62 µm, respectively. In addition, the number of concentric rings in each LC droplet increases with the increasing size of the droplet. These results indicate that when the size of the LC droplets is varied, the birefringence patterns, which are depicted by the concentric rings, across the droplet change. These bands can be attributed to the wavelength-specific retardation of light passing through the LCs which is a function of thickness (Tercero Espinoza et al. **2004;** Verhoeff et al.

2011). For droplets, the birefringence decreases when going from the drop center to the edge presumably due to the decreased length of the optical path through the drop.

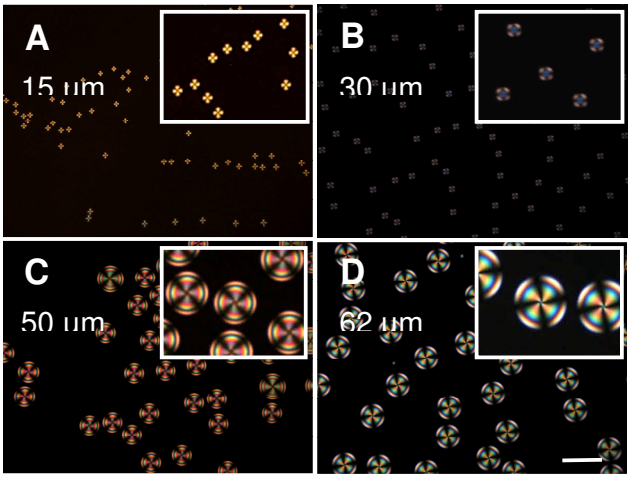

Figure 5.8 Optical textures of free LC droplets having different sizes. (A) 1 pL, (B) 10 pL, (C) 50 pL, and (D) 100 pL, respectively. Scale bar is 100 µm.

5.3.4 Using monodisperse LC droplets for detecting GA

As shown above, monodisperse LC droplets are a promising tool for creating LC-based sensors because achieving uniform sizes of the LC droplets imply a unanimous effect of the interaction of analytes with the bulk LC inside the droplets. As a proof of concept, we used monodisperse LC droplets (1 pL) to detect GA. It is well-known that the aldehyde groups of GA can react with the amine groups of PEI through imine bonds (Aliño *et al.*, **2011**). Figure 5.9 shows the optical appearance of the LC droplets before and after the addition of GA. From the figure, it is evident that the LC inside the droplets before the addition of GA exhibits a radial configuration in

which the point of defect is located at the center of the LC droplet (and that the defect does not move as the LC droplets rotates). We noted that the LC droplets still retain their radial configuration even when 10 μL of GA solution was added. This has an equivalent surface density of 2200 nm^{-2} GA. At this condition, the amount of GA molecules on the surface of the LC droplets is too low to disrupt the orientational ordering of the LC inside the droplets. After adding 40 μL of GA solution (equivalent to a surface density of 8800 nm^{-2} GA, however, the single point of defect moves away from the geometric center of the LC droplet.

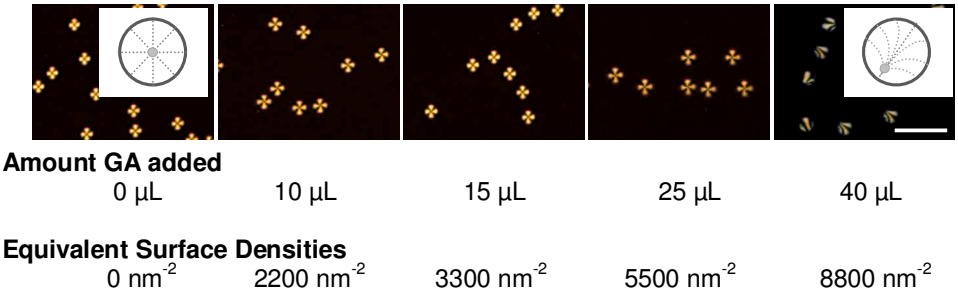

Figure 5.9 Optical appearance of the LC droplets in aqueous solution before and after the addition of GA. Equivalent GA surface densities are 2200 nm^{-2}, 3300 nm^{-2}, 5500 nm^{-2}, and 8800 nm^{-2} for 10 μL, 15 μL, 25 μL, and 40 μL of GA (5 wt%) solution added. Insets show the corresponding radial and preradial configurations, respectively. Scale bar is 100 μm.

This can be easily distinguished since the location of the defect changes as the droplets rotate. Such an observation is consistent with LC droplets exhibiting a pre-radial configuration. The pre-radial configuration can be easily distinguished from the radial configuration since the director profile of the LC radiates outward from the single point of defect and is not spherically symmetrical (Kinsinger et al. **2010**). In our past report, we show that when the surface density of GA is lower or equal to

9100 nm^{-2}, the orientational ordering of the LC inside the droplets (60 – 85 μm) is not disrupted by the GA molecules and still exhibits a bipolar configuration (Aliño *et al.*, **2011**). However, this current study shows that when the surface density of GA reaches 8800 nm^{-2}, the orientational ordering of the LC changes to a preradial configuration. We suspect that this difference is due to the different sizes of the LC droplets used. Nevertheless, the uniform transition of the LC droplets from their radial configuration to preradial configuration is evidence that the LC emulsified droplets can be used as sensing platforms to monitor chemical reactions.

5.4 Conclusion

We demonstrate a two-step method for producing monodisperse LC droplets in aqueous solutions. The first step is to dispense the LC droplets on a clean glass slide using a piezoelectric inkjet printer. Through multilayer deposition, we can control the size of the LC droplets, ranging from 1-100 pL. In the second step, the LC droplets were flushed with PEI solution in an open rectangular channel to release them into PEI solution. Flushing LC droplets supported on a clean glass at sufficiently high flow rates produces LC droplets of uniform sizes. The monodisperse LC droplets show uniform optical textures and have potential to be used in chemical and biological sensing applications.

CHAPTER 6

DETECTING PROTEINS IN MICROFLUIDIC CHANNELS DECORATED WITH LIQUID CRYSTAL SENSING DOTS

6.1 Introduction

Protein assays are important tools in food industry, biotechnology and clinical diagnostics for the quantification of proteins (Becher et al. **2006;** Wendler et al. **2005**). Recently, the incorporation of microfluidic systems in protein assays has stimulated a lot of interest both in academia and industry. Microfluidic protein assays allow the integration of standard laboratory analyses such as sample purification, separation, and detection to be carried out on a single microchip. Microfluidic protein assays have advantages over conventional techniques as they have faster response times, require fewer steps, and less sample volumes (Kuschel et al. **2002**). Nevertheless, analysis of proteins in microfluidic devices still heavily relies on conventional analytical techniques (Becher et al. **2006;** Cesaro-Tadic et al. **2004;** Gervais and Delamarche **2009;** Götz and Karst **2007;** Jiang et al. **2003;** Kim and Knapp **2001;** Koster and Verpoorte **2007;** Kuschel et al. **2002**). For example, proteins can be detected by using an ultraviolet-visible (UV/Vis) spectrometer or an ultraviolet laser induced fluorescence (UV-LIF) spectrometer after the reaction of proteins have reacted with fluorescent dyes (Gervais and Delamarche **2009**), chemical dyes (Bradford assay), or copper ions (Lowry assay). Alternatively, analytical instrumentation such as high performance liquid chromatography (HPLC), surface plasmon resonance (SPR) and mass spectrometry (MS) were recruited to analyze the solution at the outlet (Becher et al. **2006**). These techniques have their limitations as protein labeling and bulky equipment are required. This poses a challenge in the

potential utilization of these microfluidic protein assays for point-of-care (POC) applications.

Considering the limitations mentioned above, we studied the feasibility of incorporating liquid crystals (LCs) in microfluidic channels as a new sensing platform. During the past decade, LCs have been successfully exploited for the detection of proteins. The presence of proteins causes changes in the orientational ordering of an LC, which can be monitored through the intensity of light transmitted through the LC. The LC-based sensing method has advantages over conventional techniques mentioned above because it does not require any bulky equipment and labeling of proteins. In these systems, LCs are often confined in a metallic grid supported on a glass slide to avoid dewetting (Brake and Abbott **2002;** Brake et al. **2003a;** Hartono et al. **2008;** Hartono et al. **2009a;** Hartono et al. **2009b;** Jang and Hu **2010;** Park and Abbott **2008;** Yang et al. **2004**). Because LCs are immiscible with water, the interactions between target molecules (e.g. amphiphiles, polymers, proteins) in the solution and the LCs can be studied at the LC/aqueous interface. Park and Abbott, for instance, used LCs in grid to detect an enzyme, trypsin, in aqueous solutions (Park et al **2006**). They found that when trypsin cleaved oligopeptide-terminating lipids self-assembled at the LC/aqueous interface, LCs in grid gradually changed their orientation, causing a distinct optical response. A metallic grid which is not completely flat, however, may cause a distorted LC interface, and sometimes filling a small grid completely with LCs is nontrivial. Both factors may lead to inconsistent results in such system (Jang and Hu **2010**). Moreover, a grid cannot be

incorporated into a microfluidic channel because of its size. Recently, LC droplets were also considered as a new platform for sensing. Emulsified LC droplets address the need to confine the LC in the grid and the related issues mentioned previously. LC droplets can be produced in various ways particularly through vortexing, sonication, and silica templates. Nonetheless, it is still very difficult to prepare uniform and well-aligned LC droplets which fit a microfluidic channel. In this study, we exploited inkjet printing techniques to print LC dots directly on a hydrophobic surface which can retain LC droplets. Because LC dots prepared by inkjet printing are uniform, and their small sizes are comparable to the dimensions of a microfluidic channel, they can be incorporated into microfluidic channels as microscopic sensors for protein detection. Moreover, because the LC dots are embedded inside microfluidic channels, this system allows us to detect proteins in both continuous and batch systems.

To address the issue mentioned above, we exploited inkjet printing techniques (Delaney et al. **2009;** Subramanian et al. **2005;** Volkman et al. **2004;** Wijshoff **2010;** Zheng et al. **2011**) to print LC dots directly on a solid surface. Although the applications of inkjet printing for patterning nanoparticles for flexible electronic circuits (Subramanian et al. **2005;** Volkman et al. **2004**) and deposition of biomolecules (Delaney et al. **2009;** Zheng et al. **2011**) have been around for several decades, LC has never been used as "ink" in this technology to the best of our knowledge. Because LC dots prepared by inkjet printing have a uniform and small size that is comparable to the dimensions of microfluidic channel, they can be

incorporated into microfluidic channels as microscopic sensors for protein detection. Moreover, because the LC dots are embedded inside microfluidic channels, this system allows us to detect protein both in a continuous and a batch system.

6.2 Experimental Section

6.2.1 Materials

Bovine serum albumin (BSA), fluorescein 5(6)-isothiocyanate (FITC), hexadecyltrimethylammonium bromide (CTAB), and *N*,*N*-dimethyl-*N*-octadecyl-3-aminopropyltrimethoxysilylchloride (DMOAP) were purchased from Sigma-Aldrich (Singapore). Phosphate-Buffered Saline (PBS) 10× was obtained from 1st BASE (Singapore). Ethanol and methanol were purchased from Fischer (Singapore). Thermotropic liquid crystal, 4-pentyl-4'-cyano-biphenyl (5CB) was purchased from Merck (Japan) and used as received. Poly(dimethylsiloxane) (PDMS) microfluidic channels were prepared from Sylgard 184 silicone elastomer kit (Dow Corning, USA). All aqueous solutions were prepared using deionized (DI) water with a resistance of 18.2 MΩ cm^{-1} (Millipore). Glass slides were purchased from Marienfield (Germany).

6.2.2 Preparation of DMOAP-coated Slides and LC-filled Grids

Glass slides were cleaned and functionalized with DMOAP as shown in Section 3.2.4 (Aliño and Yang **2011**). Copper grids (100 square mesh, Electron

Microscopy Sciences, U.S.A.) were cleaned sequentially in ethanol and methanol, dried under nitrogen, and heated at 100 ºC for 24h. These grids were then placed on a piece of DMOAP-coated glass (~ 8 × 13 mm) and filled in manually with 0.3 μL of 5CB using a pipet. The excess LC was removed by using a capillary tube.

6.2.3 Preparation of LC dots

First, LC (5CB) was printed on a DMOAP-coated glass slide by using Dimatix Materials Printer DMP-2800 (Fujifilm, USA). The printer has a 1 pL-nozzle cartridge that is filled with 5CB, and the voltage and temperature were maintained at 25 V and 60 ºC, respectively. Pulse was fired at a slew rate of 0.38 for 3.712 μs under a maximum jetting frequency of 5 kHz. To avoid clogging, the print cartridge was periodically cleaned every 240 s during printing. The LC dots were spaced 100 μm apart. For surfactant and protein adsorption studies, 2 × 2 mm LC arrays were printed on a DMOAP-coated glass slides (~5 × 13 mm), and each array contains 441 spots. Experiments were done in triplicates.

6.2.4 Response of LC to CTAB and protein

A slide supporting LC dots was immersed into a small glass petri dish containing 1 mM of PBS buffer and 0.137 mM of CTAB. After 30 min, the optical appearances of the LC dots were observed. To investigate interactions between protein BSA and LC, the whole slide was briefly rinsed with PBS buffer and DI water

and then immersed into BSA solution. The BSA solution was prepared by dissolving BSA in PBS buffer containing 0.137 mM of CTAB. After 30 min of incubation, the optical appearances of the LC were recorded again. To quantify the luminosity of the LC image, each image was converted to gray scale (Govindaraju et al. **2007**) and the average pixel brightness of a region was calculated. For convenience, we refer to those images having luminosity greater than 2 as "bright" image whereas those images with luminosity lower than 2 are "dark" images.

We also examined the adsorption of BSA at the LC/water interface by using a fluorescence method. Firstly, a slide supporting the LC dots was rinsed with DI water to remove excess proteins. Next, the slide was immersed into PBS buffer containing 0.1 mg/mL of FITC. After 2h of incubation, the slide was rinsed repeatedly with DI. The slide was then immersed in PBS buffer and its fluorescence intensities were measured at wet state. If proteins are present, amino group in lysine residues of the protein can react with FITC and give green fluorescence. In all experiments, images of LC dots were acquired by using an optical microscope (Nikon ECLIPSE LV100POL, Japan) with a fluorescence filter set (FITC/EGFP). Experiments were done in triplicates.

6.2.5 Flushing LC dots with buffer solutions in microfluidic channels

A slide supporting the LC dots was placed on one side of the rectangular glass trough (L × W × H = 65 mm × 14 mm × 3 mm). Digital syringe pump NE-4000 (New Era Pump Systems, USA) was used to deliver CTAB solution at a constant flow rate. The CTAB solution was introduced from the other end of the trough with flow rates varying from 2 to 900 mL/h, giving equivalent linear velocities from 0.001 to 0.595 cm/s. Flushing experiments were done in triplicates. For protein detection, about 1.5 μL of BSA solution was dispensed into the inlet reservoir. The solution was allowed to fill the channel via capillary flow with a velocity of 0.41 cm/s. After 30 min of incubation, image analysis of the LC was carried out.

6.2.6 Water contact angle and interfacial tension measurements

Water contact angles were measured by using a goniometer (VCA Optima) from AST (U.S.A.) as described in previous work (Aliño et al. **2012**). Meanwhile, interfacial tension between 5CB, glass, and CTAB solution was measured using pendant drop shape analysis (KSV Cam 200) (Rotenberg et al. **1983**).

6.2.7 Preparation of Microfluidic Devices Incorporated with LC Dots

Microfluidic patterns (width w = 300 μm, height h = 160 μm and length l = 45 cm) were prepared as shown in Appendix D. These patterns were fabricated onto a silicon wafer by using photolithography with a negative photoresist (SU-8). Microfluidic channels were then molded from PDMS using standard soft lithography techniques (Xia and Whitesides **1998;** Xue et al. **2009**). PDMS was prepared by mixing PDMS elastomer with curing agent in a weight ratio of 10:1, and the mixture was degassed in vacuum to remove air bubbles. The PDMS mixture was then poured onto the silicon master and cured at 70 ºC for 3 h. After curing, the PDMS microfluidic channel was cut and peeled off from the master. One inlet and one outlet reservoirs (1.5 mm in diameter) located at both ends of the channel were punched out of the microfluidic channel. In order to bind PDMS to the DMOAP-coated slide to form a closed microfluidic system, the PDMS was treated with oxygen plasma (100W) for 45s.

6.3 Results and Discussion

6.3.1 Optical Response of LC Dots to Surfactants

We first studied optical response of LC dots to a cationic surfactant CTAB. We chose CTAB because it is well-known that the orientation of LC is sensitive to the

presence of CTAB in aqueous solutions (Bahr **2006;** Brake et al. **2003b;** Lockwood et al. **2008**). We noted that LC dots appear bright in PBS buffer (Figure 6.1A), but they change to dark in PBS buffer containing 0.137 mM of CTAB (Figure 6.1B). Finally, when the LC dots are transferred back to fresh PBS buffer, the LC dots become bright again (Figure 6.1C). This phenomenon, similar to that of LC-filled grid reported by Brake, *et. al.* (Brake et al. **2003b**), is caused by the reversible adsorption of amphiphilic CTAB the LC/water interface (Aliño et al. **2011;** Brake and Abbott **2002;** Brake et al. **2003a;** Brake et al. **2003b;** Lockwood et al. **2008**). The same authors also proposed that the long hydrocarbon chain of a monolayer of CTAB can penetrate the LC phase and cause a homeotropic orientation and dark appearance. Figure 6.1C has lower luminosity than Figure 6.1A, and that implies that the desorption rate of CTAB is slower than the adsorption. However, after 1h of incubation, the optical image in Figure 6.1C will eventually become the same as Figure 6.1A (data not shown). Surprisingly, the response time (from bright to dark) of the LC dots is very close to that of the LC in the grid (t~ 10s). No improvement in the response time can be found even though the size of the LC dots (~7.7 μm) is smaller than LC in the grid (~20 μm). The results led us to propose that the bright-to-dark response is an interface-driven phenomenon in both systems. Otherwise, the response time for LC dots would be faster than that of the LC in the grid. In Appendix D, we show that smaller LC dots do have faster response time when the optical response is bulk-driven such as the dissolution of ethanol in LC.

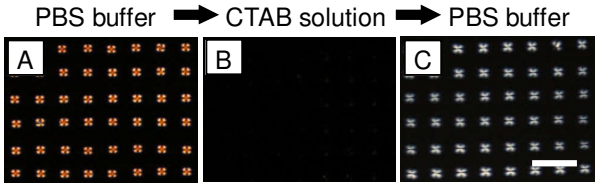

Figure 6.1 Optical images of LC dots (10 pL) in different solutions during sequential transfer. (A) PBS buffer (B) PBS buffer containing 0.137 mM of CTAB. (C) PBS buffer. Scale bar is 250 µm.

6.3.2 Effects of LC dot size on the dynamic response to CTAB

To further test the hypothesis above, we investigated how the volume of LC dots affects their optical response to CTAB. Figure 6.2 shows that the response time of all LC dots (1 pL, 5 pL, 10 pL, 50 pL and 100 pL) to CTAB is very similar (~10s). Therefore, the response time is independent of the size of the LC dots.

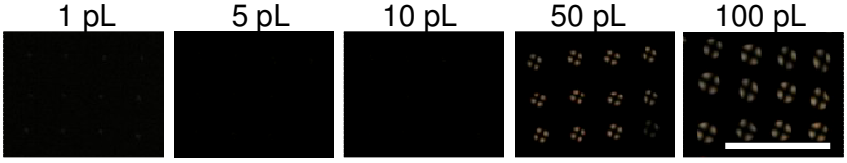

Figure 6.2 Optical appearances of LC dots having different sizes and their response to CTAB solution. Scale bar is 250 µm.

On the basis of this observation, we can conclude that the bright-to-dark response is an interface-driven phenomenon, and is independent of the LC dot size. However, we note that the final optical appearances of the LC dots are different. For smaller LC dots (1 pL, 5 pL, and 10 pL), their appearance is homogenously dark,

whereas for bigger ones (50 pL and 100 pL), they have a dark cross in the center. This is probably because bigger LC dots are similar to spherical LC droplets such that they have a curved surface. When the CTAB molecules adsorb at the LC/water interface, this causes a homeotropic boundary which can be translated into a radial configuration in the LC dots. Because the smaller LC dots give a more uniform texture, we use LC dots within the range of 1-10 pL in the following experiments.

6.3.3 Optical Response of LC Dots to Proteins

To study the response of LC dots to proteins, we immersed LC dots (supported on a slide) into a CTAB solution containing 50 μg/mL of BSA. Figure 6.3A shows that the presence of BSA causes the LC to change from dark to bright while the LC dots immersed in a CTAB solution (without BSA) remain dark. In addition, after reacting with a fluorescent dye FITC, all LC dots immersed in the CTAB solution containing BSA become fluorescent as shown in Figure 6.3A. This result confirms that the dark-to-bright transition is caused by the adsorption of BSA on the surface of the LC dots. Next, we varied the BSA concentrations, and observed the response of the LC dots after 30 min. In Figure 6.3B, LC dots show bright optical appearances when the BSA concentration is 4 μg/mL or above. On the other hand, when BSA is 3 μg/mL or lower, there is no response. This implies that there is a critical concentration of 4 μg/mL in this system. Below this value, the amount of BSA molecules adsorbed could not disturb the homeotropic orientation of the LC, thus a dark image is shown.

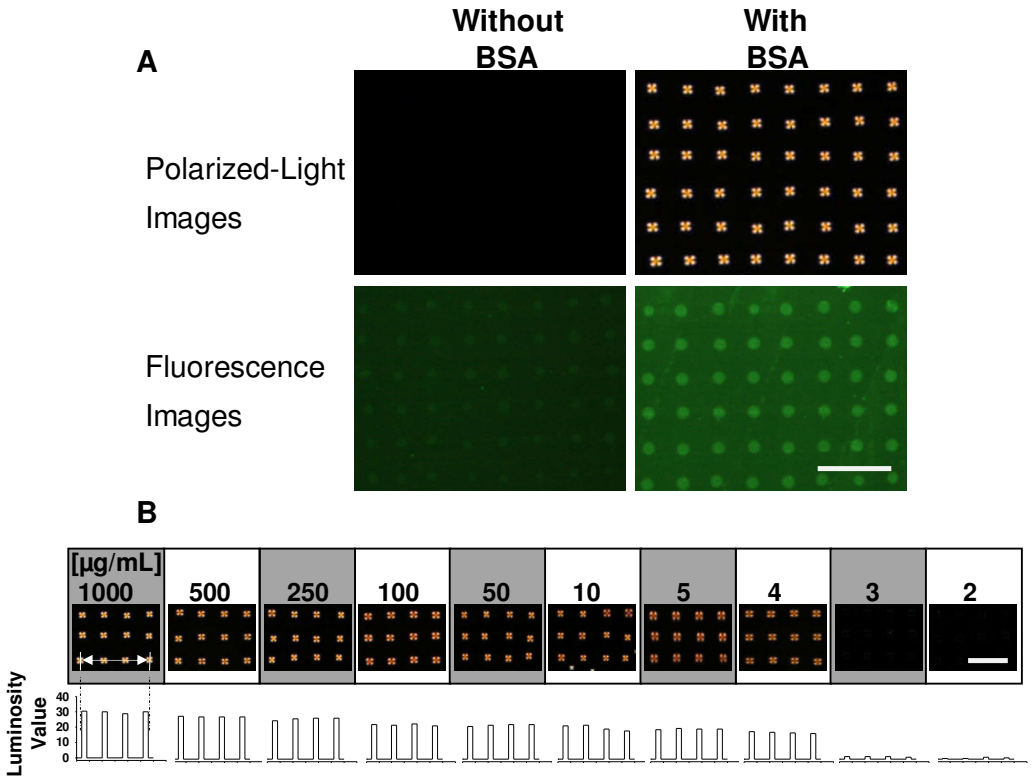

Figure 6.3 (A) Crossed-polar and fluorescence images of LCs immersed in CTAB solutions with or without BSA. (B) Crossed-polar images of LC dots immersed in solutions having different BSA concentrations. Luminosity values below 2 are referred to as a dark image. Scale bar is 250 µm.

6.3.4 Stability of LC dots under flow conditions

Although the LC dots have detection limit similar to LC in the grid, their small size allow them to be incorporated into a microfluidic channel as shown in Figures 6.4A to 6.4C. In this configuration, a number of LC dots sit in the middle of a microfluidic channel as sensing dots. To study the behavior of the LC dots in

microfluidic channels under moving solutions, we exposed LC dots of two different sizes (1 pL and 10 pL) to CTAB solution under capillary flow (0.41 cm/s) and compared their stability. Figure 6.4D shows that the 10 pL LC dots were sheared off from the surface while 1 pL LC dots remain intact (see Figure 6.4E).

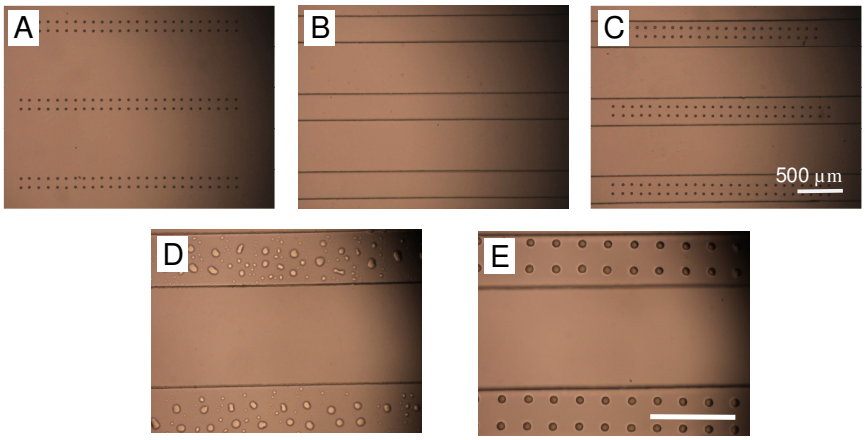

Figure 6.4 Schematic illustration of the experimental setup. (A) LC dots were spotted on a DMOAP-coated slide using inkjet printing, (B) PDMS microfluidic channel, (C) LC dots were aligned with the microfluidic channels to create a closed microfluidic system for protein detection. (D) 10 pL and (E) 1 pL LC dots after flowing CTAB solutions.

This result shows that the smaller LC dots are more stable under flow conditions. Next, we studied the behavior of the LC dots by exposing 1 pL LC dots to different flow velocities. Figure 6.5 shows that at low fluid velocities ($v < 0.198$ cm/s), the LC dots were sheared off by the solution from the surface. Meanwhile, at high fluid velocities ($v \geq 0.198$ cm/s), the LC dots remained in place.

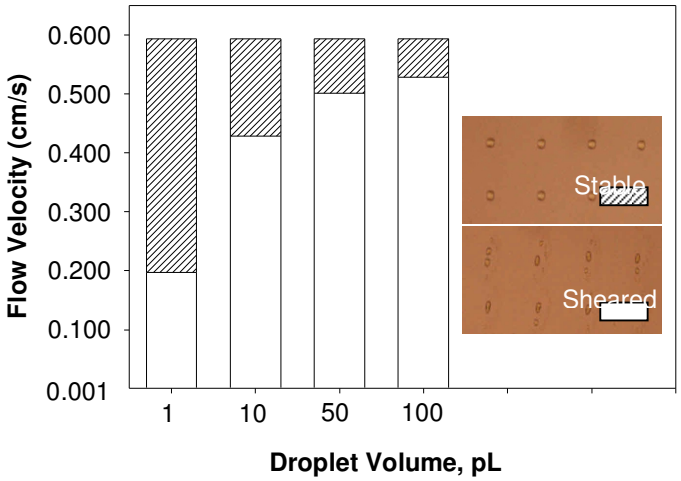

Figure 6.5 Effect of flow velocities on the stability of LC dots on DMOAP-coated surface.

This result is consistent with our previous finding that at a high flow velocity, the solution quickly submerges the entire LC dots without lifting off the LC dots (Aliño et al. **2012**). On the other hand, at a low flow velocity, the incomplete submersion of the LC dots causes some part of the LC dots is in contact with air while the other part is in the solution. Therefore, imbalance of the interfacial tension causes the detachment of LC dots from the surface and get carried away by the solution. Although the same phenomena holds true for 10, 50, and 100 pL LC dots, the fluid velocities needed to keep the LC dots in place increases as the LC dots increases (0.430, 0.503, and 0.529 cm/s, respectively). This is mainly due to the increase in the volume of the LC dots which leads to a larger contact area between the solution and LC (see Appendix D). The capillary flow velocity within the microfluidic channel is 0.41 cm/s. As a result, the 10 pL LC dots can be sheared off more easily from the

surface while the 1 pL LC dots remain in place. Because smaller LC dots are more stable, we only used 1 pL LC dots for the following experiments.

6.3.5 Detecting BSA in Microfluidic Channels

To investigate the feasibility of using 1-pL LC dots for detecting BSA in a microfluidic channel, solution containing BSA was injected into the inlet of the microfluidic channel, allowing the channel to be filled with the solution through capillary action. Because the channel is very long, the entire channel was divided into 37 sections as shown in Figure 6.6A for easy reference. Each section is 0.12-cm wide and 1.16-cm apart and contains approximately 10-12 LC dots. Figure 6.6B shows the optical appearance of LC dots in the channels after the channel is filled with BSA solution for 30 min. When the BSA concentration is 50 μg/mL, LC dots in all sections (1-37) become bright. However, when the BSA concentration is 20 μg/mL, only sections (1-20) of the microfluidic channel become bright and LC dots in sections (21-37) remain dark. This is probably due to the gradual depletion of proteins along the channel that leads to a concentration gradient of BSA in the channel. In addition, when the BSA concentration is 3 μg/mL, all sections of LC dots in the channel remain dark. This is consistent with the critical concentration of BSA (see Figure 6.3B).

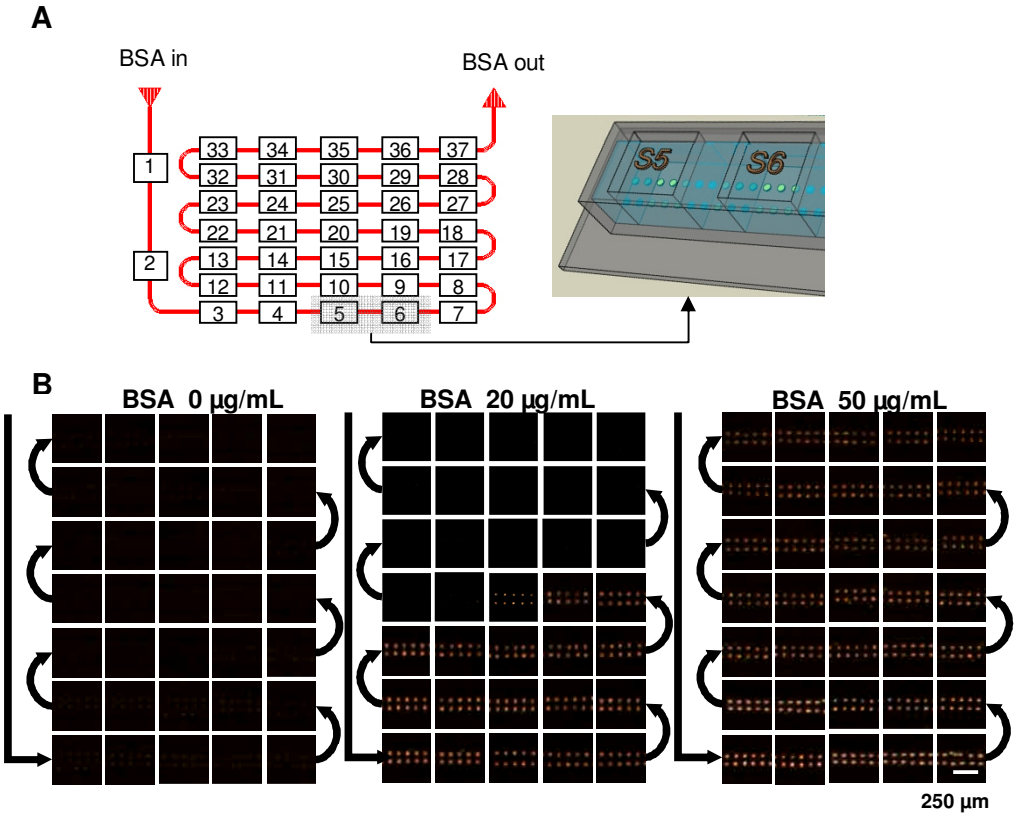

Figure 6.6 (A) Schematic diagram of the microfluidic channel. BSA solutions were dispensed into the inlet reservoir, allowing the solution to flow in capillary action through the microfluidic channel. BSA adsorbs on the surface of the LC dots and can be detected by the changes in the optical appearances of the LCs inside the channel. Sections where images are taken are spaced 1.16 cm apart. (B) Crossed-polar images of Sections (3-37) of the microfluidic channel after flowing 0, 20, and 50 µg/mL BSA solutions.

Finally, Figure 6.7 shows the correlation between the number of bright section and BSA concentration. We can see that the number of bright section increases linearly with the BSA concentration until 40 µg/mL. At this concentration, BSA covers the entire channel surface, and that causes LC dots in all sections to be bright. From Figure 6.7, it is possible to estimate BSA concentration simply by counting the

number of the bright sections in the microfluidic channels. This provides a simple method to estimate BSA concentration in an unknown sample.

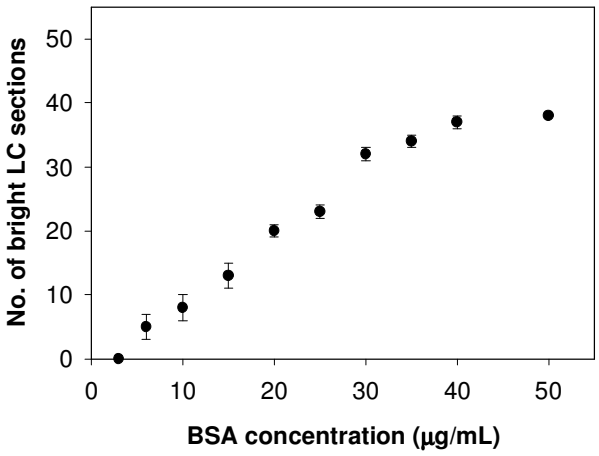

Figure 6.7 Correlations between the number of bright LC sections and BSA concentration.

6.4 Conclusions

We have successfully demonstrated the integration of LC dots inside the microfluidic channels as a sensing tool to detect BSA. These LC sensing dots can be prepared by using inkjet printing technology with LC as an ink. By using this technique, we are able to spot LC dots on a surface with a desired pattern and controllable dot size. However, only small LC dot of 1 pL shows good stability under flowing condition whereas bigger LC dots can be sheared off from the surface easily. By using the 1 pL LC dot, BSA can be detected inside the microfluidic channel, and

its concentration can be estimated by counting the number of bright section in the microfluidic channel. We anticipate that such design will be useful especially in the POC applications of microfluidic protein assay.

CHAPTER 7

CONCLUSIONS AND RECOMMENDATIONS FOR FUTURE WORK

7.1 Conclusions

The work in this thesis explores the use of LCs in developing alternative protein assays, demonstrating their potential to detect and quantify protein biomarkers in a simple, effective, and label-free way. One particular application of these protein assays is for the diagnosis and prognosis of CKD patients as demonstrated in Chapter 3 in this thesis. The novel LC-based protein assays developed in this thesis can be broadly divided into two categories: detection of proteins on a solid substrate and in aqueous solutions, respectively.

First, a label-free protein assay was developed in order to detect protein biomarkers such as HSA on a solid surface (Chapter 3). This objective was accomplished first by immobilizing AHSA antibodies on the surface for binding HSA. Subsequently, a thin LC layer was applied to the surface as signal reporters. This thin layer of LC generates bright optical textures when HSA binds to the surface. In addition, we addressed the issue of protein quantifications. Unlike previous system in which LC gives bright optical textures whenever the protein concentration is higher than the critical concentration, we incorporated a dilution protocol in this assay such that different protein concentrations can be reflected as different number of spots on the surface.

Meanwhile, the use of LC droplets as hosting and sensing platforms for protein immunoassays in solution was demonstrated in Chapter 4. In this type of protein assay, we produced LC droplets which move freely and suspend in aqueous solutions. Each LC droplet serves as an independent "microsensor" whose optical appearance is determined by the presence of target proteins in the solution. This is because orientational configurations in each LC droplet are influenced by the formation of antigen-antibody complex on the surface of the droplet. Since LC is birefringent, different orientational configurations lead to different optical textures under crossed polarizers. A great advantage of this protein immunoassay is that LC droplets can be tailored specifically for a particular protein target. This can be done in a straightforward manner by tethering different antigen probes to the surface of the LC droplets.

In Chapter 5, we presented a two-step method to generate monodisperse LC droplets in aqueous solutions. In the first step, we exploited inkjet printing to dispense uniform LC droplets on a solid surface. Uniform LC droplets, ranging from 35 to 136 μm in diameter, can be prepared by using multiple printing on the same spot. In the second step, we flushed the LC droplets with a stream of aqueous solution in an open rectangular channel. Factors that determine the polydispersity of the LC droplets include flow rates and surface wettability. Under appropriate experimental conditions (i.e. when the surface is glass and the flow rate is sufficiently

high), the LC droplets can be lifted off completely and carried away by the solution, forming free LC droplets (15 to 62 μm in diameter). These free LC droplets can respond to a chemical reaction, and change their optical textures uniformly.

Finally, a label-free microfluidic protein assay was developed in Chapter 6. This type of assay is suitable for protein detection after a primary protein separation step in microfluidic channels. The use of complex and bulky equipment such as mass spectrometry (MS) for protein detection was replaced by tiny LC sensing dots located within the channels. This is the first example of how sensitive LC materials can be integrated with a microfluidic system for protein detection, and it represents an important step toward the development of a portable microfluidic immunoassay. This unique protein assay allows real-time detection of proteins, a feature that is not possible with the surface-based protein assay.

7.2. Recommendations for Future Works

The LC-based protein assays may offer a new tool that can be used by physicians and clinical workers for the early detection, diagnosis, and progress monitoring of CKD in the future. However, this research is still at an early stage, and many efforts are still needed before such device becomes commercially reliable. During the course of this research period, we realized that the following investigations and studies are needed.

In **Chapter 3**, the detection of HSA was achieved due to the immunobinding between AHSA and HSA. However, AHSA was immobilized on the surface through physical adsorption. As a result, orientations of the AHSA molecules on the surface are random, and that may adversely affect the immunobinding between AHSA and HSA. In the future, better immobilization strategy for AHSA should be considered. This can be done, for example, by introducing molecules such as Protein A or G, which are known to orient antibody and expose the antigen-binding F_{ab} region of the antibody. This improvement may lead to higher sensitivity and lower detection limit for the LC-based immunoassay. Furthermore, more test results for real urine samples are needed. These samples need to be analyzed by using both standard methods (e.g. nephelometry) and LC-based method for detailed comparison. The performance of both methods can then be compared by performing statistical analysis.

In **Chapter 4**, we present potential applications of LC droplets to monitor multiple protein targets in solutions. The probes that detect the desired target proteins are covalently bound to the polymer-decorated LC droplets. Therefore, our future goal for this work is to expand such system to other biological and chemical sensing applications. To do this, we will investigate other polymers with specific functional groups. Second, multiplex analysis of proteins running in parallel can be studied by compartmentalizing LC droplets that are decorated with different antibodies. Lastly, from our initial experiments where we flowed these LC droplets in microfluidic

channels as microscopic sensors, we realized that it was difficult to obtain the images of the LC droplets as well as distinguish their orientational configuration. This is due to the random movement of the droplets inside the channels, thus their focal lengths from the objective lens constantly changing. Such problem can be resolved by reducing the dimensions of the channel, in order to restrict the movement of the LC droplets in the channel.

The use of vortex shown in Chapter 4 is one of the easiest methods to produce emulsified LC droplets. Nonetheless, this method generates polydisperse LC droplets and only a fraction of the LC droplets were used in the analysis. Therefore, a more controlled means of creating LC droplets of uniform size is needed. This limitation has been addressed in **Chapter 5**. The use of monodisperse LC droplets would therefore improve the study mentioned above. Still, there are several outstanding issues related to this technique. First, as shown in Appendix C, the method for production of monodisperse LC droplets we developed is not exclusive. There might be other design strategies which can be used to produce uniform LC droplets. One of such example is immersion of slides supporting LC dots into a solution-filled vial. By using this technique, it is possible to omit the open rectangular channels for flushing the printed LC dots. Second, as mentioned in Chapter 4, because the LC droplets can be specifically coated with polymers other than PEI, further examination of their respective spreading parameters as well as fluid dynamics needs to be carried out. Third, the stability of the LC droplets produced may be further enhanced. This can be done either by using polymers that can be cross-linked through UV or heat, or by

using other materials such as phospholipids. Example of UV-curable polymers including epoxy-based (e.g. NOA 51), vinyl ester-based and acrylic-based polymers can be considered, but the effects of curing time on the surface morphology of the LC droplets need to be determined. On the other hand, ligand-functionalized phospholipids (e.g. biotin-DOPE) having two-hydrophobic tails which might enhance the stability of the LC droplets might be attempted. Lastly, because we rely on a specialized material printer to print LC droplets, in the future, it would be interesting to investigate whether it is possible to retrofit a commercial inkjet printer to dispense LC droplets on the surface. This will greatly lower the cost of producing uniform LC droplets and make this approach more practical.

From the results on microfluidic protein assay embedded with LC dots in **Chapter 6**, we demonstrate the detection and quantification of protein BSA in pure solutions. A possible direction of this research work is the analysis of multiple proteins quantitatively and in parallel in a single experiment. This may be achieved by doping the LC dots with complementary antibodies prior to protein analysis. Another issue we find during the development of microfluidic protein assay is that the upper LOD of the assay is only 50 μg/mL. This makes it difficult for samples containing high protein concentrations. Therefore, the dimensions of the channels needs to be further examined either by increasing the width or the length of the channel to allow analysis of higher concentrations. It is our hope that after the implementation of these experimental plans, we can realize the application of LC sensors in POC diagnostic devices.

BIBLIOGRAPHY

Afzali, B., Jayawardene, S., Goldsmith, D., **2007**. ABC of Kidney Disease. In: Goldsmith, D., Jayawardene, S., Penny, A. (Eds.), ABC of Kidney Disease, pp. 1-12. Blackwell Publishing Ltd., Oxford, UK.

AgilentTechnologies, **2006**. Agilent Protein 230 Kit Guide. http://cat.ucsf.edu/pdfs/Protein_Analysis.pdf. Accessed last March 2008.

Alexander, R., **1980**. Comparison of radial immunodiffusion and laser nephelometry for quantitating some serum proteins. *Clin. Chem.* 2612, 314-317.

Aliño, V.J., Pang, J., Yang, K.-L., **2011**. Liquid crystal droplets as a hosting and sensing platform for developing immunoassays. *Langmuir* 27, 11784-11789.

Aliño, V.J., Tay, K.-X., Khan, S., Yang, K.-L., **2012**. Inkjet printing and release of monodisperse liquid crystal droplets from solid surfaces. *Langmuir* 28, 14540-14546.

Aliño, V.J., Yang, K.-L., **2011**. Using liquid crystals as a readout system in urinary albumin assays. *Analyst 136*, 3307-3313.

Allain, L.R., Stratis-Cullum, D.N., Vo-Dinh, T., **2004**. Investigation of microfabrication of biological sample arrays using piezoelectric and bubble-jet printing technologies. *Anal. Chim. Acta* 518, 77-85.

Anavekar, N., Gans, D., Berl, T., Rohde, R., Cooper, W., Bhaumik, A., **2004**. Predictors of cardiovascular events in patients with type 2 diabetic nephropathy and hypertension: A case of albuminuria. *Kidney Int.*, S50-55.

Bahr, C., **2006**. Surfactant-induced nematic wetting layer at a thermotropic liquid crystal/water interface. *Phys. Rev. E* 73, 0307021-0307024.

Baker, K., Rendall, M., Patel, A., Boyd, P., Hoare, M., Freedman, R., James, D., **2002**. Rapid monitoring of recombinant protein products: A comparison of current technologies. *Trends Biotecnol. 20*, 149-156.

Barikbin, Z., Rahman, M.T., Parthiban, P., Rane, A.S., Jain, V., Duraiswamy, S., Lee, S.H., Khan, S.A., **2010**. Ionic liquid-based compound droplet microfluidics for 'on-drop' separations and sensing. *Lab Chip* 10, 2458-2463.

Baroud, C., Gallaire, F., Dangla, R., **2010**. Dynamics of microfluidic droplets. *Lab Chip 10*, 2032-2045.

Barratt, J., Topham, P., **2007**. Urine proteomics: the present and future of measuring urinary protein components in disease. *Can. Med. Assoc. J.* 177, 361-368.

Barry, R., Ivanov, D., **2004**. Microfluidics in biotechnology. *J. Nanobiotechnol.* 2, 1-5.

Batteiger, B., Newhall, W., Jones, R., **1982**. The use of tween 20 as a blocking agent in the immunological detection of proteins transferred to nitrocellulose membranes. *J. Immunol. Meth. 55*, 297-307.

Bazzi, C., Petrini, C., Rizza, V., Arrigo, G., Beltrame, A., Pisano, L., D'Amico, G., **2001**. Urinary excretion of IgG and alpha(1)-microglobulin predicts clinical course better than extent of proteinuria in membranous nephropathy. *Am. J. Kidney Dis.* 38, 240-248.

Becher, F., Pruvost, A., Clement, G., Tabet, J.C., Ezan, E., **2006**. Quantification of small therapeutic proteins in plasma by liquid chromatography–tandem mass spectrometry: Application to an elastase inhibitor EPI-hNE4. *Anal. Chem.* 78, 2306-2313.

Bernard, A., Lauwerys, R., **1983**. Continuous-flow system for automation of latex immunoassay by particle counting. *Clin. Chem. 29*, 1007-1011.

Bi, X., Hartono, D., Yang, K.-L., **2009a**. Real-time liquid crystal pH sensor for monitoring enzymatic activities of penicillinase. *Adv. Funct. Mater.* 19, 3760-3765.

Bi, X., Huang, S., Hartono, D., Yang, K.-L., **2007**. Liquid-crystal based optical sensors for simultaneous detection of multiple glycine oligomers with micromolar concentrations. *Sens. Actuators, B* 127, 406-413.

Bi, X., Lai, S.L., Yang, K.-L., **2009b**. Liquid crystal multiplexed protease assays reporting enzymatic activities as optical bar charts. *Anal. Chem.* 81, 5503-5509.

Bi, X., Yang, K.-L., **2008**. A principle of detecting and differentiating dialdehydes from monoaldehydes by using surface reactions and liquid crystals. *J. Phys. Chem. C* 112, 1748-1750.

Bi, X., Yang, K.-L., **2010**. Liquid crystals decorated with linear oligopeptide FLAG for applications in immunobiosensors. *Biosens. Bioelectron.* 26, 107-111.

Bibette, J., **1991**. Depletion interactions and fractionated crystallization for polydisperse emulsion purification. *J. Colloid Interf. Sci.* 147, 474-478.

Birchall, L., Ulijn, R., Webb, S., **2008**. A combined SPS-LCD sensor for screening protease specificity. *Chem. Commun.*, 2861-2863.

Brake, J., Abbott, N., **2002**. An experimental system for imaging the reversible adsorption of amphiphiles at aqueous-liquid crystal interfaces. *Langmuir* 18, 6101-6109.

Brake, J., Daschner, M., Luk, Y.-Y., Abbott, N., **2003a**. Biomolecular interactions at phospholipid-decorated surfaces of liquid crystals. *Science* 302, 2094-2097.

Brake, J., Mezera, A., Abbott, N., **2003b**. Effect of surfactant structure on the orientation of liquid crystals at aqueous–liquid crystal interfaces. *Langmuir* 19, 6436-6442.

Burns, M.A., **2002**. Analytic chemistry: Everyone's a (future) chemist. *Science* 296, 1818-1819.

Carboni, C.; Al-Ruzaiqi, S.; Al-Siyabi, A.; Al-Harthi, S.; George, A.; Sluckin, T., **2008.** The behaviour of the interfacial surface tension of liquid-crystal materials in the vicinity of the nematic-isotropic phase transition. *Mol. Cryst. Liq. Cryst.* 494, 114-126.

Carroll, M., Temte, J., **2000**. Proteinuria in adults: A diagnostic approach. *Am. Fam. Physician* 62, 1333-1340.

Cesaro-Tadic, S., Dernick, G., Juncker, D., Buurman, G., Kropshofer, H., Michel, B., Fattinger, C., Delamarche, E., **2004**. High-sensitivity miniaturized immunoassays for tumor necrosis factor using microfluidic systems. *Lab Chip* 4, 563-569.

Chan, J.H., Timperman, A.T., Qin, D., Aebersold, R., **1999**. Microfabricated polymer devices for automated sample delivery of peptides for analysis by electrospray ionization tandem mass spectrometry. *Anal. Chem.* 71, 4437-4444.

Chan, O., Herold, D., **2006**. Chip electrophoresis as a method for quantifying total microalbuminuria. *Clin. Chem.* 52, 2141-2146.

Cheng, D., Feng, Y., Yan, J., **2007**. Dimer of calcein used as fluorescence probe in the determination of proteins. *Microchim. Acta* 157, 173.

Choi, S., Choi, E.Y., Kim, H.S., Oh, S.W., **2004**. On-site quantification of human urinary albumin by a fluorescence immunoassay. *Clin. Chem.* 50, 1052-1055.

Choong, Hui Lin, **2009**. Eighth Report of the Singapore Renal Registry 2009. www.nrdo.gov.sg. Accessed last March 2012.

Chua, J.H., Chee, R.-E., Agarwal, A., Wong, S.M., Zhang, G.-J., **2009**. Label-free electrical detection of cardiac biomarker with complementary metal-oxide semiconductor-compatible silicon nanowire sensor arrays. *Anal. Chem.* 81, 6266-6271.

Clare, B., Abbott, N., **2005**. Orientations of nematic liquid crystals on surfaces presenting controlled densities of peptides: Amplification of protein−peptide binding events. *Langmuir* 21, 6451-6461.

Clare, B., Guzmán, O., de Pablo, J., Abbott, N., **2006**. Measurement of the azimuthal anchoring energy of liquid crystals in contact with oligo(ethylene glycol)-terminated self-assembled monolayers supported on obliquely deposited gold films. *Langmuir* 22, 4654-4659.

Collings, P., Hird, M., **1997**. Introduction to Liquid Crystals: Chemistry and Physics. pp. 18-43. Taylor and Francis Inc., London, UK.

Comper, W., Jerums, G., Osicka, T., **2004a**. Differences in urinary albumin detected by four immunoassays and high-performance liquid chromatography. *Clin. Biochem.* 37, 105-111.

Comper, W., Osicka, T., Clark, M., MacIsaac, R., Jerums, G., **2004b**. Earlier detection of microalbuminuria in diabetic patients using a new urinary albumin assay. *Kidney Int.* 65, 1850-1855.

Constantiner, M., **2005**. Dipstick protein and specific gravity algorithm accurately predicts pathological proteinuria. *Am. J. Kidney Dis.* 5, 833-841.

Contois, J., Hartigan, C., Rao, L., Snyder, L., Thompson, M., **2006**. Analytical validation of an HPLC assay for urinary albumin. *Clin. Chim. Acta* 367, 150-155.

Cordero, M.L., Gallaire, F., Baroud, C.N., **2011**. Quantitative analysis of the dripping and jetting regimes in co-flowing capillary jets. *Phys. Fluids* 23, 094111-094118.

Delaney, J.T., Smith, P.J., Schubert, U.S., **2009**. Inkjet printing of proteins. *Soft Matter* 5, 4866-4877.

Derby, B., **2010**. Inkjet Printing of Functional and Structural Materials: Fluid property requirements, feature stability, and resolution. *Annu. Rev. Mater. Res.* 40, 395-414.

Deschamps, J., Trusler, J.P.M., Jackson, G., **2008**. Vapor pressure and density of thermotropic liquid crystals: MBBA, 5CB, and novel fluorinated mesogens. *J. Phys. Chem. B* 112, 3918-3926.

Deshpande, S., **1996**. Enzyme immunoassays from concept to product development. pp. 24-72. Chapman and Hall New York, NY.

Di Profio, G., Lanzo, J., Nicoletta, F., De Filpo, G., Chidichimo, G., **2001**. Fast switchable nematic emulsions with twisted director. *Appl. Phys. Lett.* 79, 4512-4514.

Di Profio, G., Nicoletta, F., De Filpo, G., Chidichimo, G., **2002**. Reverse-mode operation switchable nematic emulsions. *Langmuir* 18, 3034-3038.

Dickert, F., Bäumler, U., Zwissler, G., **1993**. Supramolecular structures and chemical sensing. *Synth. Met.* 61, 47-52.

Ding, J., Yang, Y., **1992**. Birefringence patterns of nematic droplets. *Jpn. J. Appl. Phys.* 31, 2837-2845.

Donath, E., Sukhorukov, G.B., Caruso, F., Davis, S.A., Möhwald, H., **1998**. Novel hollow polymer shells by colloid-templated assembly of polyelectrolytes. *Angew. Chem. Int. Ed* 37, 2201-2205.

Dong, Y., Wilkop, T., Xu, D., Wang, Z., Cheng, Q., **2008**. Microchannel chips for the multiplexed analysis of human Immunoglobulin G–antibody interactions by surface plasmon resonance imaging. *Anal. Bioanal. Chem.* 390, 1575-1583.

Ellekide, G., von Eyben, F., Holm, J., Hemmingsen, L., **1997**. Above normal urinary excretion of retinal-binding protein and albumin in albustix-negative hypertensive patients. *Clin. Chem.* 37, 1446-1447.

Erdmann, J., Zumer, S., Doane, J.W., **1990**. Configuration transition in a nematic liquid crystal confined to a small spherical cavity. *Phys. Rev. Lett.* 64, 1907-1910.

Fujifilm, **2008**. Jettable Fluid Formulation Guidelines. Dimatix Materials Printer DMP-2800 Series. www.fujifilm.usa. Accessed last January 2012.

Futami, J., Kitazoe, M., Maeda, T., Nukui, E., Sakaguchi, M., Kosaka, J., Miyazaki, M., Kosaka, M., Tada, H., Seno, M., Sasaki, J., Huh, N.-H., Namba, M., Yamada, H., **2005**. Intracellular delivery of proteins into mammalian living cells by polyethylenimine-cationization. *J. Biosci. Bioeng*. 99, 95-103.

Gao, J., Xu, J., Locascio, L.E., Lee, C.S., **2001**. Integrated microfluidic system enabling protein digestion, peptide separation, and protein identification. *Anal. Chem.* 73, 2648-2655.

Gervais, L., Delamarche, E., **2009**. Toward one-step point-of-care immunodiagnostics using capillary-driven microfluidics and PDMS substrates. *Lab Chip* 9, 3330-3337.

Gilbert, R., McNally, P., O'Brien, R., Taft, G., Jerums, G., **1994**. Microalbuminuria: Prognostic and therapeutic implications in diabetes mMmellitus. *Diabetic Medicine* 11, 636-645.

Gizeli, E., Lowe, C., **2002**. Biomolecular Sensors. pp. 1-32. Taylor & Francis Inc. , New York, NY.

Golemme, A., Kippelen, B., Peyghambarian, N., **1998**. Highly efficient photorefractive polymer-dispersed liquid crystals. *Appl. Phys. Lett.* 73, 2408-2410.

Goligorsky, M., Addabbo, F., O'Riordan, E., **2007**. Diagnostic potential of urine proteome: A broken mirror of renal diseases. *J. Am. Soc. Nephrol.* 18, 2233-2239.

Gonzalez-Buitrago, J., Ferreira, L., Lorenzo, I., **2007**. Urinary proteomics. *Clin. Chim. Acta* 375, 49-56.

Gonzalo, J., Dyer, P.E., Hird, M., **1997**. Pulsed laser deposition of liquid crystals. *Appl. Phys. Lett.* 71, 2752-2754.

Götz, S., Karst, U., **2007**. Recent developments in optical detection methods for microchip separations. *Anal. Bioanal. Chem.* 387, 183-192.

Govindaraju, T., Bertics, P., Raines, R., Abbott, N., **2007**. Using measurements of anchoring energies of liquid crystals on surfaces to quantify proteins captured by immobilized ligands. *J. Am. Chem. Soc.* 129, 11223-11231.

Grootendorst, D., Jager, K., Zoccali, C., Dekker, F., **2009**. Screening: why, when, and how. *Kidney Int.* 76, 694-699.

Gupta, J., Zimmerman, J., de Pablo, J., Caruso, F., Abbott, N., **2009a**. Characterization of adsorbate-induced ordering transitions of liquid crystals within monodisperse droplets. *Langmuir* 25, 9016-9024.

Gupta, J.K., Sivakumar, S., Caruso, F., Abbott, N.L., **2009b**. Size-dependent ordering of liquid crystals observed in polymeric capsules with micrometer and smaller diameters. *Angew. Chem. Int. Ed* 48, 1652-1655.

Gupta, V., Abbott, N., **1997**. Design of surfaces for patterned alignment of liquid crystals on planar and curved substrates. *Science* 276, 1533-1536.

Gupta, V., Skaife, J., Dubrovsky, T., Abbott, N., **1998**. Optical amplification of ligand-receptor binding using liquid crystals. *Science* 279, 2077-2080.

Gyure, W., **1977**. Comparison of several methods for semiquantitative determination of urinary protein. *Clin. Chem.* 23, 876-879.

Hamlington, B., Steinhaus, B., Feng, J., Link, D., Shelley, M., Shen, A., **2007**. Liquid crystal droplet production in a microfluidic device. *Liq. Cryst.* 34, 861 - 870.

Harris, T.M., Massimi, A., Childs, G., **2000**. Injecting new ideas into microarray printing. *Nat. Biotechnol.* 18, 384-385.

Hartono, D., Bi, X., Yang, K.-L., Yung, L., **2008**. Label-free characterization of phospholipases and their inhibitors. *Adv. Funct. Mater.* 18, 2938-2945.

Hartono, D., Lai, S.L., Yang, K.-L., Yung, L., **2009a**. A liquid crystal-based sensor for real-time and label-free identification of phospholipase-like toxins and their inhibitors. *Biosens. Bioelectron.* 24, 2289-2293.

Hartono, D., Qin, W.J., Yang, K.-L., Yung, L., **2009b**. Imaging the disruption of phospholipid monolayer by protein-coated nanoparticles using ordering transitions of liquid crystals. *Biomater.* 30, 843-849.

Hartono, D., Yang, K.-L., Yung, L., **2010**. The effect of cholesterol on protein-coated gold nanoparticle binding to liquid crystal-supported models of cell membranes. *Biomater. 31*, 3008-3015.

Heideman, R., Kooyman, R., Greve, J., **1993**. Polarimetric optical-fibre sensor for biochemical measurements. *Sens. Actuators, B* 12, 205-212.

Hellmich, W., Pelargus, C., Leffhalm, K., Ros, A., Anselmetti, D., **2005**. Single cell manipulation, analytics, and label-free protein detection in microfluidic devices for systems nanobiology. *Electrophoresis* 26, 3689-3696.

Heppenstall-Butler, M., Williamson, A., Terentjev, E., **2005**. Selection of droplet size and the stability of nematic emulsions. *Liq. Cryst.* 32, 77-84.

Hillege, H., Fidler, V., Diercks, G., van Gilst, W., De Zeeuw, D., van Veldhuisen, D., **2002**. Urinary albumin excretion predicts cardiovascular and noncardiovascular mortality in general population. *Circulation* 106, 1777-1178.

Hoogboom, J., Velonia, K., Rasing, T., Rowan, A., Nolte, R., **2006**. LCD-based detection of enzymatic action. *Chem. Commun.*, 434-435.

Iwata, S., **2001**. Recommended method of the Japanese Association of Medical Technologists for the determination of protein in urine by HPLC. *Clin. Chim. Acta* 303, 95-104.

Jang, C.-H., Hu, Q., **2010**. Liquid crystal-based imaging of enzymatic reactions at aqueous-liquid crystal interfaces decorated with oligopeptide amphiphiles. *Bull. Korean Chem. Soc.* 31, 1262-1266.

Jang, C.-H., Tingey, M., Korpi, N., Wiepz, G., Schiller, J., Bertics, P., **2005**. Using liquid crystals to report membrane proteins captured by affinity microcontact printing from cell lysates and membrane extracts. *J. Am. Chem. Soc.* 127, 8912-8913.

Jiang, X., Ng, J., Stroock, A., Dertinger, S., Whitesides, G., **2003**. A miniaturized, parallel, serially diluted immunoassay for analyzing multiply antigens. *J. Am. Chem. Soc.* 125, 5294-5295.

Jiang, Y., Wang, P.-C., Locascio, L., Lee, C., **2001**. Integrated plastic microfluidic devices with ESI-MS for drug screening and residue analysis. *Anal. Chem.* 73, 2048-2053.

Jimbo, M., **2007**. Nephrology. In: Heidelbaugh, J.J. (Ed.), Clinical Men's Health: Evidence in Practice, pp. 207-219, 1st ed. Elsevier, Philadelphia, PA.

Keuren, J., Wielders, S., Willems, G., Morra, M., Cahalan, L., Cahalan, P., Lindhout, T., **2003**. Thrombogenicity of polysaccharide-coated surfaces. *Biomater.* 24, 1917-1924.

Khoo, I.-C., Wu, S.-T., **1993**. Optics and nonlinear optics of liquid crystals. Series in Nonlinear Optics, pp. 282-290. World Scientific Publishing Co. Pte. Ltd., Singapore.

Kim, J.-S., Knapp, D.R., **2001**. Microfabricated PDMS multichannel emitter for electrospray ionization mass spectrometry. J. Am. Soc. Mass. Spectrom. 12, 463-469.

Kim, J.D., Choi, J.S., Kim, B.S., Choi, Y.C., Cho, Y.W., **2010**. Piezoelectric inkjet printing of polymers: Stem cell patterning on polymer substrates. *Polymer* 51, 2147-2154.

Kim, S.-R., Abbott, N., **2001**. Rubbed films of functionalized bovine serum albumin as substrates for the imaging of protein-receptor interactions using liquid crystals. *Adv. Mater.* 13, 1445-1449.

Kim, S.-R., Abbott, N., **2002**. Manipulation of the orientational response of liquid crystals to proteins specifically bound to covalently immobilized and mechanically sheared films of functionalized bovine serum albumin. *Langmuir* 18, 5269-5276.

Kim, S.-R., Shah, R., Abbott, N., **2000**. Orientations of liquid crystals on mechnanically rubbed films of bovine serum albumin: A possible substrate for biomolecular assays based on liquid crystals. *Anal. Chem.* 72, 4646-4653.

Kinsinger, M., Buck, M., Abbott, N., Lynn, D., **2010**. Immobilization of polymer-decorated liquid crystal droplets on chemically tailored surfaces. *Langmuir* 26, 10234-10242.

Klasen, I., Reichert, L., de Kat Angelino, C., Wetzels, J., **1999**. Quantitative determination of low and high molecular weight proteins in human urine: Influence of temperature and storage time. *Clin. Chem.* 45, 430-432.

Kleman, M., Lavrentovich, O.D., **2006**. Topological point defects in nematic liquid crystals. *Philos. Mag*. 86, 4117-4137.

Kocevar, K., Musevic, I., **2003**. Structural forces near phase transitions of liquid crystals. *ChemPhysChem* 4, 1049-1056.

Konta, T., Hao, Z., Takasaki, S., Abiko, H., Ishikawa, M., Takahashi, T., Ikeda, A., Ichikawa, K., Kato, T., Kawata, S., Kubota, I., **2007**. Clinical utility of trace

proteinuria for microalbuminuria screening in the general population. *Clin. Exp. Nephrol.* 11, 51-55.

Koster, S., Verpoorte, E., **2007**. A decade of microfluidic analysis coupled with electrospray mass spectrometry: An overview. *Lab Chip* 7, 1394-1412.

Kuschel, M., Neumann, T., Barthmaier, P., Kratzmeier, M., **2002**. Use of Lab-on-a-Chip Technology for Protein Sizing and Quantitation. *JBT* 13, 172-178.

Lai, S.L., Huang, S., Bi, X., Yang, K.-L., **2009**. Optical imaging of surface-immobilized oligonucleotide probes on DNA microarrays using liquid crystals. *Langmuir* 25, 311-316.

Lanzo, J., Nicoletta, F., De Filpo, G., Chidichimo, G., **1999**. Polymerization in Nematic Emulsions. *Appl. Phys. Lett.* 74, 2635-2637.

Lavrentovich, O.D., **1998**. Topological defects in dispersed words and worlds around liquid crystals, or liquid crystal drops. *Liq. Cryst.* 24, 117-126.

Lechuga, L., Lenferink, A., Kooyman, R., Greve, J., **1995**. Feasibility of evanescent wave interferometer immunosensors for pesticide detection: Chemical aspects. *Sens. Actuators, B* 24-25, 762-765.

Lian, A.-H., Huang, Y.-J., Jiang, Z.-L., **2007**. A rapid and sensitive immunoresonance scattering spectral assay for microalbumin. *Clin. Chim. Acta* 383, 73-77.

Lin, I.H., Miller, D.S., Bertics, P.J., Murphy, C., de Pablo, J., Abbott, N., **2011**. Endotoxin-induced structural transformations in liquid crystalline droplets. *Science* 332, 1297-1300.

Liu, J.-F., Wu, Y.-W., Cheng, Y.-H., Zhou, X.-W., Zhang, H.-L., Han, D.-Y., **2009**. Micellar electrokinetic chromatography assay for the simultaneous quantification of urinary transferrin and albumin. *Microchim. Acta* 165, 285-290.

Liu, X., Sun, Y., Song, D., Zhang, Q., **2006**. Enhanced optical immunosensor based on surface plasmon resonance for determination of transferrin. *Talanta* 68, 1026-1031.

Lockwood, N., Cadwell, K., Caruso, F., Abbott, N., **2006**. Formation of polyelectrolyte multilayer films at interfaces between thermotropic liquid crystals and aqueous phases. *Adv. Mater.* 18, 850-854.

Lockwood, N., Gupta, J., Abbott, N., **2008**. Self-assembly of amphiphiles, polymers and proteins at interfaces between thermotropic liquid crystals and aqueous phases. *Surf. Sci. Rep.* 63, 255-293.

Loudet, J., Richard, H., Sigaud, G., Poulin, P., **2000**. Nonaqueous liquid crystal emulsions. *Langmuir* 16, 6724-6730.

Loxley, A., Vincent, B., **1998**. Preparation of poly(methylmethacrylate) microcapsules with liquid cores. *J. Colloid Interf. Sci.* 208, 49-62.

Luk, Y.-Y., Jang, C.-H., Cheng, L.-L., Israel, B., Abbott, N., **2005**. Influence of lyotropic liquid crystals on the ability of antibodies to bind to surface-immobilized antigens. *Chem. Mater.* 17, 4774-4782.

Luk, Y.-Y., Tingey, M., Hall, D., Israel, B., Murphy, C., Bertics, P., Abbott, N., **2003**. Using liquid crystals to amplify protein–receptor interactions: Design of surfaces with nanometer-scale topography that present histidine-tagged protein receptors. *Langmuir* 19, 1671-1680.

Luo, Y., Chen, M., Wen, Q., Zhao, M., Zhang, B., Li, X., Wang, F., Huang, Q., Yao, C., Jiang, T., Cai, G., Fu, W., **2006**. Rapid and simultaneous quantification of 4 urinary proteins by piezoelectric quartz crystal microbalance immunosensor array. *Clin. Chem.* 52, 2273-2280.

Malicka, J., Gryczynski, I., Fang, J., Lakowicz, J., **2003**. Fluorescence spectral properties of cyanine dye-labeled DNA oligomers on surfaces coated with silver particles. *Anal. Biochem.* 317, 136-146.

Malmsten, M., Lassen, B., Holmberg, K., Thomas, V., Quash, G., **1996**. Effects of hydrophilization and immobilization on the interfactial behavior of immunoglobulins. *J. Colloid Interf. Sci.* 177, 70-78.

Marks, S., Girgis, R., Couch, R., **2003**. Screening for adrenal antibodies in children With Type 1 diabetes and autoimmune thyroid disease. *Diabetes Care* 26, 3187.

Marre, M., Claudel, J., Ciret, P., Luis, N., Suarez, L., Passa, P., **1987**. Laser immunonephelometry for routine quantification of urinary albumin excretion. *Clin. Chem.* 33, 209-213.

Mason, T.G., Wilking, J.N., Meleson, K., Chang, C.B., Graves, S.M., **2006**. Nanoemulsions: Formation, structure, and physical properties. Journal of Physics Condensed Matter 18(41), R635-R666.

Mathiesen, E., Oxenbøll, B., Johansen, K., Svendsen, P., Deckert, T., **1984**. Incipient nephropathy in Type 1 (insulin-dependent) diabetes. *Diabetologia* 26, 406-410.

McClements, J., Weiss, J., **2005**. Lipid emulsions. In: Shahidi, F. (Ed.), Bailey's Industrial Oil and Fat Products, pp. 457-502, 6th ed. John Wiley & Sons, Inc, Hoboken, NJ.

Meldrum, D., Holl, M., **2002**. Microscale bioanalytical systems. *Science* 297, 1197-1198.

Metzger, S., Natesan, M., Yanavich, C., Schneider, J., Lee, G., **1999**. Development and characterization of surface chemistries for microfabricated biosensors. *J. Vac. Sci. Technol. A* 17, 2623-2628.

Mladenovic, J., **2004**. Primary care secrets. pp. 298-300, 3rd edition ed. Hanley and Belfus, Philadelphia, PA.

Mohebi, M., Evans, J., **2002**. A drop-on-demand ink-jet printer for combinatorial libraries and functionally graded ceramics. *J. Comb. Chem.* 4, 267-274.

Moore, R., **2002**. Clinical Laboratory Medicine. In: McClatchey, K.D. (Ed.), Immunochemical Methods, pp. 213-238. Lippincott, Wiliams and Wilkins, Philadelphia, PA.

Muriale, L., Lee, E., Genovese, J., Trend, S., **1996**. Fatality due to acute fluoride poisoning following dermal contact with hydrofluoric acid in a palynology laboratory. *Ann. Occup. Hyg.* 40, 705-710.

Nelson, J., Kim, S.-R., Abbott, N., **2002**. Amplification of specific binding events between biological species using lyotropic liquid crystals. *Langmuir* 18, 5031-5035.

Nicoletta, F., De Filpo, G., Lanzo, J., Chidichimo, G., **1999**. A method to produce reverse-mode polymer-dispersed liquid-crystal shutters. *Appl. Phys. Lett.* 74, 3945-3947.

Nicoletta, F., Lanzo, J., De Filpo, G., Chidichimo, G., **2001**. Effect of surfactant molecules on the electrooptical properties of nematic emulsions. *Langmuir* 17, 534-536.

Ou, J., Glawdel, T., Ren, C.L., Pawliszyn, J., **2009**. Fabrication of a hybrid PDMS/SU-8/quartz microfluidic chip for enhancing UV absorption whole-channel imaging detection sensitivity and application for isoelectric focusing of proteins. *Lab Chip* 9, 1926-1932.

Pal, R., **1996**. Viscoelastic properties of polymer-thickened oil-in-water emulsions. *Chem. Eng. Sci.* 51, 3299-3305.

Pannacci, N., Bruus, H., Bartolo, D., Etchart, I., Lockhart, T., Hennequin, Y., Willaime, H., Tabeling, P., **2008**. Equilibrium and nonequilibrium states in microfluidic double emulsions. *Phys. Rev. Lett.* 101, 164502.

Park, J.-S., Abbott, N.L., **2008**. Ordering transitions in thermotropic liquid crystals induced by the interfacial assembly and enzymatic processing of oligopeptide amphiphiles. *Adv. Mater.* 20, 1185-1190.

Park, J.-S., Teren, S., Tepp, W.H., Beebe, D.J., Johnson, E.A., Abbott, N.L., **2006**. Formation of Oligopeptide-Based Polymeric Membranes at Interfaces between Aqueous Phases and Thermotropic Liquid Crystals. *Chem. Mater.*18, 6147-6151.

Pedraza-Chaverri, J., Murali, N., Croatt, A., Alam, J., Grande, J., Nath, K., **2006**. Proteinuria as a determinant of renal expression of heme oxygenase-1: studies in models of glomerular and tubular proteinuria in the rat. *Am J Physiol Renal Physiol* 290, 196-204.

Poulin, P., Stark, H., Weitz, L., **1997**. Novel colloidal interactions in anisotropic fluids. *Science* 275, 1770-1773.

Price, A., Schwartz, D., **2006**. Anchoring of a nematic liquid crystal on a wettability gradient. *Langmuir* 22, 9753-9759.

Price, A., Schwartz, D., **2008**. DNA hybridization-induced reorientation of liquid crystal anchoring at the nematic liquid crystal/aqueous interface. *J. Am. Chem. Soc.* 130, 8188-8194.

Priest, C., Quinn, A., Postma, A., Zelikin, A.N., Ralston, J., Caruso, F., **2008**. Microfluidic polymer multilayer adsorption on liquid crystal droplets for microcapsule synthesis. *Lab Chip* 8, 2182-2187.

Rifai, N., Warnick, G.R., Dominiczak, M.H., **2000**. Handbook of lipoprotein testing. pp. 298-304, 2nd ed. AACC Press, Washington, DC.

Rogers, E., **1997**. Handbook of Biosensors and Electronic Noses: Medicine, Food and the Environment, pp. 61-86, CRC Press Inc. Frankfurt, Germany. .

Rotenberg, Y., Boruvka, L., Neumann, A.W., **1983**. Determination of surface tension and contact angle from the shapes of axisymmetric fluid interfaces. *J. Colloid Interf. Sci.* 93, 169-183.

Sakai, G., Saiki, T., Uda, T., Miura, N., Yamazoe, N., **1995**. Selective and repeatable detection of human serum albumin by using piezoelectric immunosensor. *Sens. Actuators, B* 24, 134-137.

Sakai, G., Saiki, T., Uda, T., Miura, N., Yamazoe, N., **1997**. Evaluation of binding of human serum albumin (HSA) to monoclonal and polyclonal antibody by means of piezoelectric immunosensing technique. *Sens. Actuators, B* 42, 89-94.

Sakti, S., Hauptmann, P., Zimmermann, B., Buhling, F., Ansorge, S., **2001**. Disposable HSA QCM-immunosensor for practical measurement in liquid. *Sens. Actuators, B* 78, 257-262.

Schipper, E., Kooyman, R., Heideman, R., Greve, J., **1995**. Feasibility of optical waveguide immunosensors for pesticide detection: physical aspects. *Sens. Actuators, B* 24-25, 90-93.

Schrier, R., **2007**. Diseases of the Kidney and Urinary Tract, Vol. 1, pp. 302-310, 8th ed., Lippincott Williams and Wilkins, Philadelphia, PA.

Scoutaris, N., Alexander, M., Gellert, P., Roberts, C., **2011**. Inkjet printing as a novel medicine formulation technique. *J. Controlled Release* 156, 179-185.

Shah, R., Abbott, N., **2001**. Principles for measurement of chemical exposure based on recognition-driven anchoring transitions in liquid crystals. *Science* 293, 1296-1299.

Sharpe, R., Burdinski, D., Huskens, J., Zandvliet, H., Reinhoudt, D., Poelsema, B., **2005**. Chemically patterned flat stamps for microcontact printing. *J. Am. Chem. Soc.* 127, 10344-10349.

Shklyaev, O., Shen, A., **2009**. Microfluidics enhanced control of the microstructure and flow of complex fluids. *Mech. Res. Commun.* 36, 121-124.

Sia, S., Whitesides, G., **2003**. Microfluidic devices fabricated in poly(dimethylsiloxane) for biological studies. *Electrophoresis* 24, 3563-3576.

Simon, K., Sejwal, P., Gerecht, R., Luk, Y.-Y., **2007**. Water-in-water emulsions stabilized by non-amphiphilic interactions: Polymer-dispersed lyotropic liquid crystals. *Langmuir* 23, 1453-1458.

Sivakumar, S., Gupta, J., Abbott, N., Caruso, F., **2008**. Monodisperse emulsions through templating polyelectrolyte multilayer capsules. *Chem. Mater.* 20, 2063-2065.

Sivakumar, S., Wark, K., Gupta, J., Abbott, N., Caruso, F., **2009**. Liquid crystal emulsions as the basis of biological sensors for the optical detection of bacteria and viruses. *Adv. Funct. Mater.* 19, 2260-2265.

Skaife, J., Brake, J., Abbott, N., **2001**. Influence of nanometer-scale topography of surfaces on the orientational response of liquid crystals to proteins specifically bound to surface-immobilized receptors. *Langmuir* 17, 5448-5457.

Snyder, S., Pendergraph, B., **2005**. Detection and evaluation of chronic kidney disease. *Am. Fam. Physician* 72, 1723-1732.

Stevens, L., Coresh, J., Greene, T., Levey, A., **2006**. Assessing kidney function — measured and estimated glomerular filtration rate. *N. Engl. J. Med.* 354, 2473-2483.

Stevens, L., Levey, A., **2009**. Current status and future perspectivies for CKD testing. *Am. J. Kidney Dis*. 53, S17-S26.

Subramanian, V., Frechet, J.M.J., Chang, P.C., Huang, D.C., Lee, J.B., Molesa, S.E., Murphy, A.R., Redinger, D.R., Volkman, S.K., **2005**. Progress Toward Development of All-Printed RFID Tags: Materials, Processes, and Devices. IEEE 93(7), 1330-1338.

Sukhija, R., Aronow, W., Kakar, P., Garza, L., Sachdeva, R., Sinha, A., Mehta, J., **2006**. Relation of Microalbuminuria and Coronary Artery Disease in Patients With and Without Diabetes Mellitus. *Am. J. Cardiol. 98*(3), 279-281.

Sullivan, J., Krieger, G., **2001**. Hydrofluoric acid exposures. Hazardous Materials Toxicology: Clinical Principles of Environmental Health, pp. 798-805, 2nd ed. Lippincott, Williams and Wilkins, Philadelphia, PA.

Sumerel, J., Lewis, J., Doraiswamy, A., Deravi, L., Sewell, S., Gerdon, A., Wright, D., Narayan, R., **2006**. Piezoelectric ink jet processing of materials for medical and biological applications. *Biotechnol. J.* 1, 976-987.

Sviridov, D., Meilinger, B., Drake, S., Hoehn, G., Hortin, G., **2006**. Coelution of other proteins with albumin during size-exclusion HPLC: Implications for analysis of urinary albumin. *Clin. Chem.* 52, 389-397.

Tada, H., Nagayama, H., **1995**. Chemical vapor surface modification of porous glass with fluoroalkyl-functionalized silanes. 2. resistance to water. *Langmuir* 11, 136-142.

Tercero Espinoza, L., Schumann, K., Luk, Y.-Y., Israel, B., Abbott, N., **2004**. Orientational behavior of thermotropic liquid crystals on surfaces presenting electrostatically bound vesicular stomatitis virus. *Langmuir* 20, 2375-2385.

Thakkar, H., Newman, D., Holownia, P., Davey, C., Wang, C.-C., Lloyd, J., Craig, A., Price, C., **1997**. Development and validation of a particle-enhanced turbidimetric inhibition assay for urine albumin on the dade aca(R) analyzer. *Clin. Chem.* 43, 109-113.

Tingey, M., Snodgrass, E., Abbott, N., **2004**. Patterned orientations of liquid crystals on affinity microcontact printed proteins. *Adv. Mater.* 16, 1331-1336.

Tixier, T., Heppenstall-Butler, M., Terentjev, E., **2006**. Spontaneous size selection in cholesteric and nematic emulsions. *Langmuir* 22, 2365-2370.

Tjipto, E., Cadwell, K., Quinn, J., Johnston, A., Abbott, N., Caruso, F., **2006**. Tailoring the interfaces between nematic liquid crystal emulsions and aqueous phases via layer-by-layer assembly. *Nano Lett.* 6, 2243-2248.

Tongcher, O., Sigel, R., Landfester, K., **2006**. Liquid crystal nanoparticles prepared as miniemulsions. *Langmuir* 22, 4504-4511.

Torffvit, O., Wieslander, J., **1986**. A simplified enzyme-linked immunosorbent assay for urinary albumin. *Scand. J. Clin. Lab. Invest.* 46, 545-548.

Torza, S., Mason, S.G., **1970**. Three-phase interactions in shear and electrical fields. *J. Colloid Interf. Sci.* 33, 67-83.

Umbanhowar, P., Prasad, V., Weitz, D., **2000**. Monodisperse emulsion generation via drop break off in a coflowing stream. *Langmuir* 16, 347-351.

Vallon, V., Muhlbauer, B., Osswald, H., **2006**. Adenosine and kidney function. *Am. Physiological Society* 86, 901-940.

Van Tassel, P., Guemouri, L., Ramsden, J., Tarjus, G., Viot, P., Talbot, J., **1998**. A particle-level model of irreversible protein adsorption with a postadsorption transition. *J. Colloid Interf. Sci.* 207, 317-323.

Vashist, S., Raiteri, R., Tewari, R., Bajpai, R., Bharadwaj, L., **2006**. Quantification of human immunoglobulin G immobilized on gold-coated silicon chip for biosensing applications. *J. Phys. Conf. Ser.* 34, 806-811.

Verhoeff, A., Brand, R., Lekkerkerker, H., **2011**. Tuning the birefringence of the nematic phase in suspensions of colloidal gibbsite platelets. *Mol. Phys.* 109, 1363-1371.

Viberti, G., Jarrett, R., Keen, H., **1982a**. Microalbuminuria as predictor of nephropathy in diabetics. *The Lancet* 320, 611.

Viberti, G., Jarrett, R.J., Mahmud, U., Hill, R., Argyropoulos, A., Keen, H., **1982b**. Microalbuminuria as a predictor of clinical nephropathy in insulin-dependent diabetes mellitus. *The Lancet* 319, 1430-1432.

Volkman, S., Pei, Y., Redinger, D., Yin, S., Subramanian, V., **2004**. Ink-jetted silver/copper conductors for printed RFID applications. *Mat. Res. Soc. Symp. Proc.* 814, 1781-1786.

Volovik, G., Lavrentovich, O., **1983**. Topological dynamics of defects: boojums in nematic drops. *Sov. Phys. JETP* 58, 1159-1167.

Wang, Z., Stein, A., **2008**. Morphology control of carbon, silica, and carbon/silica nanocomposites: From 3D ordered macro-/mesoporous monoliths to shaped mesoporous particles. *Chem. Mater.* 20, 1029-1040.

Watts, G., Bennett, J., Rowe, D., Morris, R., Gatling, W., Shaw, K., Polak, A., **1986**. Assessment of immunochemical methods for determining low concentrations of albumin in urine. *Clin. Chem.* 32, 1544-1548.

Wendler, J., Hoffmann, A., Gross, G., Weich, H.A., Bilitewski, U., **2005**. Development of an enzyme-linked immunoreceptor assay (ELIRA) for quantification of the biological activity of recombinant human bone morphogenetic protein-2. J. Biotechnol. 119(4), 425-435.

Wijshoff, H., **2010**. The dynamics of the piezo inkjet printhead operation. *Phys. Rep.* 491, 77-177.

Wilson, J., Hawkes, J., **1998**. Optoelectronics: An introduction. pp. 527-534, 3rd ed. ed. Prentice Hall, New York, NY.

Woo, K., Lau, Y., **1998**. Strategy for urinary protein analysis. *Neprology* 4, 327-329.

Xia, Y., Whitesides, G.M., **1998**. Soft lithography. *Annu. Rev. Mater. Sci.* 28, 153-184.

Xu, H., Bi, X., Ngo, X., Yang, K.-L., **2009**. Principles of detecting vaporous thiols using liquid crystals and metal ion microarrays. *Analyst* 134, 911-915.

Xue, C.-Y., Hartono, D., Yang, K.-L., **2008**. Controlling and manipulating supported phospholipid monolayers as soft resist layers for fabricating chemically micropatterned surfaces. *Langmuir* 24, 11282-11286.

Xue, C.-Y., Khan, S., Yang, K.-L., **2009**. Exploring optical properties of liquid crystals for developing label-free and high-throughput microfluidic immunoassays. *Adv. Mater.* 21, 198-202.

Xue, C.-Y., Yang, K.-L., **2008**. Dark-to-bright optical responses of liquid crystals supported on solid surfaces decorated with proteins. *Langmuir* 24, 563-567.

Yang, K.-L., Cadwell, K., Abbott, N., **2004**. Mechanistic study of the anchoring behavior of liquid crystals supported on metal salts and their orientational responses to dimethyl methylphosphonate. *J. Phys. Chem. B* 108, 20180-20186.

Zheng, G., Patolsky, F., Cui, Y., Wang, W., Lieber, C., **2005**. Multiplexed electrical detection of cancer markers with nanowire sensor arrays. *Nat. Biotechnol.* 23, 1294-1301.

Zheng, Q., Lu, J., Chen, H., Huang, L., Cai, J., Xu, Z., **2011**. Application of inkjet printing technique for biological material delivery and antimicrobial assays. *Anal. Biochem.* 410, 171-176.

Ziegler, J., Zimmermann, M., Hunziker, P., Delamarche, E., **2008**. High-performance immunoassays based on through-stencil patterned antibodies and capillary systems. *Anal. Chem.* 80, 1763-1769.

Zou, J., Bera, T., Davis, A.A., Liang, W., Fang, J., **2011**. Director configuration transitions of polyelectrolyte coated liquid-crystal droplets. *J. Phys. Chem. B* 115, 8970-8974.

Zou, J., Fang, J., **2010**. Director configuration of liquid-crystal droplets encapsulated by polyelectrolytes. *Langmuir* 26, 7025-7028.

APPENDICES

Appendix A

A.1 AHSA surface density calculations

To obtain a calibration curve of fluorescence intensities at different AHSA surface densities, we spotted standard FITC-AHSA solutions of various concentrations (***C*** = 0, 1, 2, 5, 10, 25, 50, 65, 80 and 100μg/mL) on a DMOAP-coated slide in an array format (Bi et al. **2009b**). The array was left to dry for 2h without any further rinsing to ensure that AHSA in each droplet deposited on the surface completely. The equivalent AHSA surface density (Γ_{AHSA}), pmol/cm^2, in each dried spot can be calculated as follows:

$$\Gamma_{AHSA} = \left(\frac{10^{11}}{MW_{AHSA}} \right) \frac{CV}{\pi D^2 / 4} \qquad [A.1]$$

where ***C*** is the concentration (μg/mL), ***V*** is the volume (μL), and ***D*** is the diameter of the spherical droplet (μm), MW is the molecular weight of the protein. Based on the experimental setup, each FITC-AHSA spot has a volume (***V***) of 0.1μL, and a diameter (***D***) of 800μm. The MW of AHSA is 150kD.

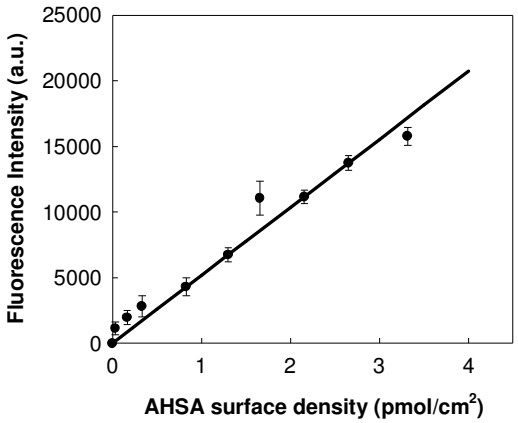

Figure A.1 Calibration curve of fluorescence intensity as a function of AHSA surface density.

FITC-AHSA solutions used in the experiment (***C*** = 0, 10, 15, 20, 25, 30, 40, 50, 90 and 100μg/mL) were then spotted to the DMOAP-coated slides and then rinsed after 2h incubation. Figure A.2 shows the fluorescence images of each spots and their corresponding AHSA surface density estimated from Figure A.1.

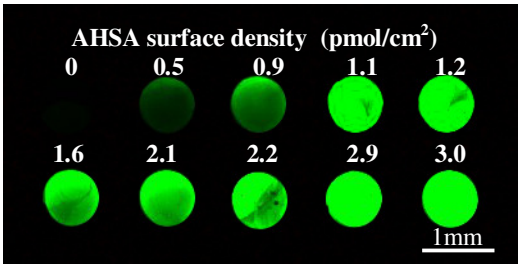

Figure A.2 Fluorescence images of the AHSA solutions used in the experiment.

Next, we studied the relationship between the AHSA concentration in the solution and the surface density of immobilized AHSA on the surface. When the concentration of AHSA in the solution is increased from 1 μg/mL to 100 μg/mL, the fluorescence intensity also increases from 1,100 to 15,800 a.u. On the basis of the fluorescence results, the maximum AHSA surface density is 3.0 ± 0.1 pmol/cm^2 (see Figure A.3).

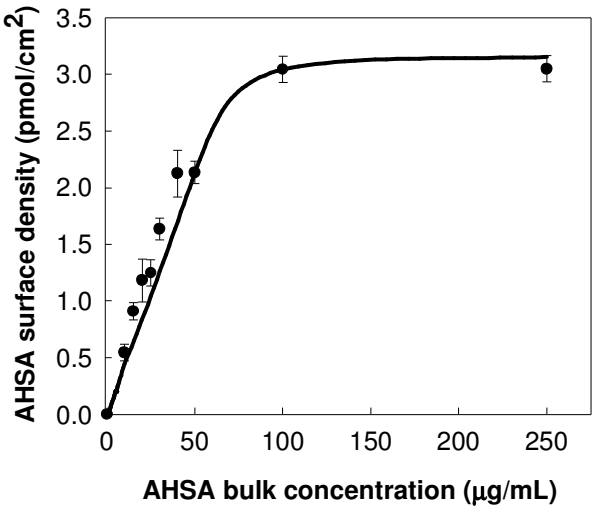

Figure A.3 AHSA surface density as a function of AHSA concentration in solution. Plotted line is a graph taken from the calibration curve. Points plotted is the actual data points taken from spotted AHSA solutions rinsed with PBS buffer.

A.2 Effect of incubation time and HSA concentrations

To find the optimum time required for the binding of HSA to surface immobilized AHSA, we spotted solutions containing different HSA concentrations (10, 25, 50, and 100 μg/mL of FITC-HSA) on AHSA-decorated slides and then varied the incubation time from 1, 5, 15, 30, 60 to 120 min. Figure A.4 shows that the amount of HSA that binds to the AHSA-decorated slide increases with time. However, this result also reveals that HSA binds very quickly onto the surface in the beginning (especially at higher concentrations), but the binding rate slows down after 30 min, probably because the surface is saturated with HSA. Since the amount of HSA bound to the surface from 30 min to 60 min is minimal, we use 30 min as the incubation time in the following experiments.

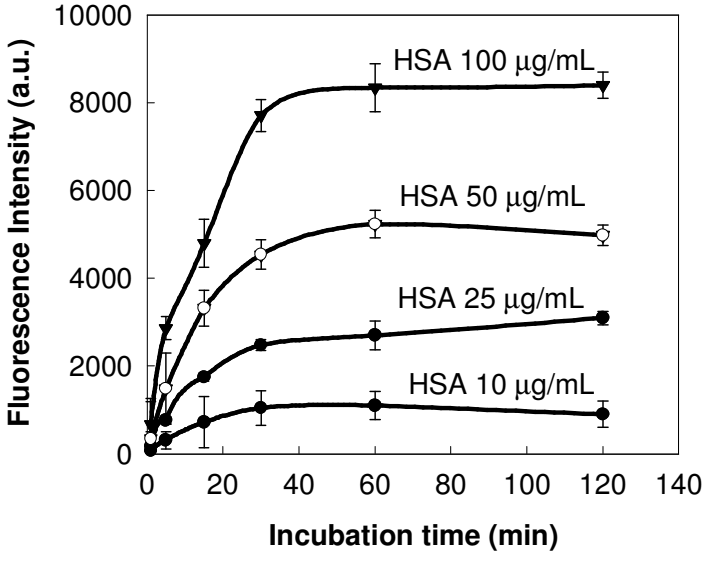

Figure A.4 Effect of incubation time on the binding of HSA to surface immobilized AHSA.

A.3 Detection of HSA using chip electrophoresis

Figure A.5 shows the runs made using several standard HSA solutions in order to determine the HSA limit of detection (LOD) of the chip electrophoresis. The figure exhibits a band near 63 kDa of the ladder which corresponds to the molecular weight of HSA. In addition, Figure A.5 (columns 1-5) shows decreasing band intensity as the amount of HSA in the solution decreases. Further decreased of the amount of HSA in the solution was done until it can no longer be detected (LOD = 20 µg/mL).

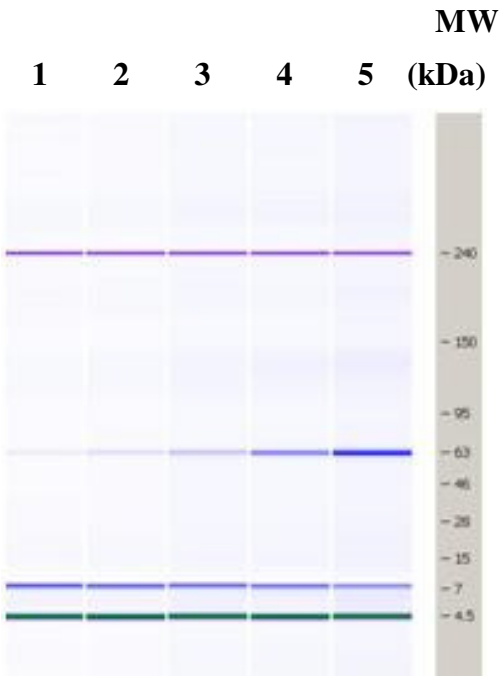

Figure A.5 Detecting HSA by using chip electrophoresis. Columns 1-5 represent standard HSA solutions whose concentrations are 20, 100, 200, 500, and 1000µg/mL, respectively.

Figure A.6 shows a representative electropherogram for samples collected from both groups. The urine sample from the group of CKD patients exhibits a band near 63 kDa which confirms the presence of HSA in the urine samples of CKD patients. In contrast, no band can be seen when the urine sample from the control group were used.

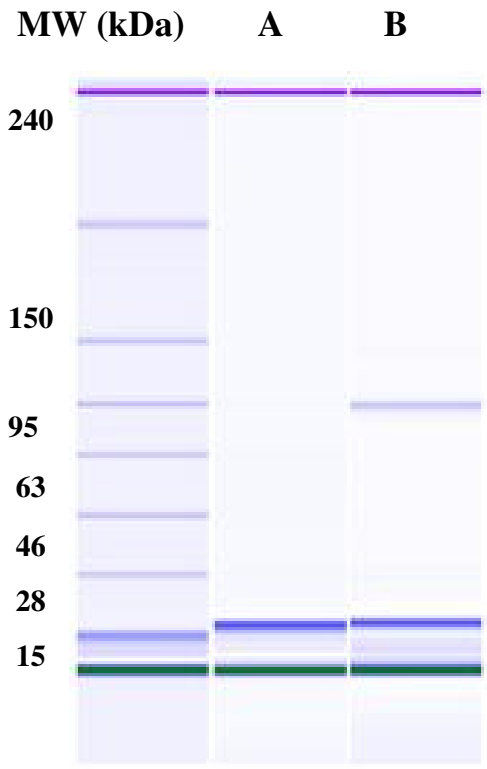

Figure A.6 Analysis of two different urine samples using chip electrophoresis. (A) sample from the control group and (B) sample from a CKD patient. The presence of HSA in the sample collected from the CKD patient is confirmed by using the protein ladder on the left.

Appendix B.

B.1 PEI surface density calculations

A calibration curve that correlates the fluorescence intensity with PEI surface density was obtained by spotting sequentially diluted Cy3-labeled PEI solutions (0, 0.078, 0.156, 0.312, 0.625, 1.25, 2.50, and 5.00 %) on a glass slide to form a dried microarray. The equivalent PEI surface density, Γ_{PEI} (nm^{-2}), in each spot can be calculated as follows:

$$\Gamma_{PEI} = \frac{CV}{\pi D^2} \times \frac{1}{MW_{PEI}} \times N_A \qquad [B.1]$$

where C is the concentration (μg/mL), V is the volume (μL), D is the diameter of the spot (μm), NA is the Avogadro's number, and MW_{PEI} = 750,745 μg/μmol. Based on the experimental setup, each Cy3-labeled PEI spot has a volume (V) of 1 μL and a diameter (D) of 4400 μm.

Figure B.1 shows a calibration curve of fluorescence intensity as a function of PEI surface density in the dry state. In order to compensate for a higher quantum yield in wet state, a correction factor f = 2.0 (the quantum ratio between wet and dry state) is used to obtain a calibration curve for wet state (Malicka et al. **2003**). Fluorescence intensity of each LC droplet was measured and averaged. Next, by using

the calibration curve (wet state), we can estimate the PEI surface density on each LC droplet.

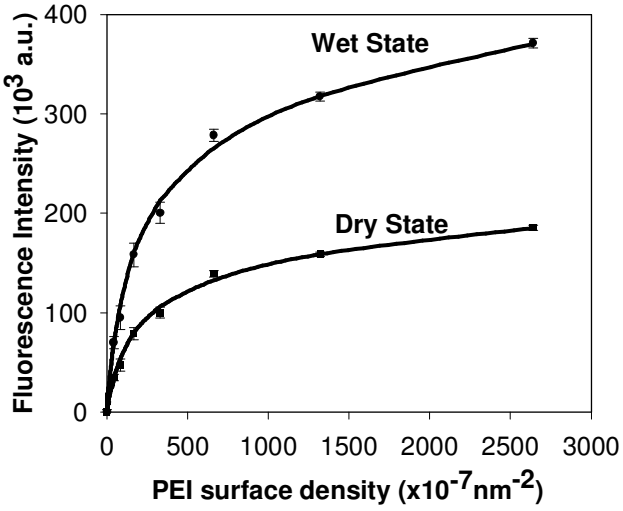

Figure B.1 Calibration curve of fluorescence intensity as a function of PEI surface density.

B.2 Effect of GA on the amount of IgG immobilized on the LC droplet surface

To determine optimum GA concentration, we measured the amount of IgG immobilized on the surface after immersing the LC droplets in a 50 μg/mL Cy3-labeled IgG solution. Figure B.2 shows an increase in the fluorescence intensity when the GA concentration is increased from 0.1% to 1.0%. This implies that the amount of immobilized IgG increases with the increasing GA concentration. This result is consistent with our previous work (Bi and Yang **2008**). However, if the GA concentration is increased further to 5%, the fluorescence intensity decreases. We suspect that the decrease is caused by overcrowding of aldehyde functional groups on

the surface. In this case, one IgG molecule can link to more than one aldehyde group and lay flat on the surface, reducing the total amount of immobilized IgG. Therefore, we decided that the optimum concentration of GA is 1% in our experiments.

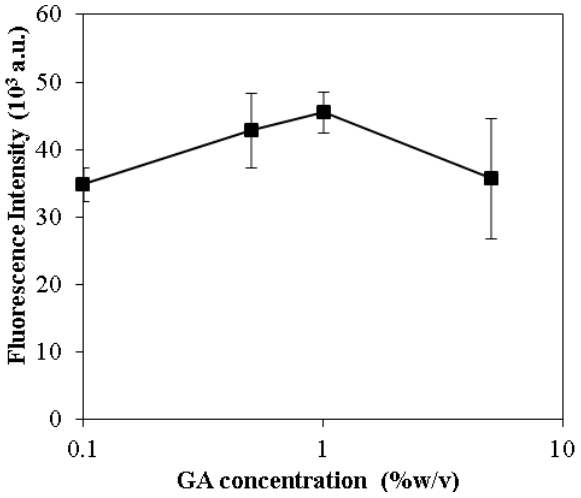

Figure B.2 Fluorescence intensity of IgG-LC droplets as a function of GA concentration.

B.3 Protein Surface Density Calculations

The calibration curve of IgG and HSA surface densities as a function of concentration were obtained similarly as Appendix B.1.

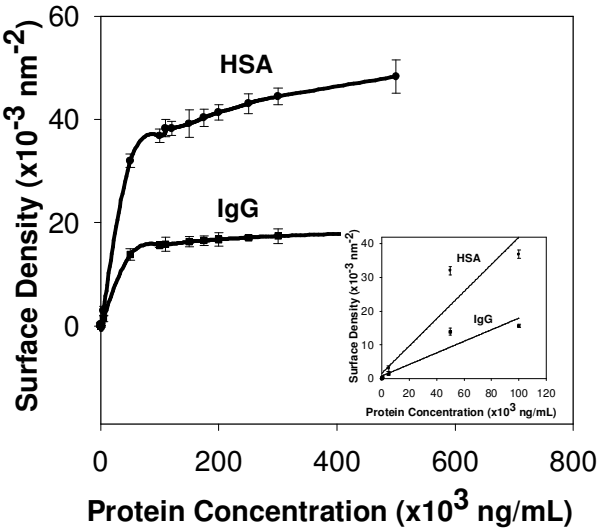

Figure B.3 Protein surface density as a function of protein concentration.

B.4 Detecting proteins using LC droplets in a microfluidic channel

We tested the use of IgG-LC droplets in a microfluidic system (Figure B.3A) to detect AIgG antibodies in solution. The microfluidic channel used has two inlets, one for the entry of LC droplets functionalized with 50 μg/mL IgG (IgG-LC droplets) and the other for the entry of 0.10 μg/mL AIgG solution. Both solutions were flowed at 0.1 μL/min. Images were taken at Locations 1 and 2 under a crossed polarized microscope.

As shown in Figure B.3B, the LC droplets still exhibit a radial configuration right after mixing the IgG-LC droplets with the AIgG solution. However, further downstream (~43 cm), the LC droplets changed to a bipolar configuration (see Figure B.3C). The transition of the LC configuration indicates antigen-antibody binding at

the LC droplets. This shows that LC droplets in a microfluidic system can give an immediate test results.

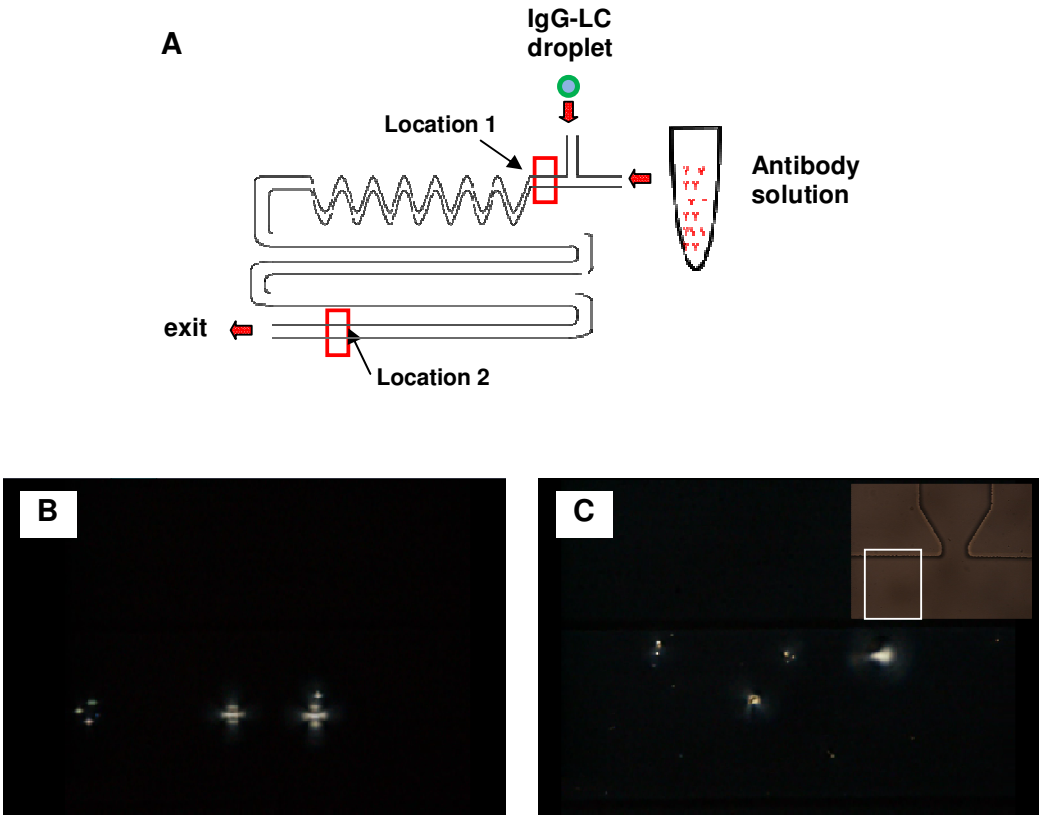

Figure B.4 (A) Schematic diagram of the microfluidic channel setup. (B) Optical appearance of IgG-LC droplets right after mixing with AIgG exhibiting a radial configuration. (C) Optical appearance of IgG-LC droplets located further downstream exhibiting a bipolar configuration (Inset: bright field image).

APPENDIX C

C.1 Jetting Parameters

According to the working principles of inkjet printing, the properties of the ink (e.g. surface tension and viscosity) need to meet a certain criteria (see Table 5.1). If the surface tension is too high ($\gamma > 42$ dynes/cm), the jetting mechanism cannot be primed and the ink will not jet. If the surface tension is too low ($\gamma < 32$ dynes/cm), however, the ink will stream out of the nozzles or form unstable drops. The nematic LC, 5CB, has a surface tension of 40 dynes/cm which meets the criteria and makes it a possible candidate to be used as an ink to the printer. Properties of 5CB are also listed in Table 5.1.

To dispense LC, we use the standard waveform for the model ink (Dimatix Model Fluid 003) (Fujifilm **2008**), as our starting point since it has similar properties as 5CB. As shown in Figure C.1, the waveform consists of 4 phases. These phases control the action brought forth by the piezo element of the fluid chamber and finally determine the drop formation of the fluid. Because the bending of the piezo element is voltage driven, we investigated the effects of firing voltage on the jetting performance and the printing patterns produced on the glass surface.

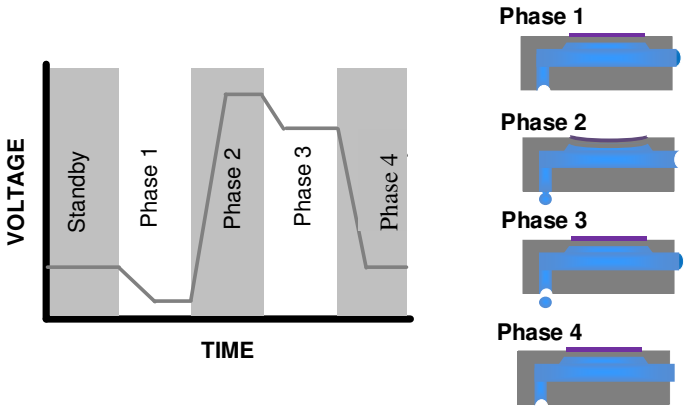

Waveform settings

	Phase 1	Phase 2	Phase 3	Phase 4
Level (%)	0	100	67	40
Slew Rate, %	0.65	.38	0.6	0.8
Duration (µs)	3.184	3.512	3.392	0.832

Figure C.1 Piezoelectric print head undergoes four phases during printing. **Phase 1**: The chamber is in a relaxed position where the fluid can pass through the inlet; **Phase 2**: The chamber is compressed to eject a drop; **Phase 3**: The chamber is decompressed partially, and; **Phase 4**: chamber is back in its original state.

C.2 Determining the appropriate voltage settings for LC ink

The Dimatix printer was calibrated by dispensing LCs from a 10 pL cartridge a 10 mm × 60 mm microarray consisting of 66,150 spots. The printing was repeated 5 times to obtain an overall volume of 33.08×10^{-4} mL. The calibration was done using 15V, 20V and 25V. By measuring the total weight of the LC droplets, we are able to approximate the LC density. From Table C.1, the computed density from 25V gave the nearest value to the theoretical value (1.016 g/mL).

Table C.1 Computed LC density from different voltage settings

	15V	**20V**	**25V**
Total Volume, mL	0.003308	0.003308	0.003308
Measured weight, g			
Trial 1	0.002844	0.003335	0.003433
Trial 2	0.002746	0.003040	0.003335
Estimated LC density, g/mL	**0.85 ± 0.02**	**0.96 ± 0.06**	**1.02 ± 0.02**

C.3 Interfacial tension measurements

The equations used for the calculation of the spreading parameter can be deduced from the Young-Dupré equation. The interfacial tension, γ_{12} (e.g. glass/PEI), can be calculated from the Young's equation using the interfacial tension measurements of γ_{13} (e.g. glass/5CB) and γ_{23} (e.g. PEI/5CB; which is obtained from the pendant drop experiment), and the contact angle of 5CB immersed in PEI:

$$\gamma_{12} = \gamma_{13} + \gamma_{23} \cos\theta \quad \text{(Young's equation)}$$

The value for γ_{13} was also computed by using Young's equation. To obtain this parameter, 5CB was in contact with air. Figure C.2 shows how the interfacial tension measurements were conducted.

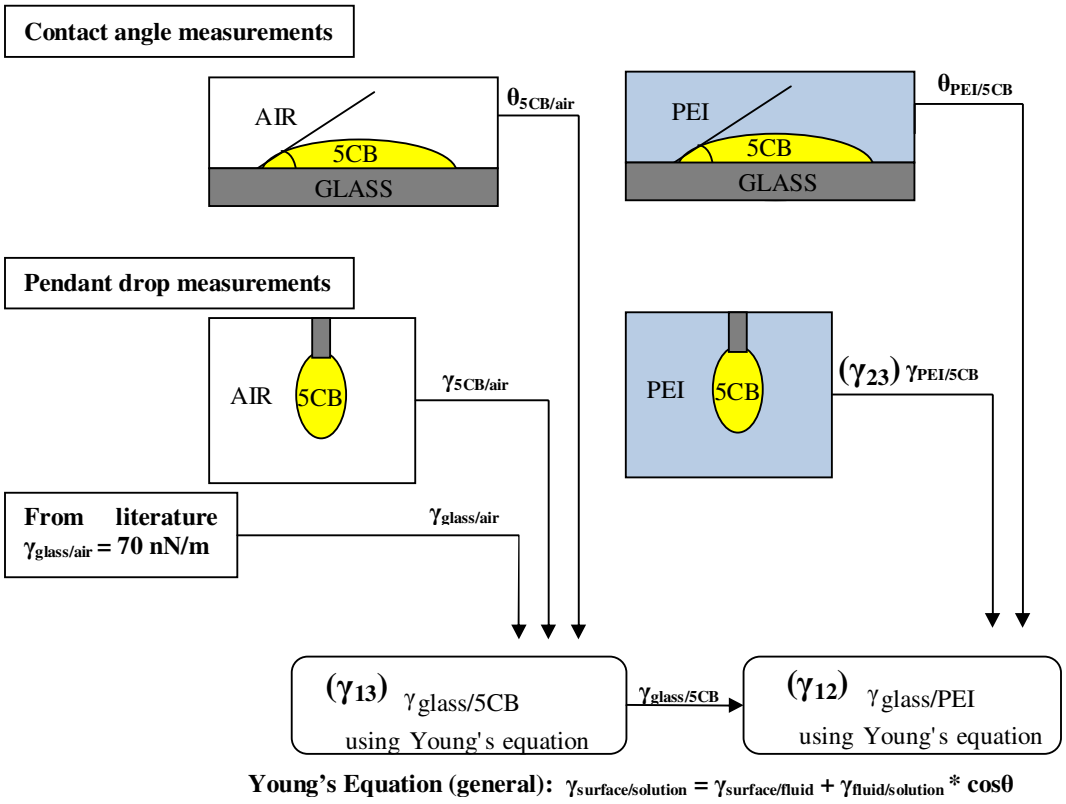

Figure C.2 Flow chart of measuring interfacial tensions between (1) glass, (2) PEI, and (3) 5CB phases.

C.4 Regulating the contact line of the continuous phase during flushing

To study whether there are any significant effects during the nature of flushing of the LC dots as shown in Figure 5.1, we positioned the slide that supports the LC dots perpendicularly on a cuvette. The cuvette was then filled with aqueous PEI solution at a constant flow rate (100 mL/h for slow flushing and 600 mL/h for fast flushing), allowing the solution to flush the LC dots vertically as shown in Figure C.3. Video images were taken during both flushing conditions at the contact line (see Movie M1 for slow flushing and Movie M2 for rapid flushing).

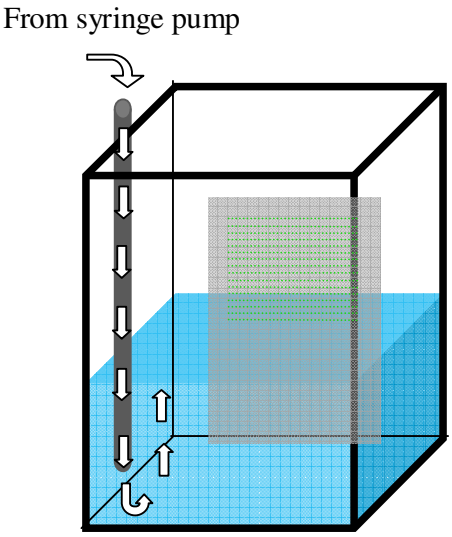

Figure C.3 A schematic diagram of the flushing setup regulating the contact line of the continuous phase. Cuvette was filled with the continuous phase at a constant flow rate, flushing the LC droplets as the solution move upwards.

Appendix D

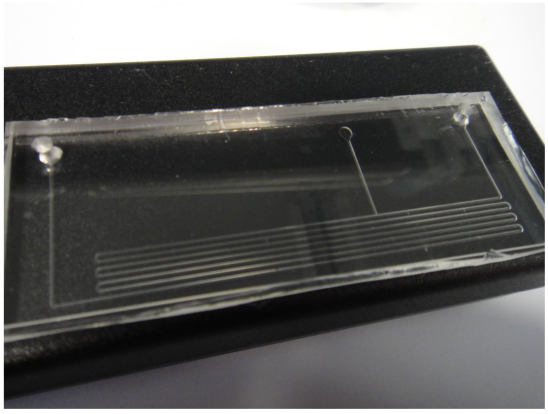

Figure D.1 PDMS microfluidic channel.

D.1 Response of LC to Ethanol Vapor

We first prepared LC in two different geometries, one is in copper grid and the other is in a microarray with LC dots. Then, we compared their response time to ethanol vapor. To do this, a LC-filled copper grid was first placed inside an closed gas chamber with polarized viewing panels (V = 0.3 cm^3). About 30 µL of ethanol was dropped onto a filter paper placed inside (both top and bottom) of the chamber. The chamber was then closed and the optical responses of the 5CB in the grid were observed over a period of time. The same procedure was repeated for the LC dot (1 pL) microarray. Experiments were done in triplicates. The results in Figure D.2 show that the LC dot microarray has faster response (t ~ 140 s) than the LC confined

in a copper grid (t ~ 1 min 48 s). This is reasonable because the LC dot has a smaller thickness; it can be more quickly saturated with ethanol than the LC in the grid. We point out this is different from the interface-driven response in which the response time is not affected by the LC thickness.

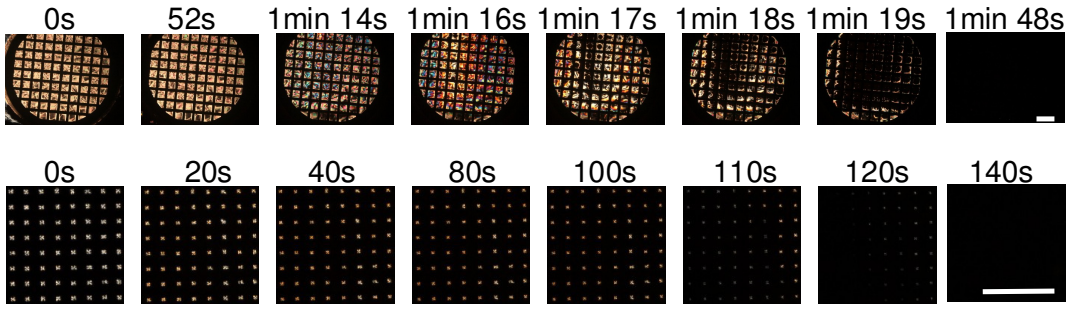

Figure D.2 Real-time response of LC to ethanol vapor using LC confined in copper grid and LC dot microarray. Scale bar is 500 µm.

We also studied the diffusion of ethanol to the different sizes of LC dots. As shown in Figure D.3, the response from bright to dark for 1-pL LC dot is only ~140s, whereas the response time for 10-pL LC dot is ~260s. This suggests that it takes longer time for bigger LC dots to be saturated with ethanol. In contrast, for interface-driven phenomenon (e.g. the adsorption of CTAB), the response time is independent of the size of LC dot.

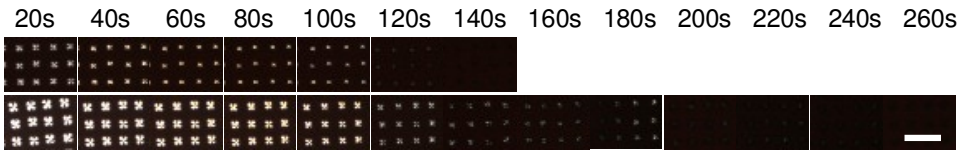

Figure D.3 Effects of LC dot size on the dynamic response to ethanol. 1-pL LC dots (top row) and 10-pL LC dots (bottom row) were used in this study for comparison. Images were taken at 20s interval. Scale bar is 250 µm.

D.2 Response time of LC dots to BSA concentrations

We observed the response times for the LC dots to give a bright signal at higher BSA concentrations to be faster than those immersed in lower BSA concentrations. These results are consistent with protein adsorption studies where the rate of adsorption increases as the protein in the solution increases (Van Tassel et al. **1998**). In addition, these results suggest that we can also monitor the protein adsorption in real-time.

Table D.1 Response time of LC dots to BSA concentrations

BSA Concentration (µg/mL)	Response time
100	58 s
50	1 min 2 s
25	1 min 15 s
10	10 min 16 s
3	no response

LIST OF PUBLICATIONS

Chapter 3

(1) Aliño, V.J., Yang, K.-L., **2011**. Using Liquid Crystals as a Readout System in Urinary Albumin Assays. *Analyst* 136, 3307-3313.

(2) Aliño, V.J., Yang, K.-L., **2009**. Applications of Liquid Crystals in Detecting Chronic Kidney Disease. International BioTraining Conference. NUS, Singapore. **Awarded** for Best Poster Presentation.

Chapter 4

(3) Aliño, V.J., Pang, J., Yang, K.-L., **2011**. Liquid Crystal Droplets as a Hosting and Sensing Platform for Developing Immunoassays. *Langmuir* 27, 11784-11789.

(4) Aliño, V.J., Pang, J., Yang, K.-L., **2011**. Liquid Crystal Droplets as Sensing Platform for Developing Protein Immunoassays. AICHE Annual Conference. Salt Lake City, Utah, USA.

Chapter 5

(5) Aliño, V.J., Tay, K. X., Khan, S. A., Yang, K.-L., **2012**. Inkjet Printing and Release of Monodisperse Liquid Crystal Droplets from Solid Surfaces. *Langmuir* 28, 14540-14546.

Chapter 6

(6) Aliño, V.J., Sim, P. H., Choy, W. T., Fraser, A., Yang, K.-L., **2012**. Detecting Proteins in Microfluidic Channels Decorated with Liquid Crystal Sensing Dots. *Langmuir* 28, 17571-17577.